

Neutrino non-standard interactions as a portal to test flavour symmetries

TseChun Wang ^{*} Ye-Ling Zhou [†]

Institute for Particle Physics Phenomenology, Department of Physics,
Durham University, Durham DH1 3LE, United Kingdom

Abstract

Imposing non-Abelian discrete flavour symmetries to neutrino non-standard interactions (NSIs) is discussed for the first time. For definiteness, we choose A_4 as the flavour symmetry, which is subsequently broken to the residual symmetry Z_2 in the neutrino sector. We provide a general discussion on flavour structures of NSIs from higher-dimensional operators ($d \leq 8$) without inducing unnecessary tree-level 4-charged-fermion interactions. Both A_4 - and Z_2 -motivated NSI textures are obtained. UV completions of higher-dimensional operators lead to extra experimental constraints on NSI textures. We study the implementation of matter-effect NSIs in DUNE from phenomenological point of view, and discover that DUNE can test A_4 with a high level of statistics. We also present exclusion limits of sum rules suggested by UV-complete models. Our result shows that the NSI effects, though predicted to be small for DUNE, could provide useful information that might extend our understanding of the flavour symmetry.

PACS number(s): 11.30.Hv, 12.15.Ff, 13.15.+g, 14.60.Pq

Keywords: non-standard interaction, neutrino oscillation, flavour symmetries

^{*}E-mail: tse-chun.wang@durham.ac.uk

[†]E-mail: ye-ling.zhou@durham.ac.uk

1 Introduction

Neutrino oscillation experiments have achieved great success in the last two decades [1–4]. Two neutrino mass-squared differences (Δm_{21}^2 , $|\Delta m_{31}^2|$) and three mixing angles (θ_{12} , θ_{23} , θ_{13}) have been measured in the standard three-neutrino framework. Several next-generation oscillation experiments are proposed, such as the long-baseline accelerator experiments DUNE [5], T2HK [6], the intermediate-baseline reactor experiment JUNO [7,8], SBN programme [9], and muon-decay experiments NuSTORM [10], MOMENT [11], Neutrino Factory [12], etc. They are aimed at answering the remaining questions in neutrino oscillations: if CP is violated in neutrino oscillations, what the value of the Dirac-type CP-violating phase δ is, and which mass ordering ($\Delta m_{31}^2 > 0$ or $\Delta m_{31}^2 < 0$) is true. In addition, the already known oscillation parameters can be measured to the percent level and the octant of θ_{23} ($\theta_{23} < 45^\circ$ or $\theta_{23} > 45^\circ$) will be determined [13,14].

These experiments will also test the standard three-neutrino mixing scenario and might unveil new neutrino couplings beyond the Standard Model (SM). Neutrino nonstandard interactions (NSIs) provide a model-independent framework of studying new physics in neutrino oscillation experiments (for some reviews, see [15]). They are usually considered as effective descriptions of contributions from higher-dimensional operators mediated by heavy mediators [16–18,20], although they may also be induced by light mediators with very weak couplings (see e.g., [21,22]). In neutrino oscillation experiments, NSIs may appear at neutrino sources, detectors or during neutrino propagation. There are no experimental hints for NSIs at the source and the detector [15,26]. Current global-fit results for NSIs during neutrino propagation, i.e., matter-effect NSIs, reach the precision from a few to tens of percentages of the strength of the standard matter effect induced by the weak interaction [27]. Due to precision upgrades and because of nonnegligible matter effects, the testability of NSIs in DUNE and T2HK (as well as its alternative T2HKK), and the influences on measurements of mass ordering and CP violation have received a lot of attentions (see, e.g., in [28–32]). For NSIs studied in other future experiments, see, e.g., Refs. [33–37].

One important theoretical development promoted by neutrino oscillations is the application of flavour symmetries for understanding lepton flavour mixing. It is directly triggered by the measured values of mixing angles, $\sin^2 \theta_{12} \sim 1/3$ and $\sin^2 \theta_{23} \sim 1/2$. In the framework of flavour symmetries, it is assumed that an underlying discrete flavour symmetry G_f exists at some high energy scale. It unifies the three flavours together. After the flavour symmetry is broken at a lower energy scale, special flavour structures arise. The most famous group used as a flavour symmetry is the tetrahedral group A_4 [38]. Most A_4 models naturally predict $\sin^2 \theta_{12} = 1/3$, $\sin^2 \theta_{23} = 1/2$ but $\sin^2 \theta_{13} = 0$ [39–41], i.e., the so-called tri-bimaximal (TBM) mixing [42]. One important feature of these models are the correspondence between the mixing and the existence of the residual symmetries Z_3 and Z_2 after A_4 breaking (for some reviews, see e.g. [43]). Z_3 and Z_2 are subgroups of A_4 . They are approximately preserved in the charged lepton and neutrino sectors, respectively, acting on charged leptons and neutrinos separately as

$$\begin{aligned} Z_3 : \quad & e \rightarrow e, \quad \mu \rightarrow e^{-i2\pi/3} \mu, \quad \tau \rightarrow e^{i2\pi/3} \tau; \\ Z_2 : \quad & \nu_e \rightarrow \frac{1}{3}(-\nu_e + 2\nu_\mu + 2\nu_\tau), \quad \nu_\mu \rightarrow \frac{1}{3}(-\nu_\mu + 2\nu_\tau + 2\nu_e), \quad \nu_\tau \rightarrow \frac{1}{3}(-\nu_\tau + 2\nu_e + 2\nu_\mu). \end{aligned} \quad (1)$$

Slight breakings of the residual symmetries provide small corrections to the mixing, specifically generating a non-zero θ_{13} and making all mixing parameters compatible with oscillation data. The preferred parameters of these models will be tested by the future neutrino oscillation experiments.

Imposing flavour symmetries may not only influence the flavour mixing measured by neutrino oscillation experiments, but also contribute to other flavour-dependent phenomenological signatures, such

as the charged lepton flavour violation (CLFV). The influence of flavour symmetries on CLFV processes has been discussed in [44–50]. In particular, the essential contribution of A_4 and Z_3 on the CLFV decays of charged leptons have been carefully analysed in [49]. The branching ratio sum rules of these processes have been obtained therein, which can be regarded as specific features of flavour symmetries. In the neutrino sector, as the couplings are too weak, the phenomenological signatures of flavour symmetries beyond the standard neutrino oscillation measurements have been rarely discussed.

Previous discussions of NSIs in flavour symmetries are limited only in the Abelian case [21–25]. In these papers, by assuming a gauged $U(1)$ flavour symmetry, relatively sizeable NSIs are generated via flavour-dependent gauge interaction mediated by a gauge boson with the mass around or below the GeV scale. Note that $U(1)$ symmetries proposed in these works are not supposed to explain the lepton flavour mixing. Thus we do not expect any connection between NSIs and lepton flavour mixing.

In the non-Abelian case, as e , μ and τ lepton doublets are arranged as a triplet in the flavour space, which both complicates the NSI construction and strengthens experimental constraints. However, if the non-Abelian discrete symmetry is a true symmetry behind, a combined study of the flavour symmetry and NSIs will be required in the future neutrino experiments. Regarding the A_4 case, the measurement of NSIs in neutrino oscillations provides an excellent opportunity to study the connection with A_4 and the residual symmetry Z_2 in the neutrino sector, as we will see later.

This work is aimed at discussing how to hint flavour symmetries and residual symmetries in the NSI measurements in neutrino oscillation experiments. We fix the flavour symmetry A_4 and residual symmetry Z_2 for definiteness. It is a complementarity to studies of A_4 and Z_3 in CLFV processes and in the standard neutrino oscillation measurements. Imposing the flavour symmetry in the fermion sectors, interesting NSI textures or sum rules of NSI parameters are obtained. Both NSIs directly from higher-dimensional operators in the EFT approach with respecting to the electroweak symmetry and those mediated by specified BSM particles will be discussed. The rest of this paper is organised as follows. We briefly review the TBM mixing realised in A_4 models in Section 2. Section 3 is devoted to a systematic analysis of how to impose A_4 or Z_2 to higher-dimensional operators (with the dimension $d \leq 8$) which result in NSIs. A class of NSI textures based on A_4 and Z_2 are obtained, respectively. We only require that the three lepton doublets form a triplet of A_4 , no requirement for representations of other fermions in the flavour space. In Section 4, we consider the UV completion of these operators. New particles in the UV sector impose additional experimental constraints to NSI parameters and thus, some textures are less constrained than the others. We suggest that these textures have a priority to be discussed in the NSI measurement. In Section 5, based on the DUNE experiment set up, we analyse the potential for the discovery of these textures. We summarise our paper in Section 6. In the main text of this paper, we focus on NSIs in matter. Connections of flavour symmetries with NSIs at the source and detector are strongly dependent upon representations of the other fermions.

2 Flavour symmetries and residual symmetries in lepton mixing

We briefly review the realisation of the TBM mixing in A_4 models and residual symmetries after A_4 is broken. A_4 is generated by two generators \mathcal{S} and \mathcal{T} with the requirements $\mathcal{S}^2 = \mathcal{T}^3 = (\mathcal{ST})^3 = 1$ and contains 12 elements. It has four irreducible representations: three singlet representations $\mathbf{1}$, $\mathbf{1}'$, $\mathbf{1}''$ and one triplet representation $\mathbf{3}$. Kronecker products of two irreducible representations are reduced in the

following way:

$$\begin{aligned} \mathbf{1} \times \mathbf{1}^{(\prime,\prime)} &= \mathbf{1}^{(\prime,\prime)}, \quad \mathbf{1}' \times \mathbf{1}' = \mathbf{1}'', \quad \mathbf{1}'' \times \mathbf{1}'' = \mathbf{1}', \quad \mathbf{1}' \times \mathbf{1}'' = \mathbf{1}, \\ \mathbf{3} \times \mathbf{1}^{(\prime,\prime)} &= \mathbf{3}, \quad \mathbf{3} \times \mathbf{3} = \mathbf{1} + \mathbf{1}' + \mathbf{1}'' + \mathbf{3}_S + \mathbf{3}_A, \end{aligned} \quad (2)$$

where the subscripts $_S$ and $_A$ stand for the symmetric and anti-symmetric components, respectively.

We work in the Altarelli-Feruglio (AF) basis [40], where \mathcal{T} and \mathcal{S} are respectively given by

$$\mathcal{T} = \begin{pmatrix} 1 & 0 & 0 \\ 0 & \omega^2 & 0 \\ 0 & 0 & \omega \end{pmatrix}, \quad \mathcal{S} = \frac{1}{3} \begin{pmatrix} -1 & 2 & 2 \\ 2 & -1 & 2 \\ 2 & 2 & -1 \end{pmatrix}. \quad (3)$$

This basis is widely used in the literature since the charged lepton mass matrix invariant under \mathcal{T} is diagonal in this basis. The products of each two triplet representations $a = (a_1, a_2, a_3)^T$ and $b = (b_1, b_2, b_3)^T$ can be expressed as

$$\begin{aligned} (ab)_{\mathbf{1}} &= a_1 b_1 + a_2 b_3 + a_3 b_2, \\ (ab)_{\mathbf{1}'} &= a_3 b_3 + a_1 b_2 + a_2 b_1, \quad (ab)_{\mathbf{3}_S} = \frac{1}{2} \begin{pmatrix} 2a_1 b_1 - a_2 b_3 - a_3 b_2 \\ 2a_3 b_3 - a_1 b_2 - a_2 b_1 \\ 2a_2 b_2 - a_3 b_1 - a_1 b_3 \end{pmatrix}, \quad (ab)_{\mathbf{3}_A} = \frac{1}{2} \begin{pmatrix} a_2 b_3 - a_3 b_2 \\ a_1 b_2 - a_2 b_1 \\ a_3 b_1 - a_1 b_3 \end{pmatrix}. \end{aligned} \quad (4)$$

The A_4 symmetry is broken at a certain lower scale. After the A_4 breaking, residual symmetries Z_3 and Z_2 , which are generated by \mathcal{T} and \mathcal{S} , respectively, are approximately preserved in the charged lepton and neutrino sectors, separately. Residual symmetries constrain the lepton mass matrices and lead to the TBM mixing [42]. A sketch for how to realise TBM from A_4 is shown in Figure 1.

The Lagrangian terms for generating charged lepton and neutrino masses are effectively realised by some higher-dimensional operators. In the flavour space, the lepton doublets $L_1 = (\nu_{eL}, e_L)$, $L_2 = (\nu_{\mu L}, \mu_L)$, $L_3 = (\nu_{\tau L}, \tau_L)$ are often arranged as a triplet $L \equiv (L_1, L_2, L_3)^T$. This arrangement holds for most flavour models with non-Abelian discrete symmetries, not just for A_4 models, in which the flavour symmetry contains a triplet irreducible representation [43]. In A_4 models, the right-handed charged leptons e_R , μ_R and τ_R are often assigned as singlets $\mathbf{1}$, $\mathbf{1}'$ and $\mathbf{1}''$, respectively [39, 40]. The relevant Lagrangian terms are effectively written as

$$\begin{aligned} -\mathcal{L}_l &= \frac{y_e}{\Lambda} (\bar{L}\varphi)_{\mathbf{1}} e_R H + \frac{y_\mu}{\Lambda} (\bar{L}\varphi)_{\mathbf{1}''} \mu_R H + \frac{y_\tau}{\Lambda} (\bar{L}\varphi)_{\mathbf{1}'} \tau_R H + \text{h.c.}, \\ -\mathcal{L}_\nu &= \frac{y_1}{2\Lambda\Lambda_W} ((\bar{L}\tilde{H}\tilde{H}^T L^c)_{\mathbf{3}_S} \chi)_{\mathbf{1}} + \frac{y_2}{2\Lambda_W} ((\bar{L}\tilde{H}\tilde{H}^T L^c)_{\mathbf{1}} + \text{h.c.}), \end{aligned} \quad (5)$$

where the Higgs $H \sim \mathbf{1}$ of A_4 and $\tilde{H} = i\sigma_2 H^*$. We apply the dimension-5 Weinberg operator $(\bar{L}\tilde{H}\tilde{H}^T L^c)$ to generate neutrino masses and Λ_W is the corresponding UV-complete scale. Operators in Eq. (5) involve flavons, denoted by φ and χ and a new scale Λ corresponding to the decoupling of some heavy A_4 multiplets.

Flavons play the key role in the flavour mixing. They gain VEVs, leading to the breaking of the flavour symmetry and leaving residual symmetries in the charged lepton and neutrino sectors, respectively. The flavon VEVs φ and χ preserving Z_3 and Z_2 , respectivelyⁱ, i.e.,

$$\mathcal{T}\varphi = \varphi, \quad \mathcal{S}\chi = \chi \quad (6)$$

ⁱIn the following, we do not specify notations of flavons with flavon VEVs.

take the following forms,

$$\varphi = (1, 0, 0)^T v_\varphi, \quad \chi = (1, 1, 1)^T v_\chi. \quad (7)$$

The resulting lepton mass matrices are represented as

$$M_l = \begin{pmatrix} y_e & 0 & 0 \\ 0 & y_\mu & 0 \\ 0 & 0 & y_\tau \end{pmatrix} \frac{v v_\varphi}{\sqrt{2}\Lambda}, \quad M_\nu = \begin{pmatrix} 2a + b & -a & -a \\ -a & 2a & -a + b \\ -a & -a + b & 2a \end{pmatrix}, \quad (8)$$

where $v = 246$ GeV is the Higgs VEV, $a \equiv y_1 v_\chi v^2 / (4\Lambda\Lambda_W)$ and $b \equiv y_2 v^2 / (2\Lambda_W)$. It is straightforward to check that the lepton mass matrices M_l and M_ν satisfy the Z_3 and Z_2 , respectively,

$$\mathcal{T} M_l M_l^\dagger \mathcal{T}^\dagger = M_l M_l^\dagger, \quad \mathcal{S} M_\nu \mathcal{S}^T = M_\nu. \quad (9)$$

They are consistent with the residual symmetries satisfied by the flavon VEVs in Eq. (6). The charged lepton mass matrix M_l is diagonal and the neutrino mass matrix M_ν is diagonalised by the unitary matrix

$$U_{\text{TBM}} = \begin{pmatrix} \frac{2}{\sqrt{6}} & \frac{1}{\sqrt{3}} & 0 \\ -\frac{1}{\sqrt{6}} & \frac{1}{\sqrt{3}} & \frac{1}{\sqrt{2}} \\ -\frac{1}{\sqrt{6}} & \frac{1}{\sqrt{3}} & -\frac{1}{\sqrt{2}} \end{pmatrix} \quad (10)$$

and has eigenvalues $m_1 = |3a + b|$, $m_2 = |b|$ and $m_3 = |3a - b|$. The mixing matrix is identical to U_{TBM} . This is the so-called TBM mixing pattern, from which we obtain $\sin \theta_{13} = 0$, $\sin \theta_{12} = 1/\sqrt{3}$ and $\sin \theta_{23} = 1/\sqrt{2}$. We conclude how to realise TBM from A_4 in the sketch shown in Figure 1.

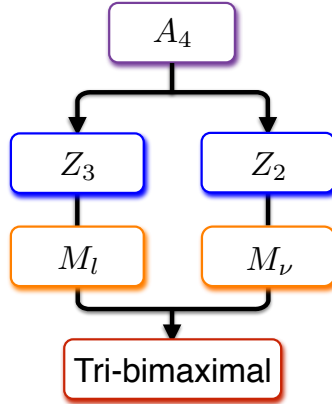


Figure 1: A sketch showing how the TBM mixing is generated in A_4 models. After A_4 is broken, residual symmetries (Z_3 in the charged lepton sector and Z_2 in the neutrino sector) are preserved. These symmetries constrain charged lepton and neutrino mass matrices, respectively and finally result in the TBM mixing. The residual symmetries are just approximate symmetries in the model. Besides, there may be additional accidental symmetries in the model, which are not shown here.

The TBM mixing should be only considered as leading order result since it is not consistent with neutrino oscillation data. Deviations from TBM have to be included in flavour model construction. The deviations are usually obtained from certain subleading interactions which break the Z_3 or Z_2 residual symmetries. It is crucial to obtain suitable deviations which are all compatible with current data (For

very recent A_4 models consistent with current oscillation data, see, e.g., [51, 52] and references therein). These deviations may contribute to NSIs as subleading effects. However, there are various of successful flavour models, and the deviations are usually model-dependent. In addition, these subleading effects are negligible in current NSI measurements. Therefore, we will not consider small corrections to NSIs resulted from small deviations from the TBM mixing.

3 NSI textures predicted by flavour symmetries in EFT

In neutrino oscillation experiments, NSIs may appear in processes of neutrino production at the source, propagation in matter and detection at the detector. The matter-effect NSIs are customarily described by a 3×3 Hermitian matrix ϵ added to an effective Hamiltonian H in the flavour basis,

$$H = \frac{1}{2E} \left\{ U \begin{pmatrix} 0 & 0 & 0 \\ 0 & \Delta m_{21}^2 & 0 \\ 0 & 0 & \Delta m_{31}^2 \end{pmatrix} U^\dagger + A \begin{pmatrix} 1 & 0 & 0 \\ 0 & 0 & 0 \\ 0 & 0 & 0 \end{pmatrix} + A \begin{pmatrix} \epsilon_{ee} & \epsilon_{e\mu} & \epsilon_{e\tau} \\ \epsilon_{\mu e} & \epsilon_{\mu\mu} & \epsilon_{\mu\tau} \\ \epsilon_{\tau e} & \epsilon_{\tau\mu} & \epsilon_{\tau\tau} \end{pmatrix} \right\}, \quad (11)$$

where $\epsilon_{\alpha\beta} = \epsilon_{\beta\alpha}^*$ holds, and $A = 2\sqrt{2}G_F N_e E$ is the usual matter effect with N_e the electron number density in the Earth and E the neutrino beam energy. The effective Hamiltonian for antineutrino oscillation is obtained after the replacements $U \rightarrow U^*$, $A \rightarrow -A$ and $\epsilon_{\alpha\beta} \rightarrow \epsilon_{\alpha\beta}^*$. In this section, by assuming NSIs obtained from higher-dimensional operators, we embed A_4 or its residual symmetry Z_2 to these operators and systematically analyse how to obtain NSI textures from the symmetry.

3.1 NSIs from higher-dimensional operators

We assume that NSIs arise from effective higher-dimensional operators and these operators satisfy the following conditions.

- Lorentz invariance and the SM gauge symmetry $SU(2)_L \times U(1)_Y$ around or above the electroweak scale are required.
- Since neutrino oscillation experiments cannot test lepton-number-violating (LNV) or baryon-number-violating (BNV) processes, we select lepton- and baryon-number-conserving operatorsⁱⁱ.
- We will only focus on operators in which the number of fermions is 4. The simplest operators have the dimension $d = 6$, and the operators with $d > 6$ are formed by 4 fermions and $d - 6$ Higgsⁱⁱⁱ. In the following, we briefly denote the rest SM fermion contents as

$$E_R = (e_R, \mu_R, \tau_R)^T, \quad U_R = (u_R, c_R, t_R)^T, \quad D_R = (d_R, s_R, b_R)^T, \quad Q = (Q_1, Q_2, Q_3)^T, \quad (12)$$

where $Q_1 = (u_L, d_L)$, $Q_2 = (c_L, s_L)$, $Q_3 = (t_L, b_L)$.

- For neutrinos propagating in matter, at least two L 's must be involved in the relevant operators. As a comparison, operators for neutrino production and detection involves at least one L .

ⁱⁱThis does not mean that the lepton number or baryon number cannot be broken in the UV-complete scale, as will be discussed in the next section.

ⁱⁱⁱOperators modifying neutrino kinetic terms may also contribute to the NSIs through the non-diagonal Z mediation. These effects are small, $\lesssim 10^{-3}$, from the constraints of the PMNS non-unitarity [32, 56], and will not be our case here.

- Furthermore, we will impose one more requirement: we only consider NSIs which avoid the strong constraints from 4-charged-fermion interactions, e.g., rare lepton-flavour-violating decays of leptons and hadrons. Since left-handed charged leptons and neutrinos belong to the same electroweak doublet in the SM, any NSI effects from higher-dimensional operators are related to an interaction involving at least one charged lepton. Once all final and initial states of the latter interaction are electrically charged fermions, i.e., charged leptons and quarks, the operator and the relevant NSI parameters should have been strongly constrained by these “visible” processes. For example, the non-standard $\nu_\mu + (e, u, d) \rightarrow \nu_e + (e, u, d)$ propagation in matter may be constrained by $\mu + (e, u, d) \rightarrow e + (e, u, d)$ in the CLFV measurement.

The following classes of operators and their conjugates are allowed by the first four requirements,

$$\bar{L}E_R\bar{D}_RQ, \bar{L}E_R\bar{Q}U_R, \bar{L}L\bar{F}F \text{ with } F = L, E_R, Q, U_R, D_R \quad (13)$$

for $d = 6$ and

$$\begin{aligned} &\bar{L}L\bar{D}_R\bar{U}_RH^*H^*, \bar{L}E_R\bar{U}_RQH, \bar{L}E_R\bar{Q}D_RHH, \bar{L}E_R\bar{L}E_RHH, \\ &\bar{L}E_R\bar{D}_RQH^*H, \bar{L}E_R\bar{Q}U_RH^*H, \bar{L}L\bar{F}FH^*H \text{ with } F = L, E_R, Q, U_R, D_R \end{aligned} \quad (14)$$

for $d = 8$. Here we have not written out the necessary Γ matrices, gauge indices and flavour indices. The lepton and baryon number conservations forbid any dimension-7 operators involving 4 fermions. After the Higgs gets the VEV $\langle H \rangle = (0, 1)^T(2\sqrt{2}G_F)^{-1/2}$, these operators classified into two types, those preserving electroweak symmetry and those not. Taking the last requirement into account, we extract the following operators:

- The first class are explicitly given by

$$\varepsilon_{ac}\varepsilon_{bd}(\bar{L}_{a\alpha}\gamma^\mu L_{b\beta})(\bar{L}_{c\gamma}\gamma_\mu L_{d\delta}), \quad \varepsilon_{ac}\varepsilon_{bd}(\bar{L}_{a\alpha}\gamma^\mu L_{b\beta})(\bar{L}_{c\gamma}\gamma_\mu L_{d\delta})H^\dagger H, \quad (15)$$

where $\alpha, \beta, \gamma, \delta = 1, 2, 3$ are flavour indices, $a, b, c, d = 1, 2$ are $SU(2)_L$ doublet indices, and non-vanishing entries of ε_{ab} are given by $\varepsilon_{12} = -\varepsilon_{21} = 1$. Specifically, we denote the flavour indices in the lepton sector as $(1, 2, 3) = (e, \mu, \tau)$. Using the relation $\varepsilon_{ac}\varepsilon_{cd} = \delta_{ab}\delta_{cd} - \delta_{ad}\delta_{bc}$ and the Fierz identity, we expand the first term of the above equation and obtain $(\bar{L}_{a\alpha}\gamma^\mu L_{a\beta})(\bar{L}_{c\gamma}\gamma_\mu L_{c\delta}) - (\bar{L}_{a\alpha}\gamma^\mu L_{a\delta})(\bar{L}_{c\gamma}\gamma_\mu L_{c\beta})$, i.e.,

$$(\bar{\nu}_{\alpha L}\gamma^\mu \nu_{\beta L})(\bar{E}_{\gamma L}\gamma_\mu E_{\delta L}) + (\bar{\nu}_{\gamma L}\gamma^\mu \nu_{\delta L})(\bar{E}_{\alpha L}\gamma_\mu E_{\beta L}) - (\bar{\nu}_{\alpha L}\gamma^\mu \nu_{\delta L})(\bar{E}_{\gamma L}\gamma_\mu E_{\beta L}) - (\bar{\nu}_{\gamma L}\gamma^\mu \nu_{\beta L})(\bar{E}_{\alpha L}\gamma_\mu E_{\delta L}), \quad (16)$$

which we denote as $\mathcal{O}_{\alpha\beta\gamma\delta}^1$. Note that $\mathcal{O}_{\alpha\beta\gamma\delta}^1 = -\mathcal{O}_{\gamma\beta\alpha\delta}^1 = -\mathcal{O}_{\alpha\delta\gamma\beta}^1 = \mathcal{O}_{\gamma\delta\alpha\beta}^1$ is satisfied. This term can lead to NSIs of neutrino interacting with the electron $\nu_\alpha e \rightarrow \nu_\beta e$ during the neutrino propagation, but have no influence on 4-charged-lepton interactions such as the scattering $\mu e \rightarrow ee$ or the rare decay $\mu \rightarrow eee$, and thus are not directly constrained by the latter. The second term in Eq. (15) gives no more information than $\mathcal{O}_{\alpha\beta\gamma\delta}^1$, which is not necessary to be considered separately.

- The second class of operators are:

$$\begin{aligned} &(\bar{L}_\alpha\tilde{H}\gamma^\mu\tilde{H}^\dagger L_\beta)(\bar{U}_{\gamma R}\gamma_\mu U_{\delta R}), (\bar{L}_\alpha\tilde{H}\gamma^\mu\tilde{H}^\dagger L_\beta)(\bar{D}_{\gamma R}\gamma_\mu D_{\delta R}), (\bar{L}_\alpha\tilde{H}\gamma^\mu\tilde{H}^\dagger L_\beta)(\bar{E}_{\gamma R}\gamma_\mu E_{\delta R}), \\ &(\bar{L}_\alpha\tilde{H}\gamma^\mu\tilde{H}^\dagger L_\beta)(\bar{Q}_{\gamma R}\gamma_\mu Q_{\delta R}), (\bar{L}_\alpha\tilde{H}\gamma^\mu\tilde{H}^\dagger L_\beta)(\bar{L}_{\gamma R}\gamma_\mu L_{\delta R}), \\ &(\bar{L}_\alpha\tilde{H}\gamma^\mu L_{b\beta})(\bar{Q}_{b\gamma}\gamma_\mu\tilde{H}^\dagger Q_\delta), \varepsilon_{bc}(\bar{L}_\alpha\tilde{H}\gamma^\mu L_{b\beta})(\bar{Q}_{\gamma R}\gamma_\mu Q_{c\delta}), \\ &(\bar{L}_\alpha\tilde{H}\gamma^\mu H^\dagger L_\beta)(\bar{D}_{\gamma R}\gamma_\mu U_{\delta R}), (\bar{L}_\alpha\tilde{H}\sigma^{\mu\nu} E_{\beta R})(\bar{Q}_{\gamma R}H\sigma_{\mu\nu} U_{\delta R}), \\ &(\bar{L}_\alpha\tilde{H}E_{\beta R})(\bar{D}_{\gamma R}\tilde{H}^\dagger Q_\delta), (\bar{L}_\alpha\tilde{H}E_{\beta R})(\bar{Q}_{\gamma R}HU_{\delta R}). \end{aligned} \quad (17)$$

After the Higgs gets the VEV, the above operators are effectively reduced to 11 four-fermion interactions,

$$\begin{aligned}
& (\overline{\nu_{\alpha L}} \gamma^\mu \nu_{\beta L})(\overline{U_{\gamma R}} \gamma_\mu U_{\delta R}), (\overline{\nu_{\alpha L}} \gamma^\mu \nu_{\beta L})(\overline{D_{\gamma R}} \gamma_\mu D_{\delta R}), (\overline{\nu_{\alpha L}} \gamma^\mu \nu_{\beta L})(\overline{E_{\gamma R}} \gamma_\mu E_{\delta R}), \\
& (\overline{\nu_{\alpha L}} \gamma^\mu \nu_{\beta L})(\overline{U_{\gamma L}} \gamma_\mu U_{\delta L} + \overline{D_{\gamma L}} \gamma_\mu D_{\delta L}), (\overline{\nu_{\alpha L}} \gamma^\mu \nu_{\beta L})(\overline{\nu_{\gamma L}} \gamma_\mu \nu_{\delta L} + \overline{E_{\gamma L}} \gamma_\mu E_{\delta L}), \\
& (\overline{\nu_{\alpha L}} \gamma^\mu \nu_{\beta L})(\overline{U_{\gamma L}} \gamma_\mu U_{\delta L}) + (\overline{\nu_{\alpha L}} \gamma^\mu E_{\beta L})(\overline{D_{\gamma L}} \gamma_\mu U_{\delta L}), (\overline{\nu_{\alpha L}} \gamma^\mu \nu_{\beta L})(\overline{D_{\gamma L}} \gamma_\mu D_{\delta L}) - (\overline{\nu_{\alpha L}} \gamma^\mu E_{\beta L})(\overline{D_{\gamma L}} \gamma_\mu U_{\delta L}), \\
& (\overline{\nu_{\alpha L}} \gamma^\mu E_{\beta L})(\overline{D_{\gamma R}} \gamma_\mu U_{\delta R}), (\overline{\nu_{\alpha L}} \sigma^{\mu\nu} E_{\beta R})(\overline{D_{\gamma L}} \sigma_{\mu\nu} U_{\delta R}), \\
& (\overline{\nu_{\alpha L}} E_{\beta R})(\overline{D_{\gamma R}} U_{\delta L}), (\overline{\nu_{\alpha L}} E_{\beta R})(\overline{D_{\gamma L}} U_{\delta R}).
\end{aligned} \tag{18}$$

In the above operators, the first 5 terms, denoted by $\mathcal{O}_{\alpha\beta\gamma\delta}^{2,3,4,5,6}$, respectively, contribute to NSIs in matter during neutrino propagation. The next 2 terms, denoted by $\mathcal{O}_{\alpha\beta\gamma\delta}^{7,8}$, contribute to both NSIs at the neutrino source and detector, and NSIs for neutrino mediation in matter, and correlate them together. And the final 4 terms, denoted by $\mathcal{O}_{\alpha\beta\gamma\delta}^{9,10,11,12}$, respectively, contribute to NSIs in the neutrino production and detection processes. For more discussions on textures of NSIs in these processes, please see appendix B.

Label	Before EW breaking	After EW breaking	observation
\mathcal{O}^1	$\varepsilon_{ac}\varepsilon_{bd}(\overline{L_{a\alpha}}\gamma^\mu L_{b\beta})(\overline{L_{c\gamma}}\gamma_\mu L_{d\delta}),$ $\varepsilon_{ac}\varepsilon_{bd}(\overline{L_{a\alpha}}\gamma^\mu L_{b\beta})(\overline{L_{c\gamma}}\gamma_\mu L_{d\delta})H^\dagger H$	$(\overline{\nu_{\alpha L}}\gamma^\mu \nu_{\beta L})(\overline{E_{\gamma L}}\gamma_\mu E_{\delta L}) + (\overline{\nu_{\gamma L}}\gamma^\mu \nu_{\delta L})(\overline{E_{\alpha L}}\gamma_\mu E_{\beta L})$ $-(\overline{\nu_{\alpha L}}\gamma^\mu \nu_{\delta L})(\overline{E_{\gamma L}}\gamma_\mu E_{\beta L}) - (\overline{\nu_{\gamma L}}\gamma^\mu \nu_{\beta L})(\overline{E_{\alpha L}}\gamma_\mu E_{\delta L})$	M
\mathcal{O}^2	$(\overline{L_{\alpha}}\tilde{H}\gamma^\mu \tilde{H}^\dagger L_{\beta})(\overline{U_{\gamma R}}\gamma_\mu U_{\delta R})$	$(\overline{\nu_{\alpha L}}\gamma^\mu \nu_{\beta L})(\overline{U_{\gamma R}}\gamma_\mu U_{\delta R})$	M
\mathcal{O}^3	$(\overline{L_{\alpha}}\tilde{H}\gamma^\mu \tilde{H}^\dagger L_{\beta})(\overline{D_{\gamma R}}\gamma_\mu D_{\delta R})$	$(\overline{\nu_{\alpha L}}\gamma^\mu \nu_{\beta L})(\overline{D_{\gamma R}}\gamma_\mu D_{\delta R})$	M
\mathcal{O}^4	$(\overline{L_{\alpha}}\tilde{H}\gamma^\mu \tilde{H}^\dagger L_{\beta})(\overline{E_{\gamma R}}\gamma_\mu E_{\delta R})$	$(\overline{\nu_{\alpha L}}\gamma^\mu \nu_{\beta L})(\overline{E_{\gamma R}}\gamma_\mu E_{\delta R})$	M
\mathcal{O}^5	$(\overline{L_{\alpha}}\tilde{H}\gamma^\mu \tilde{H}^\dagger L_{\beta})(\overline{Q_{\gamma}}\gamma_\mu Q_{\delta})$	$(\overline{\nu_{\alpha L}}\gamma^\mu \nu_{\beta L})(\overline{U_{\gamma L}}\gamma_\mu U_{\delta L} + \overline{D_{\gamma L}}\gamma_\mu D_{\delta L})$	M
\mathcal{O}^6	$(\overline{L_{\alpha}}\tilde{H}\gamma^\mu \tilde{H}^\dagger L_{\beta})(\overline{L_{\gamma}}\gamma_\mu L_{\delta})$	$(\overline{\nu_{\alpha L}}\gamma^\mu \nu_{\beta L})(\overline{\nu_{\gamma L}}\gamma_\mu \nu_{\delta L} + \overline{E_{\gamma L}}\gamma_\mu E_{\delta L})$	M
\mathcal{O}^7	$(\overline{L_{\alpha}}\tilde{H}\gamma^\mu L_{b\beta})(\overline{Q_{b\gamma}}\gamma_\mu \tilde{H}^\dagger Q_{\delta})$	$(\overline{\nu_{\alpha L}}\gamma^\mu \nu_{\beta L})(\overline{U_{\gamma L}}\gamma_\mu U_{\delta L}) + (\overline{\nu_{\alpha L}}\gamma^\mu E_{\beta L})(\overline{D_{\gamma L}}\gamma_\mu U_{\delta L})$	S,M,D
\mathcal{O}^8	$\varepsilon_{bc}(\overline{L_{\alpha}}\tilde{H}\gamma^\mu L_{b\beta})(\overline{Q_{\gamma}}\gamma_\mu Q_{c\delta})$	$(\overline{\nu_{\alpha L}}\gamma^\mu \nu_{\beta L})(\overline{D_{\gamma L}}\gamma_\mu D_{\delta L}) - (\overline{\nu_{\alpha L}}\gamma^\mu E_{\beta L})(\overline{D_{\gamma L}}\gamma_\mu U_{\delta L})$	S,M,D
\mathcal{O}^9	$\varepsilon_{bc}(\overline{L_{\alpha}}\tilde{H}\gamma^\mu L_{b\beta})(\overline{Q_{\gamma}}\gamma_\mu Q_{c\delta})$	$(\overline{\nu_{\alpha L}}\gamma^\mu E_{\beta L})(\overline{D_{\gamma R}}\gamma_\mu U_{\delta R})$	S,D
\mathcal{O}^{10}	$(\overline{L_{\alpha}}\tilde{H}\sigma^{\mu\nu} E_{\beta R})(\overline{Q_{\gamma}}\gamma_\mu \sigma_{\mu\nu} U_{\delta R})$	$(\overline{\nu_{\alpha L}}\sigma^{\mu\nu} E_{\beta R})(\overline{D_{\gamma L}}\sigma_{\mu\nu} U_{\delta R})$	S,D
\mathcal{O}^{11}	$(\overline{L_{\alpha}}\tilde{H}E_{\beta R})(\overline{D_{\gamma R}}\tilde{H}^\dagger Q_{\delta})$	$(\overline{\nu_{\alpha L}}E_{\beta R})(\overline{D_{\gamma R}}U_{\delta L})$	S,D
\mathcal{O}^{12}	$(\overline{L_{\alpha}}\tilde{H}E_{\beta R})(\overline{Q_{\gamma}}\tilde{H}U_{\delta R})$	$(\overline{\nu_{\alpha L}}E_{\beta R})(\overline{D_{\gamma L}}U_{\delta R})$	S,D

Table 1: Higher-dimensional operators ($d \leq 8$) which may contribute to NSIs in neutrino oscillation experiments. S, M, and D represent NSIs at a source, in matter and at a detector, respectively.

The effective operators describing neutrino NSIs for neutrino propagation can be expressed as

$$\mathcal{L}_{\text{NSI}} = 2\sqrt{2}G_F \sum_{p=1}^8 c_{\alpha\beta\gamma\delta}^p \mathcal{O}_{\alpha\beta\gamma\delta}^p + \text{h.c.}, \tag{19}$$

where two same flavour indices should be summed. Operators in Eqs. (16) and (18) form a full list of NSI operators with $d \leq 8$ before electroweak symmetry breaking. We have checked that all the other NSIs with $d \leq 8$ operators can be represented as a linear combination of these $\mathcal{O}_{\alpha\beta\gamma\delta}^p$. Matching with the effective NSI matrix ϵ in Eq. (11), we obtain

$$\epsilon_{\alpha\beta} = \epsilon_{\alpha\beta}^e + \left(2 + \frac{N_n}{N_e}\right) \epsilon_{\alpha\beta}^u + \left(1 + 2\frac{N_n}{N_e}\right) \epsilon_{\alpha\beta}^d \tag{20}$$

with N_n the neutron number density and

$$\begin{aligned}\epsilon_{\alpha\beta}^e &= c_{\alpha\beta 11}^1 + c_{\alpha\beta 11}^4 + c_{\alpha\beta 11}^6, \\ \epsilon_{\alpha\beta}^u &= c_{\alpha\beta 11}^2 + c_{\alpha\beta 11}^5 + c_{\alpha\beta 11}^7, \\ \epsilon_{\alpha\beta}^d &= c_{\alpha\beta 11}^3 + c_{\alpha\beta 11}^5 + c_{\alpha\beta 11}^8.\end{aligned}\tag{21}$$

For $\mathcal{O}_{\alpha\beta\gamma\delta}^1$, it is easy to confirm $c_{\alpha\beta\gamma\delta}^1 = -c_{\gamma\beta\alpha\delta}^1 = c_{\alpha\delta\gamma\beta}^1$, and thus $c_{e\beta 11}^1$ and $c_{ae 11}^1$ always vanish. Therefore, $\mathcal{O}_{\alpha\beta\gamma\delta}^1$ will not contribute to the first column or first row of ϵ .

3.2 NSI textures predicted by A_4

We consider how neutrino NSIs from the higher-dimensional operators are constrained by A_4 . We require that the higher-dimensional operators are invariant under the symmetry A_4 and consider which kinds of NSI textures we could gain from the symmetry. As we only care about matter-effect NSI textures, we limit our discussion in the operators \mathcal{O}^{1-8} . In appendix B, we list the NSI textures at the source and detector from the operators \mathcal{O}^{7-12} .

We follow Section 2 in which the lepton doublets $L = (L_1, L_2, L_3)^T$ are often arranged as a triplet **3** of A_4 ^{iv}. Besides, we do not specify the representations for the other fermions in the flavour space. In other words, the right-handed charged leptons, left-handed quarks and right-handed quarks could be any irreducible representations of A_4 , **1**, **1'**, **1''** or **3**. It is worth noting that we do not specify if A_4 can be responsible for the quark mixing in this work. If all quarks are arranged as the singlet representation **1**, quark flavour mixing is totally independent of A_4 . We scan for all these possibilities, and find the following NSI textures:

$$\mathbb{T}_{11} \equiv \mathbb{1} = \begin{pmatrix} 1 & 0 & 0 \\ 0 & 1 & 0 \\ 0 & 0 & 1 \end{pmatrix}, \quad \mathbb{T}_{12} = \begin{pmatrix} 2 & 0 & 0 \\ 0 & -1 & 0 \\ 0 & 0 & -1 \end{pmatrix}, \quad \mathbb{T}_{13} = \begin{pmatrix} 0 & 0 & 0 \\ 0 & 1 & 0 \\ 0 & 0 & -1 \end{pmatrix}.\tag{22}$$

In the following, we explain how to get these textures.

The first operator $c_{\alpha\beta\gamma\delta}^1 \mathcal{O}_{\alpha\beta\gamma\delta}^1$, i.e., the dimension-6 $\varepsilon_{ac}\varepsilon_{bd}c_{\alpha\beta\gamma\delta}^1(\overline{L}_{a\alpha}\gamma^\mu L_{b\beta})(\overline{L}_{c\gamma}\gamma_\mu L_{d\delta})$, satisfy the anti-permutation property of two L 's and two \overline{L} 's, as shown in Eq. (16), which results in $c_{e\beta 11}^1 = c_{ae 11}^1 = 0$. There are 5 independent A_4 -invariant operators:

$$(\overline{L}L)_{\mathbf{1}}(\overline{L}L)_{\mathbf{1}}, (\overline{L}L)_{\mathbf{1}'}(\overline{L}L)_{\mathbf{1}''}, (\overline{L}L)_{\mathbf{3}_S}(\overline{L}L)_{\mathbf{3}_S}, (\overline{L}L)_{\mathbf{3}_A}(\overline{L}L)_{\mathbf{3}_A}, (\overline{L}L)_{\mathbf{3}_S}(\overline{L}L)_{\mathbf{3}_A}.\tag{23}$$

Here, we have ignored the unnecessary flavour-independent notations, including the $SU(2)_L$ indices, Γ matrices and the Higgs field. The representations in the subscripts are understood as in Eq. (4). Taking account of the CG coefficients in Eq. (4), we obtain

$$c_{\mu\mu 11}^1 = c_{\tau\tau 11}^1, \quad c_{ee 11}^1 = c_{\alpha\beta 11}^1 = 0 \text{ for } \alpha \neq \beta\tag{24}$$

for the first 4 operators which lead to the NSI texture

$$\mathbb{T}'_{12} \equiv \begin{pmatrix} 0 & 0 & 0 \\ 0 & 1 & 0 \\ 0 & 0 & 1 \end{pmatrix} \propto 2\mathbb{T}_{11} - \mathbb{T}_{12}.\tag{25}$$

^{iv}In the AF basis, the conjugate of L should be arranged as $\overline{L} = (\overline{L}_1, \overline{L}_3, \overline{L}_2)^T$.

The last operator gives vanishing $c_{\alpha\beta 11}^1$ and thus does not contribute to NSIs.

For the second one in Table 1, $c_{\alpha\beta\gamma\delta}^2 \mathcal{O}_{\alpha\beta\gamma\delta}^2$, i.e., the dimension-8 $(\bar{L}_\alpha \tilde{H} \gamma^\mu \tilde{H}^\dagger L_\beta)(\bar{U}_{\gamma R} \gamma_\mu U_{\delta R})$, the A_4 -invariant operators depend on the flavour representation of U_R :

- If U_{1R} is arranged to be a singlet $\mathbf{1}^{(\prime\prime)}$ of A_4 , there is only one A_4 -invariant operator

$$(\bar{L}L)_1(\bar{U}_{1R}U_{1R})_1. \quad (26)$$

It leads to the relation of the coefficients

$$c_{ee11}^2 = c_{\mu\mu 11}^2 = c_{\tau\tau 11}^2, \quad c_{\alpha\beta 11}^2 = 0 \text{ for } \alpha \neq \beta. \quad (27)$$

Representations of U_{2R} and U_{3R} are irrelevant for our discussion since U_{2R} and U_{3R} do not attend to the low energy NSIs.

- If $U_R = (U_{1R}, U_{2R}, U_{3R})^T$ is a triplet $\mathbf{3}$ of A_4 , there are 7 independent A_4 -invariant operators

$$\begin{aligned} &(\bar{L}L)_1(\bar{U}_R U_R)_1, (\bar{L}L)_{1'}(\bar{U}_R U_R)_{1''}, (\bar{L}L)_{1''}(\bar{U}_R U_R)_{1'}, \\ &(\bar{L}L)_{3_S}(\bar{U}_R U_R)_{3_S}, (\bar{L}L)_{3_A}(\bar{U}_R U_R)_{3_S}, (\bar{L}L)_{3_S}(\bar{U}_R U_R)_{3_A}, (\bar{L}L)_{3_A}(\bar{U}_R U_R)_{3_A}. \end{aligned} \quad (28)$$

The first operator gives the same correlation as in Eq. (27), $(\bar{L}L)_{3_S}(\bar{U}_R U_R)_{3_S}$ and $(\bar{L}L)_{3_A}(\bar{U}_R U_R)_{3_S}$ give rise to

$$\begin{aligned} c_{ee11}^2 &= -2c_{\mu\mu 11}^2 = -2c_{\tau\tau 11}^2, \quad c_{\alpha\beta 11}^2 = 0 \text{ for } \alpha \neq \beta; \\ c_{\mu\mu 11}^2 &= -c_{\tau\tau 11}^2, \quad c_{ee11}^2 = c_{\alpha\beta 11}^2 = 0 \text{ for } \alpha \neq \beta, \end{aligned} \quad (29)$$

respectively, where all non-vanishing values are real. The rest, $(\bar{L}L)_{1'}(\bar{U}_R U_R)_{1''}$, $(\bar{L}L)_{1''}(\bar{U}_R U_R)_{1'}$, $(\bar{L}L)_{3_S}(\bar{U}_R U_R)_{3_A}$, and $(\bar{L}L)_{3_A}(\bar{U}_R U_R)_{3_S}$ have no contribution to $c_{\alpha\beta 11}^2$.

The correlations of the coefficients $c_{\alpha\beta 11}^2$ directly determine the flavour structure of matter-effect NSIs. In detail, Eq. (27) directly gives rise to \mathbb{T}_{11} , and Eq. (29) leads to \mathbb{T}_{12} and \mathbb{T}_{13} . The discussion of $\mathcal{O}_{\alpha\beta\gamma\delta}^2$ applies to $\mathcal{O}_{\alpha\beta\gamma\delta}^{3-8}$. In other words, the NSI textures \mathbb{T}_{11} , \mathbb{T}_{12} and \mathbb{T}_{13} can be derived from

$$(\bar{L}L)_1(\bar{F}F)_1, (\bar{L}L)_{3_S}(\bar{F}F)_{3_S}, (\bar{L}L)_{3_A}(\bar{F}F)_{3_S}, \quad (30)$$

respectively, where F represents any fermions in the SM.

3.3 NSI textures predicted by the residual symmetry of A_4

In order to break A_4 and obtain residual symmetries, we include the flavon VEV in the NSI operators. We consider that the operators $c_{\alpha\beta\gamma\delta}^p \mathcal{O}_{\alpha\beta\gamma\delta}^p$ are effectively realised via^v

$$c_{\alpha'\alpha\beta\gamma\delta}^{\varphi,p} \frac{\varphi_{\alpha'}}{v_\varphi} \mathcal{O}_{\alpha\beta\gamma\delta}^p \quad \text{or} \quad c_{\alpha'\alpha\beta\gamma\delta}^{\chi,p} \frac{\chi_{\alpha'}}{v_\chi} \mathcal{O}_{\alpha\beta\gamma\delta}^p. \quad (31)$$

These operators are A_4 -invariant before flavons get VEVs. Taking the VEVs in Eq. (7), we obtain $c_{\alpha\beta\gamma\delta}^p \mathcal{O}_{\alpha\beta\gamma\delta}^p$ with

$$c_{\alpha\beta\gamma\delta}^p = c_{1\alpha\beta\gamma\delta}^{\varphi,p} \quad \text{or} \quad c_{1\alpha\beta\gamma\delta}^{\chi,p} + c_{2\alpha\beta\gamma\delta}^{\chi,p} + c_{3\alpha\beta\gamma\delta}^{\chi,p}. \quad (32)$$

^vSince the conjugates of φ and χ are identical with φ and χ , respectively, it is not necessary to write out operators realised by φ^* or χ^* separately.

They are not A_4 -invariant any more, but preserves only a Z_3 or Z_2 symmetry, since φ and χ preserve Z_3 and Z_2 symmetries, respectively. The Z_3 -invariant operators $\varphi\mathcal{O}$ will not give nothing new, but Eq. (22). The reason is that the generator of Z_3 , \mathcal{T} , is diagonal, and the predicted NSI textures must be also diagonal. In the following, we will not consider the Z_3 -invariant operator $\varphi\mathcal{O}$ anymore.

Now we focus on the A_4 -breaking Z_2 -invariant operators $\chi\mathcal{O}$. We first define the following non-diagonal textures:

$$\begin{aligned}\mathbb{T}_{21} &= \begin{pmatrix} 0 & 1 & 1 \\ 1 & 0 & 1 \\ 1 & 1 & 0 \end{pmatrix}, & \mathbb{T}_{22} &= \begin{pmatrix} 0 & -1 & -1 \\ -1 & 0 & 2 \\ -1 & 2 & 0 \end{pmatrix}, & \mathbb{T}_{23} &= \begin{pmatrix} 0 & -1 & 1 \\ -1 & 0 & 0 \\ 1 & 0 & 0 \end{pmatrix}, \\ \mathbb{T}_{31} &= \begin{pmatrix} 0 & -i & i \\ i & 0 & -i \\ -i & i & 0 \end{pmatrix}, & \mathbb{T}_{32} &= \begin{pmatrix} 0 & i & -i \\ -i & 0 & -2i \\ i & 2i & 0 \end{pmatrix}, & \mathbb{T}_{33} &= \begin{pmatrix} 0 & i & i \\ -i & 0 & 0 \\ -i & 0 & 0 \end{pmatrix}.\end{aligned}\quad (33)$$

\mathbb{T}_{2n} represent non-diagonal real NSI textures, while \mathbb{T}_{3n} represent pure imaginary NSI textures.

For $c_{\alpha'\alpha\beta\gamma\delta}^{\chi,1}\chi_{\alpha'}\mathcal{O}_{\alpha\beta\gamma\delta}^1$, there are 9 Z_2 -invariant operators that can contribute to NSIs:

$$\begin{aligned}&\chi(\bar{L}L)_{\mathbf{3}_S}(\bar{L}L)_{\mathbf{1}}, \chi(\bar{L}L)_{\mathbf{3}_S}(\bar{L}L)_{\mathbf{1}'}, \chi(\bar{L}L)_{\mathbf{3}_S}(\bar{L}L)_{\mathbf{1}''}, \\&\chi(\bar{L}L)_{\mathbf{3}_A}(\bar{L}L)_{\mathbf{1}}, \chi(\bar{L}L)_{\mathbf{3}_A}(\bar{L}L)_{\mathbf{1}'}, \chi(\bar{L}L)_{\mathbf{3}_A}(\bar{L}L)_{\mathbf{1}''}, \\&\chi((\bar{L}L)_{\mathbf{3}_S}(\bar{L}L)_{\mathbf{3}_S})_{\mathbf{3}_S}, \chi((\bar{L}L)_{\mathbf{3}_A}(\bar{L}L)_{\mathbf{3}_A})_{\mathbf{3}_S}, \\&\chi((\bar{L}L)_{\mathbf{3}_S}(\bar{L}L)_{\mathbf{3}_A})_{\mathbf{3}_S}, \chi((\bar{L}L)_{\mathbf{3}_S}(\bar{L}L)_{\mathbf{3}_A})_{\mathbf{3}_A}.\end{aligned}\quad (34)$$

Due to the antisymmetric property between α and γ and that between β and δ , $c_{e\beta 11}^1 = c_{ae 11}^1 = 0$ for all cases. The other coefficients satisfy the following relations, respectively. Taking the CG coefficients in Eq. (4) into account, we obtain

$$2c_{\mu\mu 11}^1 = 2c_{\tau\tau 11}^1 = c_{\mu\tau 11}^1 = c_{\tau\mu 11}^1 \quad (35)$$

for $\chi((\bar{L}L)_{\mathbf{3}_S}(\bar{L}L)_{\mathbf{1},\mathbf{1}',\mathbf{1}''})_{\mathbf{3}}$, $\chi((\bar{L}L)_{\mathbf{3}_S}(\bar{L}L)_{\mathbf{3}_S})_{\mathbf{3}_S}$, $\chi((\bar{L}L)_{\mathbf{3}_A}(\bar{L}L)_{\mathbf{3}_A})_{\mathbf{3}_S}$ and

$$c_{\mu\mu 11}^1 = -c_{\tau\tau 11}^1, \quad c_{\mu\tau 11}^1 = c_{\tau\mu 11}^1 = 0 \quad (36)$$

for $\chi((\bar{L}L)_{\mathbf{3}_A}(\bar{L}L)_{\mathbf{1},\mathbf{1}',\mathbf{1}''})_{\mathbf{3}}$, $\chi((\bar{L}L)_{\mathbf{3}_S}(\bar{L}L)_{\mathbf{3}_A})_{\mathbf{3}_S}$, $\chi((\bar{L}L)_{\mathbf{3}_S}(\bar{L}L)_{\mathbf{3}_A})_{\mathbf{3}_A}$. The first two relations give

$$\frac{1}{3}(2\mathbb{T}_{11} - \mathbb{T}_{12} + 2\mathbb{T}_{21} + 2\mathbb{T}_{23}) = \begin{pmatrix} 0 & 0 & 0 \\ 0 & 1 & 2 \\ 0 & 2 & 1 \end{pmatrix} \quad (37)$$

and \mathbb{T}_{13} , respectively.

For $c_{\alpha'\alpha\beta\gamma\delta}^{\chi,2}\chi_{\alpha'}\mathcal{O}_{\alpha\beta\gamma\delta}^2$, i.e., the first dimension-8 operator $(\bar{L}_\alpha\tilde{H}\gamma^\mu\tilde{H}^\dagger L_\beta)(\bar{U}_{\gamma R}\gamma_\mu U_{\delta R})$, depending on the representation of U_R , there are several Z_2 -invariant operators:

- If U_{1R} is a trivial singlet $\mathbf{1}$, $\mathbf{1}'$, or $\mathbf{1}''$ of A_4 , there are two Z_2 -invariant operators

$$\chi(\bar{L}L)_{\mathbf{3}_S}(\bar{U}_{1R}U_{1R})_{\mathbf{1}}, \chi(\bar{L}L)_{\mathbf{3}_A}(\bar{U}_{1R}U_{1R})_{\mathbf{1}}. \quad (38)$$

They lead to the correlations of the coefficients

$$\begin{aligned}c_{ee 11}^2 &= c_{\mu\tau 11}^2 = c_{\tau\mu 11}^2 = -2c_{\mu\mu 11}^2 = -2c_{\tau\tau 11}^2 = -2c_{e\mu 11}^2 = -2c_{\mu e 11}^2 = -2c_{e\tau 11}^2 = -2c_{\tau e 11}^2; \\-c_{\mu\mu 11}^2 &= c_{\tau\tau 11}^2 = c_{e\mu 11}^2 = c_{\mu e 11}^2 = -c_{e\tau 11}^2 = -c_{\tau e 11}^2, \quad c_{ee 11}^2 = c_{e\tau 11}^2 = c_{\tau e 11}^2 = 0,\end{aligned}\quad (39)$$

respectively. They give rise to two textures $\mathbb{T}_2 \equiv \mathbb{T}_{12} + \mathbb{T}_{22}$ and $\mathbb{T}_3 \equiv \mathbb{T}_{13} + \mathbb{T}_{23}$, respectively.

- If U_{1R} is arranged as one component of a triplet $U_R = (U_{1R}, U_{2R}, U_{3R})^T \sim \mathbf{3}$ of A_4 , there are 6 independent Z_2 -invariant operators contributing to NSIs,

$$\begin{aligned} & \chi(\overline{LL})_{\mathbf{3}_S}(\overline{U_R}U_R)_{\mathbf{1}}, \chi(\overline{LL})_{\mathbf{3}_A}(\overline{U_R}U_R)_{\mathbf{1}}, \chi((\overline{LL})_{\mathbf{3}_S}(\overline{U_R}U_R)_{\mathbf{3}_S})_{\mathbf{3}_S}, \\ & \chi((\overline{LL})_{\mathbf{3}_S}(\overline{U_R}U_R)_{\mathbf{3}_S})_{\mathbf{3}_A}, \chi((\overline{LL})_{\mathbf{3}_A}(\overline{U_R}U_R)_{\mathbf{3}_S})_{\mathbf{3}_S}, \chi((\overline{LL})_{\mathbf{3}_A}(\overline{U_R}U_R)_{\mathbf{3}_S})_{\mathbf{3}_A}. \end{aligned} \quad (40)$$

The first two give the two correlations as in Eq. (39). The rest four give rise to

$$\begin{aligned} c_{ee11}^2 &= -2c_{\mu\mu11}^2 = -2c_{\tau\tau11}^2 = -2c_{\mu\tau11}^2 = -2c_{\tau\mu11}^2 = 4c_{e\mu11}^2 = 4c_{\mu e11}^2 = c_{e\tau11}^2 = 4c_{\tau e11}^2; \\ c_{\mu\mu11}^2 &= -c_{\tau\tau11}^2 = 2c_{e\mu11}^2 = 2c_{\mu e11}^2 = -2c_{e\tau11}^2 = 2c_{\tau e11}^2, \quad c_{ee11}^2 = c_{e\tau11}^2 = c_{\tau e11}^2 = 0; \\ ic_{\mu\tau11}^2 &= -ic_{\tau\mu11}^2 = -2ic_{e\mu11}^2 = 2ic_{\mu e11}^2 = 2ic_{e\tau11}^2 = -2ic_{\tau e11}^2, \quad c_{ee11}^2 = c_{\mu\mu11}^2 = c_{\tau\tau11}^2 = 0; \\ ic_{e\mu11}^2 &= -ic_{\mu e11}^2 = ic_{e\tau11}^2 = -ic_{\tau e11}^2, \quad c_{ee11}^2 = c_{\mu\mu11}^2 = c_{\tau\tau11}^2 = c_{\mu\tau e11}^2 = c_{\tau\mu11}^2 = 0, \end{aligned} \quad (41)$$

respectively, where all non-vanishing values are real, required by the Hermitean of the Lagrangian. They give rise to

$$2\mathbb{T}_{12} - \mathbb{T}_{22} = \begin{pmatrix} 4 & 1 & 1 \\ 1 & -2 & -2 \\ 1 & -2 & -2 \end{pmatrix}, \quad 2\mathbb{T}_{13} - \mathbb{T}_{23} = \begin{pmatrix} 0 & 1 & -1 \\ 1 & 2 & 0 \\ -1 & 0 & -2 \end{pmatrix}, \quad (42)$$

and \mathbb{T}_{32} and \mathbb{T}_{33} , respectively.

The similar discussion applies to \mathcal{O}^{3-8} and the same textures as predicted by \mathcal{O}^2 are obtained from these operators.

Nine textures \mathbb{T}_{mn} in Eqs. (22) and (33) form a complete basis for a Hermitian 3×3 matrix. Any two of these textures are orthogonal in the Hilbert-Schmidt inner product, $\text{tr}(\mathbb{T}_{mn}^\dagger \mathbb{T}_{m'n'}) \propto \delta_{mm'} \delta_{nn'}$. Matter-effect NSIs contribute to the effective Hamiltonian term via the matrix

$$\epsilon \equiv \begin{pmatrix} \epsilon_{ee} & \epsilon_{e\mu} & \epsilon_{e\tau} \\ \epsilon_{\mu e} & \epsilon_{\mu\mu} & \epsilon_{\mu\tau} \\ \epsilon_{\tau e} & \epsilon_{\tau\mu} & \epsilon_{\tau\tau} \end{pmatrix} \equiv \begin{pmatrix} \epsilon_{ee} & |\epsilon_{e\mu}|e^{i\phi_{e\mu}} & |\epsilon_{e\tau}|e^{i\phi_{e\tau}} \\ |\epsilon_{\mu e}|e^{-i\phi_{e\mu}} & \epsilon_{\mu\mu} & |\epsilon_{\mu\tau}|e^{i\phi_{\mu\tau}} \\ |\epsilon_{e\tau}|e^{-i\phi_{e\tau}} & |\epsilon_{\mu\tau}|e^{-i\phi_{\mu\tau}} & \epsilon_{\tau\tau} \end{pmatrix} = \sum_{m,n=1,2,3} \alpha_{mn} \mathbb{T}_{mn} / N_{mn}, \quad (43)$$

where N_{mn} are normalization factor $N_{11} = \sqrt{3}$, $N_{12} = \sqrt{6}$, $N_{13} = \sqrt{2}$, $N_{21} = N_{31} = \sqrt{6}$, $N_{22} = N_{32} = 2\sqrt{3}$ and $N_{23} = N_{33} = 2$. The relations between $\epsilon_{\alpha\beta}$ and α_{mn} are shown in Table 3, and the following properties are satisfied

$$\text{tr}(\epsilon\epsilon^\dagger) = \sum_{\alpha,\beta=e,\mu,\tau} |\epsilon_{\alpha\beta}|^2 = \sum_{m,n=1,2,3} \alpha_{mn}^2. \quad (44)$$

Note that $\mathbb{T}_{11} \equiv \mathbb{1}$ is unobservable in neutrino oscillations experiments.

We list all A_4 - and Z_2 -motivated matter-effect NSI textures predicted by A_4 - and Z_2 -invariant operators \mathcal{O}^p and $\chi\mathcal{O}^p$ in Table 2, where χ is the flavon VEV inducing A_4 breaking to Z_2 . As seen in the table, an NSI texture predicted by an A_4 -invariant (Z_2 -invariant) operator usually does not preserve A_4 (Z_2). This is because the matter-effect NSIs have specified the first-generation charged fermions. These charged fermions, if not arranged as a singlet $\mathbf{1}$ of A_4 , is not invariant in A_4 (Z_2), and thus the NSI texture does not respect A_4 (Z_2). In a specific A_4 model, the NSI matrix ϵ could be a linear combinations of \mathbb{T}_{mn} . However, it is notable that \mathbb{T}_{31} cannot be obtained directly from the above analysis. The analysis based on higher-dimensional operators cannot determine which texture is more important and dominant in oscillation experiments. However, as what we will discuss in the next section, once we consider UV completion for these textures and include experimental constraints, some of them are suppressed and cannot be measured in neutrino experiments.

	Representations	A_4 -invariant operators	NSI textures
\mathcal{O}^1	$L \sim \mathbf{3}$	$(\bar{L}L)_1(\bar{L}L)_1, (\bar{L}L)_{1'}(\bar{L}L)_{1''}, (\bar{L}L)_{\mathbf{3}_S}(\bar{L}L)_{\mathbf{3}_S}, (\bar{L}L)_{\mathbf{3}_A}(\bar{L}L)_{\mathbf{3}_A}$	$2\mathbb{T}_{11} - \mathbb{T}_{12}$
\mathcal{O}^{2-8}	$L \sim \mathbf{3}, F \sim \mathbf{1}, \mathbf{1}', \mathbf{1}'', \mathbf{3}$	$(\bar{L}L)_1(\bar{F}F)_1$	\mathbb{T}_{11}
	$L \sim \mathbf{3}, F \sim \mathbf{3}$	$(\bar{L}L)_{\mathbf{3}_S}(\bar{F}F)_{\mathbf{3}_S}$	\mathbb{T}_{12}
		$(\bar{L}L)_{\mathbf{3}_A}(\bar{F}F)_{\mathbf{3}_S}$	\mathbb{T}_{13}
	Representations	Z_2 -invariant operators	NSI textures
$\chi\mathcal{O}^1$	$\chi \sim \mathbf{3}, L \sim \mathbf{3}$	$\chi((\bar{L}L)_{\mathbf{3}_S}(\bar{L}L)_{\mathbf{1}, \mathbf{1}', \mathbf{1}''})_{\mathbf{3}}, \chi((\bar{L}L)_{\mathbf{3}_S}(\bar{L}L)_{\mathbf{3}_S})_{\mathbf{3}_S}, \chi((\bar{L}L)_{\mathbf{3}_A}(\bar{L}L)_{\mathbf{3}_A})_{\mathbf{3}_S}$	$\frac{1}{3}(2\mathbb{T}_{11} - \mathbb{T}_{12} + 2\mathbb{T}_{21} + 2\mathbb{T}_{23})$
		$\chi((\bar{L}L)_{\mathbf{3}_A}(\bar{L}L)_{\mathbf{1}, \mathbf{1}', \mathbf{1}''})_{\mathbf{3}}, \chi((\bar{L}L)_{\mathbf{3}_S}(\bar{L}L)_{\mathbf{3}_A})_{\mathbf{3}_S}$	\mathbb{T}_{13}
		$\chi(\bar{L}L)_{\mathbf{3}_S}(\bar{F}F)_1$	$\mathbb{T}_{12} + \mathbb{T}_{22}$
$\chi\mathcal{O}^{2-8}$	$\chi \sim \mathbf{3}, L \sim \mathbf{3}, F \sim \mathbf{1}, \mathbf{1}', \mathbf{1}'', \mathbf{3}$	$\chi(\bar{L}L)_{\mathbf{3}_A}(\bar{F}F)_1$	$\mathbb{T}_{13} + \mathbb{T}_{23}$
		$\chi((\bar{L}L)_{\mathbf{3}_S}(\bar{F}F)_{\mathbf{3}_S})_{\mathbf{3}_S}$	$2\mathbb{T}_{12} - \mathbb{T}_{22}$
	$\chi \sim \mathbf{3}, L \sim \mathbf{3}, F \sim \mathbf{3}$	$\chi((\bar{L}L)_{\mathbf{3}_A}(\bar{F}F)_{\mathbf{3}_S})_{\mathbf{3}_S}$	$2\mathbb{T}_{13} - \mathbb{T}_{23}$
		$\chi((\bar{L}L)_{\mathbf{3}_S}(\bar{F}F)_{\mathbf{3}_S})_{\mathbf{3}_A}$	\mathbb{T}_{32}
		$\chi((\bar{L}L)_{\mathbf{3}_A}(\bar{F}F)_{\mathbf{3}_S})_{\mathbf{3}_A}$	\mathbb{T}_{33}

Table 2: NSI Textures in matter predicted by A_4 and the residual symmetry Z_2 , where F represents any SM fermion. The textures \mathbb{T}_{1n} are defined in Eq. (22), \mathbb{T}_{2n} and \mathbb{T}_{3n} are defined in Eq. (33), and χ is defined in Eq. (7).

4 NSI textures realised in renormalisable flavour models

In this section, we consider how to realise higher-dimensional operators in UV-complete models. We follow the widely used technique in [16, 17], where the dimension-6 operator is mediated by singly-charged gauge-singlet scalars and the dimension-8 operators can be realised with the help of singly-charged gauge-singlet scalars and neutral fermions. Imposing the A_4 symmetry differs the analysis in the following ways: 1) It requires to extend the heavy particles as relevant multiplets of A_4 . 2) Mass matrices of these particles gain special structures constrained by A_4 or Z_2 (if the Z_2 -invariant flavon VEV χ is included), which further contribute the NSI structure. 3) Although experimental constraints to the heavy particles have been studied in [16, 17] and later work, e.g., [18, 19], the non-Abelian flavour symmetry connects channels of different flavours together and may result in stronger constraints. Due to these differences, NSIs with A_4 -invariant UV completion deserve a careful consideration.

4.1 UV completion of the dimension-6 operator

We first consider the UV completion of \mathcal{O}^1 , $\varepsilon_{ac}\varepsilon_{bd}(\overline{L_{a\alpha}}\gamma^\mu L_{b\beta})(\overline{L_{c\gamma}}\gamma_\mu L_{d\delta})$. The only way is to introduce a singly charged scalar S which is a $SU(2)_L$ singlet with $Y = +1$ and assume that it couples to L in an ‘‘antisymmetric’’ form [16]. Together with the kinetic and mass term of S , we write down the renormalisable Lagrangian terms as

$$\mathcal{L}_S = (D_\mu S)^\dagger(D^\mu S) - (M_S^2)_{\alpha\beta}S_\alpha^*S_\beta + \lambda_{\alpha\beta\gamma}\varepsilon_{ab}\overline{L_{a\alpha}}L_{b\beta}S_\gamma + \text{h.c.}, \quad (45)$$

where $\lambda_{\alpha\beta\gamma} = -\lambda_{\beta\alpha\gamma}$. In the framework of A_4 , S cannot be arranged as a singlet representation $\mathbf{1}, \mathbf{1}'$ or $\mathbf{1}''$ of A_4 since the symmetric CG coefficients of A_4 and the anti-symmetric property of λ lead to

$S(\overline{L^C}L)_{\mathbf{1}(\mu,\nu)} \equiv 0$. Similarly by arranging $S \sim \mathbf{3}$, we obtain $S(\overline{L^C}L)_{\mathbf{3}_S} = 0$. The only term that can contribute to the operator in Eq. (45) is $S(\overline{L^C}L)_{\mathbf{3}_A}$ for $S \sim \mathbf{3}$. All non-vanishing coefficients satisfy

$$\lambda_{123} = \lambda_{231} = \lambda_{312} = -\lambda_{132} = -\lambda_{213} = -\lambda_{321} \equiv \lambda_0. \quad (46)$$

After S decouples and by using the Fierz identity, we obtain \mathcal{O}^1 and the resulted NSI parameters are obtained as

$$\epsilon_{\alpha\beta}^e = \frac{1}{\sqrt{2}G_F} \lambda_{\beta e} (M_S^2)^{-1} \lambda_{\alpha e}^\dagger, \quad (47)$$

where each $\lambda_{\alpha\beta}$ is the 1×3 matrix given by $\lambda_{\alpha\beta} = (\lambda_{\alpha\beta 1}, \lambda_{\alpha\beta 2}, \lambda_{\alpha\beta 3})$.

The structures of $\epsilon_{\alpha\beta}^e$ are fully determined by the flavour structure of M_S^2 . We will see how to constrain the M_S^2 structure.

- An A_4 -invariant mass term for the charged scalar can only take the form $\mu_S^2 (S^* S)_{\mathbf{1}} = \mu_S^2 \sum_{\alpha} S_{\alpha}^* S_{\alpha}$ with $\mu_S^2 > 0$, leading to the charged scalar mass matrix $M_S^2 = \mu_S^2 \mathbb{1}$. From this mass matrix, we obtain the texture $\epsilon^e = \alpha_0 \mathbb{T}'_{12}$ with $\alpha_0 = \frac{\mu_S^2}{\sqrt{2}G_F}$.
- In order to obtain non-vanishing off-diagonal NSI entries, A_4 has to be broken. As shown in the last section, the key is to introduce a flavon with the Z_2 -preserving VEV χ . We add the following renormalisable couplings to the Lagrangian,

$$\frac{\mu_S^2}{v_{\chi}} \left[\frac{2}{3} h_S (\chi (S^* S)_{\mathbf{3}_S})_{\mathbf{1}} - \frac{2}{\sqrt{3}} h_A (\chi (S^* S)_{\mathbf{3}_A})_{\mathbf{1}} \right], \quad (48)$$

where h_S and h_A are real dimensionless coefficients as required by the Hermiticity of the Lagrangian. Then, the S mass matrix is non-diagonal and the resulted NSI matrix becomes

$$\epsilon^e = \alpha_0 \left[\mathbb{T}'_{12} + \frac{1}{3} \begin{pmatrix} 0 & 0 & 0 \\ 0 & h_S - h_S^2 & 2h_S + h_S^2 \\ 0 & 2h_S + h_S^2 & h_S - h_S^2 \end{pmatrix} + \frac{1}{3} \begin{pmatrix} 0 & 0 & 0 \\ 0 & \sqrt{3}h_A - h_A^2 & h_A^2 \\ 0 & h_A^2 & -\sqrt{3}h_A - h_A^2 \end{pmatrix} \right], \quad (49)$$

where $\alpha_0 = |\lambda_0|^2 / [\sqrt{2}G_F \mu_S^2 (1 - h_S^2 - h_A^2)]$. ϵ^e contains three real parameters $\epsilon_{\mu\mu}$, $\epsilon_{\tau\tau}$ and $|\epsilon_{\mu\tau}|$. The renormalisable quartic terms $((\chi\chi)_{\mathbf{3}_S} (S^* S)_{\mathbf{3}_S})_{\mathbf{1}}$ and $((\chi\chi)_{\mathbf{3}_S} (S^* S)_{\mathbf{3}_A})_{\mathbf{1}}$ are also allowed by the symmetry, such terms do not modify the flavour structures of M_S^2 and ϵ^e except redefinitions of h_S and h_A .

However, sizeable NSI textures are hard to be realised in this approach due to the strong constraint from the radiative charged LFV measurements. Although the tree-level 4-charged-fermion interactions have been avoided, radiative decays $E_{\alpha} \rightarrow E_{\beta} \gamma$ involving S and neutrinos in the loop are triggered by the interaction $\overline{L^C} L S$, and the relative branching ratios are $\propto |G_F^{-1} \lambda_{\alpha\gamma} (M_S^2)^{-1} \lambda_{\beta\gamma}^\dagger|^2$, where $\gamma \neq \alpha, \beta$. General upper bounds of $\tau \rightarrow e\gamma$ and $\tau \rightarrow \mu\gamma$ branching ratios are around 10^{-8} [58] and [59], and that of $\mu \rightarrow e\gamma$ is 4.2×10^{-13} [60]. Without flavour symmetries, the coefficients $\lambda_{\alpha\beta\gamma}$ and mass terms $(M_S^2)_{\alpha\beta}$ are free parameters, and $\tau \rightarrow e\gamma$ and $\mu \rightarrow e\gamma$ do not provide direct constraints to NSIs [16]. Once the flavour symmetry is included, relations such as Eqs. (46) and (48) are satisfied. In the limit $h_S, h_A \rightarrow 0$, all radiative decays are forbidden. However, off-diagonal NSIs are also forbidden in this case, becoming less interesting in oscillation experiments. On the other hand, by assuming h_S or $h_A \sim \mathcal{O}(1)$, very strong constraint, $|\epsilon_{\alpha\beta}^e| < 7 \times 10^{-5}$, is obtained from the upper limit of $\mu \rightarrow e\gamma$.

4.2 UV completions of dimension-8 operators

In the following, we will only consider NSIs from UV completions of dimension-8 operators. Before performing a detailed analysis, we directly point out our main result that, in UV-complete models with the Z_2 residual symmetry, only linear combinations of the following NSI textures are worth for phenomenological studies in neutrino oscillation experiments,

$$\mathbb{T}_1 = \frac{1}{3} \begin{pmatrix} 2 & -1 & -1 \\ -1 & 2 & -1 \\ -1 & -1 & 2 \end{pmatrix}, \mathbb{T}_2 = \frac{1}{3} \begin{pmatrix} 2 & -1 & -1 \\ -1 & -1 & 2 \\ -1 & 2 & -1 \end{pmatrix}, \mathbb{T}_3 = \frac{1}{\sqrt{3}} \begin{pmatrix} 0 & -1 & 1 \\ -1 & 1 & 0 \\ 1 & 0 & -1 \end{pmatrix}, \mathbb{T}_4 = \frac{1}{\sqrt{3}} \begin{pmatrix} 0 & -i & i \\ i & 0 & -i \\ -i & i & 0 \end{pmatrix}. \quad (50)$$

We refer them to major NSI textures. They are combinations of some \mathbb{T}_{mn} , $\mathbb{T}_1 = \frac{1}{3}(2\mathbb{T}_{11} - \mathbb{T}_{21})$, $\mathbb{T}_2 = \frac{1}{3}(\mathbb{T}_{12} + \mathbb{T}_{22})$, $\mathbb{T}_3 = \frac{1}{\sqrt{3}}(\mathbb{T}_{13} + \mathbb{T}_{23})$, and $\mathbb{T}_4 = \frac{1}{\sqrt{3}}\mathbb{T}_{31}$. As discussed later in this section, the rest NSI textures \mathbb{T}_{12} , \mathbb{T}_{13} , \mathbb{T}_{32} , \mathbb{T}_{33} and their combinations are strongly constrained by non-oscillation data. Therefore, we call them ‘minor NSI texture’. Here, we classify them into ‘major’ and ‘minor’ due to their testability. In the former case, although they are small, we may still have the opportunity to detect them, while in the later case, we will have no chance to test them in the next-generation neutrino experiments. Throughout this paper, we will put our focus on the ‘major NSIs texture’.

Major NSI textures realised in UV-complete A_4 models

We consider how to realise the major NSI textures in the renormalisable A_4 models and consider their experimental constraints. Before electroweak symmetry breaking, the operators \mathcal{O}^{2-6} take the form as dimension-8 operator $(\bar{L}\tilde{H}\gamma^\mu\tilde{H}^\dagger L)(\bar{F}\gamma_\mu F)$. A popular way to realise large NSIs is introducing a vector boson Z' . Then, the 4-charged-fermion interaction $(\bar{F}\gamma^\mu F)(\bar{F}\gamma_\mu F)$ is unavoidable. In order to be consistent with experimental data, the coupling must be very small. Here, we will carefully avoid the 4-charged-fermion interactions newly introduced after the decouple of the new particles in the UV sector. Thus, interactions mediated by Z' will not be considered.

We focus on \mathcal{O}^4 by using a singly charged scalar ϕ and a neutral fermion N to realise major NSI textures. The renormalisable interactions are given by

$$\begin{aligned} \mathcal{L}_{\phi,N} = & (D_\mu\phi)^\dagger(D^\mu\phi) - (M_\phi^2)_{\alpha\beta}\phi_\alpha^*\phi_\beta + \bar{N}i\not{\partial}N - M_{N\alpha\beta}\bar{N}_{\alpha R}\overline{N_{\beta L}} \\ & - \kappa_{\alpha\beta\gamma}\overline{E_{\alpha R}}N_{\beta L}\phi_\gamma^* - y_{\alpha\beta}\bar{L}_\alpha\tilde{H}N_{\beta R} + \text{h.c.}, \end{aligned} \quad (51)$$

where $D_\mu = \partial_\mu + ieA_\mu$. The charged scalar is a $SU(2)_L$ singlet with $Y = -1$. In order to distinguish it from S in the last subsection, we denote it as ϕ . There is no lepton-number-violating (LNV) coupling in the above interactions. For the neutral fermion N , we require a vector-like mass term $M_N\bar{N}_R N_L$ as shown in the above. If there is an additional small LNV mass term $\mu\bar{N}_L^C N_L$ and hierarchical masses $y/\sqrt{G_F} \ll M_N$, we recover the inverse seesaw model [57]. But here we do not specify if N is related to the origin of active neutrino masses. No matter whether there is a small LNV mass term, we can always arrive at a dimension-8 operator $\sim \frac{\kappa^2 y^2}{M_\phi^2 M_N^2}(\bar{L}\tilde{H}E_R)(\bar{E}_R\tilde{H}^\dagger L)$ after the decouple of the charged scalar and sterile neutrinos, from which we obtain \mathcal{O}^4 . Once the flavour structure is included, the 3×3 NSI parameter matrix ϵ^e is expressed as

$$\epsilon^e = \frac{1}{8G_F^2}(yM_N^{-1}\kappa_e)(M_\phi^2)^{-1}(yM_N^{-1}\kappa_e)^\dagger, \quad (52)$$

where κ_e is a 3×3 matrix defined via $(\kappa_\alpha)_{\beta\gamma} = \kappa_{\alpha\beta\gamma}$ for $\alpha = e, \mu, \tau$.

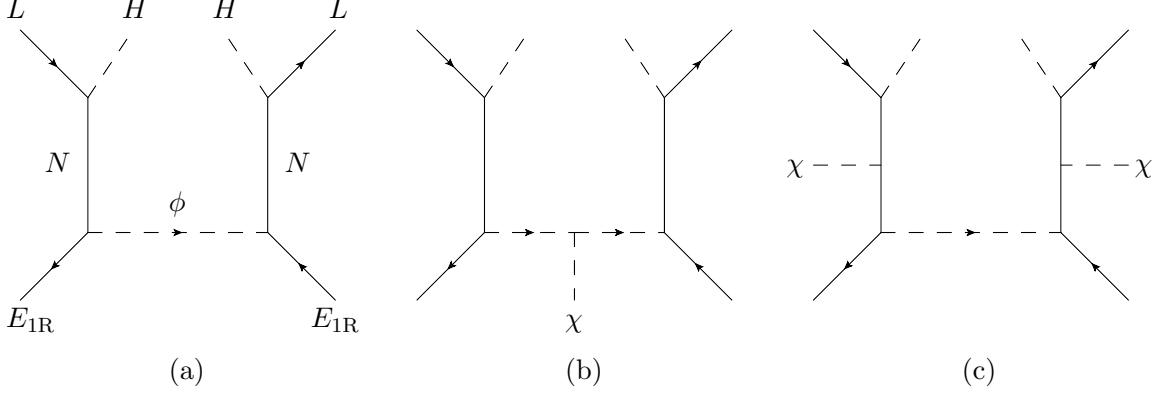


Figure 2: Diagrams to realise sizeable NSI textures corresponding to dimension-8 operator \mathcal{O}^4 in leptonic A_4 models.

We will discuss how the A_4 symmetry can constrain NSIs originating from this renormalisable model. We first consider A_4 -motivated NSI textures without the involvement of flavons. In the flavour space, since we have arranged $L \sim \mathbf{3}$, the fields N_L , N_R and ϕ must be triplets to ensure the invariance of Lagrangian in A_4 . We follow the setup of most A_4 models that E_{1R} is fixed as a singlet $\mathbf{1}$ of A_4 . An A_4 -invariant mass term for the charged scalar can only take the form $\mu_\phi^2(\phi^*\phi)_\mathbf{1} = \mu_\phi^2 \sum_i \phi_i^* \phi_i$ with $\mu_\phi^2 > 0$, i.e., the charged scalar mass matrix $M_\phi^2 = \mu_\phi^2 \mathbb{1}$. Similarly, to be invariant under transformations of A_4 , the Dirac mass matrix of the sterile neutrinos M_N and the Yukawa coupling between L and N_R , y is also proportional to an identity matrix, $M_N = \mu_N \mathbb{1}$, $y = y_0 \mathbb{1}$. The structures of the couplings y and κ depend on representations of E_R . Interactions involving ϕ and N are given by

$$\kappa_0 \overline{E_{1R}} (N_L \phi^*)_\mathbf{1} + y_0 (\bar{L} \tilde{H} N_R)_\mathbf{1} + \text{h.c.} . \quad (53)$$

Thus, both coupling matrices κ and y appear to be proportional to the identity matrix, $\kappa = \kappa_0 \mathbb{1}$, $y = y_0 \mathbb{1}$. After ϕ and N are integrated out from the Lagrangian, we obtain that the \mathcal{O}^4 takes the $(\bar{L}L)_\mathbf{1}(\bar{F}F)_\mathbf{1}$ form as listed in Table 2 for $F = E_R$. Finally, we obtain the NSI texture $\epsilon^e = \alpha_0 \mathbb{1}$, where

$$\alpha_0 = \frac{|y_0 \kappa_0|^2}{8 G_F^2 \mu_N^2 \mu_\phi^2} . \quad (54)$$

Since $\mathbb{1}$ is an identity matrix, ϵ^e in this special case has no observable signatures in neutrino oscillation experiments.

The involvement of χ breaks A_4 to Z_2 and modifies the correlation relations of NSI parameters. In order to realise relatively large and measurable NSI effects, we only consider the contribution of renormalisable couplings of χ . There are cases, as shown in Figure 2 (b) and (c), where χ couples to ϕ and N , modifying their mass matrices, respectively.

- The charged scalar ϕ mass matrix modified by the coupling between χ and ϕ . We add the following renormalisable coupling to the Lagrangian,

$$\frac{\mu_\phi^2}{v_\chi} \left[\frac{2}{3} f_S (\chi (\phi^* \phi)_{\mathbf{3}_S})_\mathbf{1} - \frac{2}{\sqrt{3}} f_A (\chi (\phi^* \phi)_{\mathbf{3}_A})_\mathbf{1} \right] , \quad (55)$$

where f_S and f_A are real dimensionless coefficients as required by the Hermiticity of the Lagrangian. The relevant higher-dimensional operators after ϕ and N integrated out take the forms

as $\chi(\overline{LL})_{\mathbf{3}_S}(\overline{FF})_{\mathbf{1}}$ and $\chi(\overline{LL})_{\mathbf{3}_A}(\overline{FF})_{\mathbf{1}}$, respectively. The modified ϕ mass matrix turns out to be

$$M_\phi^2/\mu_\phi^2 = \mathbb{1} + f_S \mathbb{T}_2 + f_A \mathbb{T}_3. \quad (56)$$

Terms such as $((\chi\chi)_{\mathbf{3}_S}(\phi^*\phi)_{\mathbf{3}_S})_{\mathbf{1}}$, $((\chi\chi)_{\mathbf{3}_S}(\phi^*\phi)_{\mathbf{3}_A})_{\mathbf{1}}$ are also renormalisable and should be considered for completeness. These terms will not induce new structures different from Eq. (56).

- The Dirac mass matrix of N is modified by couplings between χ and N . The related renormalisable Lagrangian term is given by

$$\frac{\mu_N}{v_\chi} \left[\frac{2}{3} g_S (\chi(\overline{N}_L N_R)_{\mathbf{3}_S})_{\mathbf{1}} - \frac{2}{\sqrt{3}} g_A (\chi(\overline{N}_L N_R)_{\mathbf{3}_A})_{\mathbf{1}} \right] + \text{h.c.}, \quad (57)$$

where g_S and g_A are in general complex parameters. Dirac mass matrix M_N is modified to

$$M_N/\mu_N = \mathbb{1} + g_S \mathbb{T}_2 + g_A \mathbb{T}_3. \quad (58)$$

Taking the flavon-modified mass matrices of ϕ and N into account, we state that the final detectable (i.e., ignoring the undetectable $\mathbb{1}$) NSI matrix ϵ^e in Eq. (52) is always a linear combination of \mathbb{T}_i for $i = 1, 2, 3, 4$. This is guaranteed by the algebra of \mathbb{T}_i and can be straightforwardly proven by implying Eqs. (88) and (89) in Appendix C. From Table 2, one can expect that the textures \mathbb{T}_2 and \mathbb{T}_3 will be predicted. The other two textures, \mathbb{T}_1 and \mathbb{T}_4 , which are not predicted from higher-dimensional operators, are obtained from the inverse transformations of M_ϕ^2 and M_N , and matrix product $\mathbb{T}_2 \mathbb{T}_3 = -i \mathbb{T}_4$. \mathbb{T}_1 and \mathbb{T}_4 appear at the second order of f_S, f_A and g_S, g_A . If $f_S, f_A, g_S, g_A \ll 1$ is satisfied, the \mathbb{T}_1 and \mathbb{T}_4 parts are negligible compared with the \mathbb{T}_2 and \mathbb{T}_3 parts. However, these coefficients, as coefficients of renormalisable terms, may take $\mathcal{O}(1)$ values, and thus in this case, \mathbb{T}_1 and \mathbb{T}_4 may have comparable NSI effects to \mathbb{T}_2 and \mathbb{T}_3 .

The flavour structures of NSIs can be further discussed in the following scenarios, dependent on the role of the flavon VEV χ :

- With the assumption of additional symmetries, χ may only couple to ϕ , not to N , i.e., $g_A, g_S = 0$. The resulted detectable NSI matrix is explicitly expressed as

$$\epsilon^e = \alpha_0 [(f_S^2 + f_A^2) \mathbb{T}_1 - f_S \mathbb{T}_2 - f_A \mathbb{T}_3]. \quad (59)$$

Here, only \mathbb{T}_1 , \mathbb{T}_2 and \mathbb{T}_3 appear, and α_0 has been redefined.

- On the other hand, if χ only couple to N , we obtain the following NSI matrix

$$\begin{aligned} \epsilon^e = \alpha_0 \{ & [-(2 + |g_S|^2 + |g_A|^2)(|g_S|^2 + |g_A|^2) + 4\text{Re}(g_S^2 + g_A^2) + 4[\text{Im}(g_S^* g_A)]^2] \mathbb{T}_1 \\ & - 2\text{Re}(g_S) \mathbb{T}_2 - 2\text{Re}(g_A) \mathbb{T}_3 - 2\text{Im}(g_S^* g_A) \mathbb{T}_4 \}. \end{aligned} \quad (60)$$

where α_0 has been redefined. It is a linear combination of all four \mathbb{T}_i , but \mathbb{T}_4 is important only if both $|g_S|$ and $|g_A|$ are sizeable and there is a relative phase between g_S and g_A .

- If the anti-symmetric couplings f_A and g_A are forbidden, the NSI matrix can be simplified to a linear combination of \mathbb{T}_1 and \mathbb{T}_2 . On the other hand, if the symmetric couplings f_S and g_S are forbidden, the NSI matrix is a linear combination of \mathbb{T}_1 and \mathbb{T}_3 . These two cases are valid if the group A_4 is replaced by larger groups. For example, in the hexahedron group S_4 [61], there

are two triplet irreducible representations, and the symmetric and anti-symmetric products $\mathbf{3}_S$ and $\mathbf{3}_A$ correspond to two different representations. By arranging χ to be one of the triplets, the anti-symmetric (or symmetric) products can be forbidden, and thus only the symmetric (or anti-symmetric) couplings are left.

Naively, one may expect that NSIs from the UV completion of the dimension-8 operator is more constrained than that of the dimension-6 operator, but this is not the case in the framework of the flavour symmetry. First of all, no tree-level CLFV interactions have been introduced from the Lagrangian in Eq. (51) as required. Although radiative CLFV processes are induced by the coupling $\overline{E}_R N_L \phi$, they essentially rely on the coupling with the second or third generation charged lepton E_{2R} or E_{3R} . By arranging E_{1R} , E_{2R} and E_{3R} as different singlets of A_4 , the relevant coefficients are theoretically independent of those involving in matter NSIs [62, 63]. Constraints on CLFV do not apply to NSIs. On the side of collider searches, with a careful treatment of ϕ decaying to e/μ plus missing transverse momentum or τ plus missing transverse momentum, the existing LEP and LHC data still allow a singlet charged scalar as light as 65 GeV [64]. The main constraint in this model is the bound of the non-unitarity of the lepton mixing. The decouple of sterile neutrinos contributes to the active neutrino kinetic mixing as $\frac{y^2}{M_N^2}(\overline{L}\tilde{H})\not{\partial}(\tilde{H}^\dagger L)$. After rescaling the kinetic terms of active neutrinos, non-unitarity of the PMNS matrix is

$$\eta \equiv V_{\text{PMNS}}^\dagger V_{\text{PMNS}} - \mathbf{1} = \frac{1}{2\sqrt{2}G_F}(yM_N^{-1})(yM_N^{-1})^\dagger. \quad (61)$$

The non-unitarity bound from a global analysis of LFV decays, probes of the universality of weak interactions, CKM unitarity bounds and electroweak precision data is around $\eta \sim 10^{-3}$ [56]. Combining with the above constraints, we see that it is still possible to achieve the major NSI textures with coefficients $\sim \eta/(G_F M_\phi^2)$ at 10^{-2} or 10^{-3} level. These values may be potentially measured by the next-generation accelerator neutrino oscillation experiments.

In the above, we have constructed UV-complete models for \mathcal{O}^4 and $\chi\mathcal{O}^4$. A similar discussion can be directly extended to the $\mathcal{O}^{2,3,5}$ and $\chi\mathcal{O}^{2,3,5}$ by replacing the singly-charged scalar ϕ by $\phi_{U_R, D_R, Q}$ which are $SU(2)_L$ gauge singlet, single and doublet with hypercharge $Y = -2/3, +1/3$ and $-1/6$, respectively, and replacing the singlet $F = E_{1R}$ with $F = U_{1R}, D_{1R}$ and Q_1 , respectively. The resulted NSI matrix is also a linear combination of the textures $\mathbb{T}_1, \mathbb{T}_2, \mathbb{T}_3$ and \mathbb{T}_4 . The textures $\mathbb{T}_1, \mathbb{T}_2, \mathbb{T}_3$ and \mathbb{T}_4 are obtained by assuming the charged fermion as singlets of A_4 . This treatment can avoid strong constraints from the second- and third-generation charged fermions. These textures are less constrained than the other textures discussed below and thus, we call them major NSI textures.

Minor NSI textures realised in UV-complete A_4 models

The minor NSI textures $\mathbb{T}_{12}, \mathbb{T}_{13}, \mathbb{T}_{32}, \mathbb{T}_{33}$ and their combinations cannot be realised in the above discussions. This is compatible with Table 2, where the minor textures are obtained by setting $F \sim \mathbf{3}$. To achieve these textures, as shown in Table 2, F has to be assumed to be a triplet of A_4 . Then F cannot be chosen as right-handed charged leptons and not realised in the \mathcal{O}^4 and $\chi\mathcal{O}^4$ series. We will discuss how to realise them in UV-complete A_4 models as a complement.

To realise the A_4 -motivated \mathbb{T}_{12} and \mathbb{T}_{13} , we choose $F = U_R \equiv (U_{1R}, U_{2R}, U_{3R})^T \sim \mathbf{3}$ of A_4 and consider the UV completion of \mathcal{O}^2 . The latter is obtained by replacing the singly charged scalar ϕ with a fractionally charged scalar ϕ_{U_R} , i.e., a scalar leptoquark, with the hypercharge $Y = -2/3$, and

coupling to N_L and U_R . The renormalisable couplings are given by

$$\kappa_S^{U_R}((\overline{U_R}N_L)\mathbf{3}_S\phi_{U_R}^*)\mathbf{1} + \kappa_A^{U_R}((\overline{U_R}N_L)\mathbf{3}_A\phi_{U_R}^*)\mathbf{1} + \text{h.c.} . \quad (62)$$

Then, coupling matrix κ is modified to $\kappa_{U_R} = \kappa_S^{U_R}\mathbb{T}_{12} + \kappa_A^{U_R}\mathbb{T}_{13}$ and the A_4 -preserved NSI texture

$$\epsilon^u \equiv \frac{1}{8G_F^2}(yM_N^{-1}\kappa_{U_R})(M_{\phi_{U_R}}^2)^{-1}(yM_N^{-1}\kappa_{U_R})^\dagger \quad (63)$$

is obtained as a linear combination of \mathbb{T}_{12} and \mathbb{T}_{13} . Finally, we include the A_4 -breaking effect in the ϕ_{U_R} and N mass matrices, as in Eqs. (56) and (58). Non-zero \mathbb{T}_{32} and \mathbb{T}_{33} can be extracted out in principle.

The minor textures \mathbb{T}_{12} , \mathbb{T}_{13} , \mathbb{T}_{32} and \mathbb{T}_{33} are expected to receive stronger constraints. The main reason is that $U_R = (U_{1R}, U_{2R}, U_{3R})$ is arranged as a triplet of A_4 and constraints from the second- and third-generation charged fermions should be included. The neutrino kinetic mixing leads to coupling $\overline{U_R}\nu_L\phi_{U_R}^*$. It further modifies processes, e.g., (semi-)leptonic decays $U_\alpha \rightarrow U_\beta\nu\bar{\nu}$ at tree level, radiative decays $U_\alpha \rightarrow U_\beta\gamma\gamma$ at loop level and FCNC processes $U_\alpha \rightarrow U_\beta\overline{U}_\gamma U_\delta$ at loop level, from their SM predictions. As a consequence, precision measurements of charm mesons and baryons can give strong constraints to ϵ^u . A detailed discussion of these constraints is not our subject in this paper. Realisations of sizeable NSI textures \mathbb{T}_{12} , \mathbb{T}_{13} , \mathbb{T}_{32} and \mathbb{T}_{33} via UV completions of the other dimension-8 operators are also hard. Those via $\mathcal{O}^{3,5,7,8}$ gain strong constraints from K and B decays, and those via \mathcal{O}^6 gain constraints from $E_\alpha \rightarrow E_\beta\gamma$ decays again. Since it is hard to generate sizeable NSI for textures \mathbb{T}_{12} , \mathbb{T}_{13} , \mathbb{T}_{32} , \mathbb{T}_{33} or their combinations, we refer them to minor NSI textures.

5 Testing NSI textures at LBL experiments

The long baseline experiment with the wide-band beam and sizeable matter effects is expected to measure more than one $\epsilon_{\alpha\beta}$, which implies that the flavour dependence of NSIs $\epsilon_{\alpha\beta}$ can be tested. As a result, an experiment of this kind is possible to study the flavour symmetry model through the operators \mathcal{O}^{1-8} . In this section we will study the matter NSI effects for DUNE experiment under the flavour symmetry A_4 or Z_2 . We summarise the connection of texture parameters α_{mn} to the conventional parameters $\epsilon_{\alpha\beta}$ in Table 3. Some benefits can be seen to consider matter-effect NSIs under flavour symmetries. When we assume that A_4 symmetry is not broken, only two types of NSIs could be seen, and they are both flavour-conserving ones. If A_4 is broken and the residual Z_2 symmetry is preserved, there is no such benefits as all textures are predicted under this symmetry, until we impose an UV complete model. Therefore, we expect a good performance for DUNE to figure out these scenarios. We will test the NSI textures from the A_4 symmetry without assuming any UV complete model in Section 5.2. In section 5.3, we will study on the Z_2 testing, following with the discussion in Section 4.2. The approximation to oscillation probabilities with NSI matter effects is presented in Appendix D; the true value used for oscillation parameters through out the simulation in this section is given in Table 9.

The current global fit for matter-effect NSIs [27] includes solar, atmospherical, reactor and LBL neutrino data. With the assumption that all NSIs coming entirely from up quark or down quark to avoid NSIs at the source and the detector, the current global fit to standard NSI parameters $\epsilon_{\alpha\beta}^u$ and $\epsilon_{\alpha\beta}^d$ has been performed in [27], respectively. We adopt these results to estimate the bounds for $\alpha_{mn}^{u,d}$. We only take the bound for each $\epsilon_{\alpha\beta}^{u,d}$, i.e., the results of 1-D projection. Furthermore, we neglect underlying corrections between any two or among more than two parameters, which are $\epsilon_{\alpha\beta}$, or mixing angles, mass-squared differences. Assuming Gaussian distributions, taken 90% C.L. limits from [27], bounds on

$\tilde{\epsilon}_{ee}(\equiv \epsilon_{ee} - \epsilon_{\mu\mu})$	$3\alpha_{12}/\sqrt{6} - \alpha_{13}/\sqrt{2}$
$\tilde{\epsilon}_{\tau\tau}(\equiv \epsilon_{\tau\tau} - \epsilon_{\mu\mu})$	$-2\alpha_{13}/\sqrt{2}$
$\epsilon_{e\mu}$	$\alpha_{21}/\sqrt{6} - \alpha_{22}/\sqrt{12} - \alpha_{23}/2 + i(-\alpha_{31}/\sqrt{6} + \alpha_{32}/\sqrt{12} + \alpha_{33}/2)$
$\epsilon_{e\tau}$	$\alpha_{21}/\sqrt{6} - \alpha_{22}/\sqrt{12} + \alpha_{23}/2 + i(\alpha_{31}/\sqrt{6} - \alpha_{32}/\sqrt{12} + \alpha_{33}/2)$
$\epsilon_{\mu\tau}$	$\alpha_{21}/\sqrt{6} + 2\alpha_{22}/\sqrt{12} + i(-\alpha_{31}/\sqrt{6} - \alpha_{32}/\sqrt{12})$

Table 3: Expressions of conventional parameters $\epsilon_{\alpha\beta}$ in terms of texture parameters α_{mn} according to Eqs. (22), (33), (43).

$\epsilon_{\alpha\beta}^{u,d}$ at 1σ are shown in Table 4. Since in their analysis the imaginary part is assumed to be 0 or π , we directly translate their bounds to $\alpha_{1n}^{u,d}$ and $\alpha_{2n}^{u,d}$ by setting the imaginary $\alpha_{3n}^{u,d} = 0$, and the results are shown in Table 5. NSIs with down quarks $\epsilon_{\alpha\beta}^{u,d}$ have very similar constraints as those with $\epsilon_{\alpha\beta}^{u,d}$. As we neglect some correlations among parameters, our results can be viewed as optimal. In Table 5, we see that most parameters are constrained around or below the percent level of weak interactions, except for $\alpha_{12}^{u,d}$, for which 1σ bounds are around 15%.

1 σ bounds of global fit results			
$\tilde{\epsilon}_{ee}^u$	[0.188, 0.376]	$\tilde{\epsilon}_{ee}^d$	[0.203, 0.384]
$\tilde{\epsilon}_{\tau\tau}^u$	[-0.003, 0.012]	$\tilde{\epsilon}_{\tau\tau}^d$	[-0.003, 0.012]
$\epsilon_{e\mu}^u$	[-0.046, 0.002]	$\epsilon_{e\mu}^d$	[-0.048, 0]
$\epsilon_{e\tau}^u$	[-0.038, 0.065]	$\epsilon_{e\tau}^d$	[-0.036, 0.066]
$\epsilon_{\mu\tau}^u$	[-0.004, 0.003]	$\epsilon_{\mu\tau}^d$	[-0.004, 0.003]

Table 4: Taken from the current global fit results [27] for $\epsilon_{\alpha\beta}^u$ and $\epsilon_{\alpha\beta}^d$. In these results, the authors assume that off-diagonal elements $\epsilon_{\alpha\neq\beta}$ are real, consider that NSIs is only contributed by u (d) quarks for $\epsilon_{\alpha\beta}^u$ ($\epsilon_{\alpha\beta}^d$), but do not include NSIs at the source and the detector.

1 σ bounds by global fit results			
α_{12}^u	[0.089, 0.247]	α_{12}^d	[0.099, 0.26]
α_{13}^u	[-0.003, 0.007]	α_{13}^d	[-0.003, 0.007]
α_{21}^u	[-0.045, 0.049]	α_{21}^d	[-0.045, 0.047]
α_{22}^u	[-0.037, 0.03]	α_{22}^d	[-0.035, 0.0302]
α_{23}^u	[-0.019, 0.096]	α_{23}^d	[-0.0154, 0.096]

Table 5: The 1σ bounds for α_{12}^u (α_{12}^d), α_{13}^u (α_{13}^d) and α_{2i}^u (α_{2i}^d), with fixed $\alpha_{3i}^u = 0$ ($\alpha_{3i}^d = 0$), by global fit results [27] shown in Table 4. More details can be seen in the text.

The smallness of matter effect NSIs is predicted as we see in Table 4. Fortunately, DUNE can improve the sensitivity and is possible to detect these effects. In this section, our goal is to see if these minor features^{vi} appearing in DUNE can provide any extra information for the flavour symmetry. We firstly discuss how matter-effect NSIs α_{mn} affect neutrino oscillations in DUNE and then, study the physics capacity for DUNE to test A_4 symmetry and Z_2 residual symmetry via the NSI measurement. We emphasis that the results in Sections 5.2 and 5.3 are in the general point of view; we consider all possible correlations by using the conventional parametrisation (3 mixing angles, 1 Dirac CP phase and 2

^{vi} Assuming an equal amount of NSI effects with u , d quarks and electrons, the 1σ size of total NSI matter effects in the earth is roughly 3 times of the 1σ region shown Table 4. This estimate will be applied in the following (Tables 6 and 8) for the comparison.

mass-squared differences), instead of implementing any possible flavour model for oscillation parameters. The final note is that for a given model that consistently predicts values for both oscillation and NSI parameters, we should further adopt the Wilks' theorem that the $\Delta\chi^2$ value for nested hypothesis testing asymptotically follows the χ^2 -distribution with the degrees of freedom that equals to the difference in the number of free parameters between two models [65]. Therefore, we will further study two cases with the maximum and the minimum of the possible degrees of freedom for χ^2 -distribution.

5.1 Oscillation probabilities in DUNE

As mentioned in the introduction, matter-effect NSIs in DUNE have been widely discussed. Because of the propagation in such long distance (1300 km) of neutrino in the earth, nonnegligible matter density, and the GeV-energy-scale neutrino beam, matter effects play a substantial role in the oscillation. Before discussing the physics potential for understanding any flavour symmetries, we firstly study the impact of α_{mn} on the oscillation probability for DUNE.

The DUNE experiment consists of a neutrino source known as Long Baseline Neutrino Facility (LBNF), a detector based at Fermilab and a LArTPC detector complex located in SURF a distance of 1300 km away. The beam design is considered based on both LBNE (reference design) and LBNF studies (optimised design). The optimisation is according to the physics capability of δ discovery. Over 1 MW power generates large amount of ν_μ (POT/year $\sim 10^{21}$) to 1300 km away. On the other side, the detector configuration is planned of four 10-kiloton LArTPC detectors. LArTPC technology has a particularly strong particle identification capability as well as good energy resolution which are both crucial in providing high efficiency searches and low backgrounds. DUNE covers the 1st maximum of appearance channel (0.5 \sim 5 GeV); with the wide-band design and LArTPC technology, it allows to read the behaviour of $P(\nu_\mu \rightarrow \nu_e)$ in energy around the 1st maximum for the appearance channel with the high precision.

We show the difference of oscillation probabilities with one nonzero α_{mn} and those without NSIs, $\delta P_{\text{NSI}}(\nu_\alpha \rightarrow \nu_\beta) \equiv P(\nu_\alpha \rightarrow \nu_\beta) - P_0(\nu_\alpha \rightarrow \nu_\beta)$ in Figure 3. The coefficient α_{mn} is fixed at 0.1, but the other NSI parameters are fixed at zeros. The Dirac phase $\delta = 270^\circ$ and the normal mass ordering are assumed.

For appearance channels in the upper 2 panels of Figure 3, we see that the NSI parameters non-trivially modify the oscillation probability. NSIs modify the amplitude of oscillation probability and distort the oscillation behaviour against L/E . α_{23} , α_{31} and α_{33} have larger impacts on δP_{NSI} than the other NSI parameters, and δP_{NSI} around the 1st maximum reaches up to or over 0.01 for the neutrino mode. These impacts are slightly larger in the neutrino mode than the antineutrino mode, and this is due to our assumption of the normal mass ordering. DUNE with the wide-band-beam fluxes (the grey shadows) reads the variation of δP_{NSI} around the 1st maximum. As a result, the sophisticated behaviour in the appearance channel around the 1st maximum plays a role of distinguishing different textures.

In lower 2 panels of Figure 3, we observe the oscillation behaviour of δP_{NSI} in L/E in disappearance channels, and except for α_{13} it goes to 0 at the 1st and 2nd minimums. As a result, this is clear that we would not see the NSI effects if we focus on the first minimum, where roughly peaks of DUNE fluxes are. As the grey shadows shown in this figure, the wide-band beam feature of DUNE provides more information about how much α_{mn} affects on the disappearance channels around the 1st minimum. Further, it is obvious that the disappearance channels can be sensitive to α_{21} and α_{22} as their impacts

δP_{NSI} are significantly larger than the others. An interesting feature is that for neutrino and antineutrino modes δP_{NSI} behaves oppositely, i.e. $\delta P_{\text{NSI}}(\nu_\mu \rightarrow \nu_\mu) \cong -\delta P_{\text{NSI}}(\bar{\nu}_\mu \rightarrow \bar{\nu}_\mu)$. This is because $P(\nu_\mu \rightarrow \nu_\mu; \delta, A) \cong P(\bar{\nu}_\mu \rightarrow \bar{\nu}_\mu; -\delta, -A)$, and also due to the fact that the contribution of α_{mn} is proportional to A in the leading approximation for the disappearance channel. We see this correlation in Figure 4, in which the event rates with $\alpha_{21} = 0.1$ (green spectra), $\alpha_{22} \approx 0.7$ (blue circle) and that without NSIs (red spectra) are presented in ν and $\bar{\nu}$ disappearance channels. We see the overlapping between the blue circles and the green spectra demonstrates the difficulty of distinguishing α_{21} and α_{22} in disappearance channels.

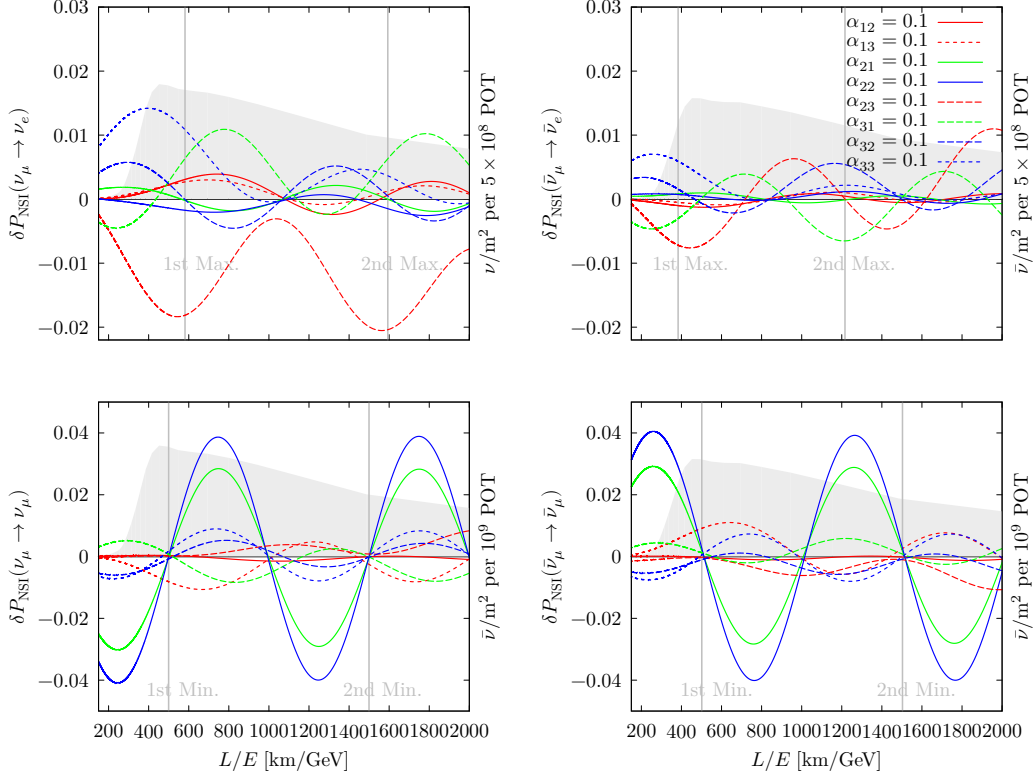


Figure 3: Oscillation probabilities $\delta P_{\text{NSI}}(\nu_\mu \rightarrow \nu_e)$ (upper left), $\delta P_{\text{NSI}}(\bar{\nu}_\mu \rightarrow \bar{\nu}_e)$ (upper right), $\delta P_{\text{NSI}}(\nu_\mu \rightarrow \nu_\mu)$ (lower left) and $\delta P_{\text{NSI}}(\bar{\nu}_\mu \rightarrow \bar{\nu}_\mu)$ (lower right) against L/E [km/GeV] for the case with one α_{mn} , fixed at 0.1. The oscillation parameters are used the current global fit results [68] (shown in Table 9) for the normal ordering with $\delta = 270^\circ$, and the oscillation baseline is considered 1300 km. In the left (right) panels, the grey shadow shows ν ($\bar{\nu}$) flux of the 2-horn-optimised design for DUNE at the far detector without oscillations.

We conclude that the wide-band-beam feature of DUNE is an advantage to detect NSI textures. Different NSI textures result in different distortions of the probabilities in the appearance channel. Therefore, we can distinguish different textures by reading out the variation of $P(\nu_\mu \rightarrow \nu_e)$ along energy. In addition, this feature helps us to measure the size of NSI effects in the disappearance channel.

5.2 Testing “ A_4 symmetry” in DUNE

Matter NSI effects predicted by A_4 -invariant operators only allow diagonal entries. After the breaking of A_4 by the Z_2 -preserving flavon VEV χ , textures \mathbb{T}_{2n} , \mathbb{T}_{3n} , or their linear combinations is involved in the NSI matrix ϵ . Eqs. (90) and (91) indicate us that accelerator LBL experiments can be sensitive to off-diagonal terms in ϵ , because of the fact that $\epsilon_{\mu\tau}$ is the leading term in the disappearance channel, and

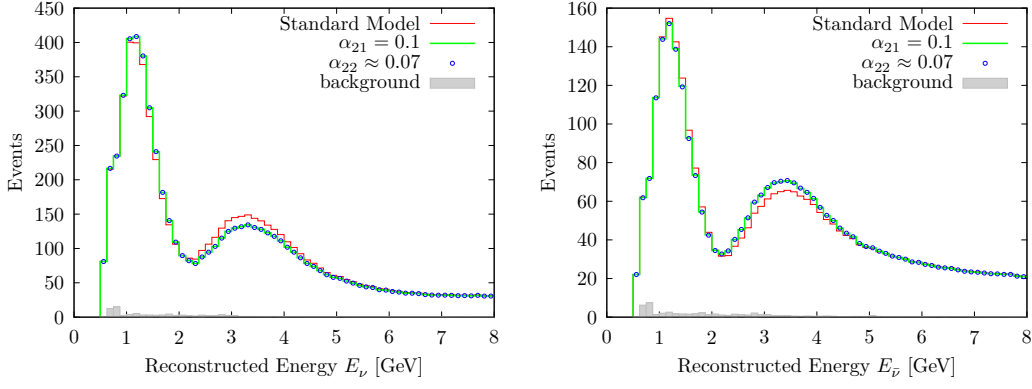


Figure 4: The event spectral with $\alpha_{21} = 0.1$ (green line), $\alpha_{22} \approx 0.07$ (blue circles), and the case without NSIs (red line). The overlapping between green and blue curves; this present the correlation between α_{21} and α_{22} .

$\epsilon_{e\mu}$, $\epsilon_{e\tau}$ are for the appearance channel. As a result, experiments of this kind can test the conservation of A_4 symmetry.

Through out the study in this section, we adopt General Long Baseline Experiment Simulator (GLOBES) library [66, 67]. To simulate probabilities with matter-effect NSIs, we modify the default probability engine of GLOBES, by simply adding the matrix $A\epsilon$ in the Hamiltonian. For the simulation for DUNE, we implement the simulation package in Ref. [69], with run time fixed by 7 years total (corresponding to 300 MW \times kton \times years) and 2-horn optimised beam design with 80 GeV protons. The other sets for oscillation parameters are described in Appendix A.

We study the capacity for DUNE to rule out the “ A_4 symmetry” hypothesis. The statistics quantity that we study is

$$\Delta\chi_{A_4}^2 \equiv \chi^2|_{\alpha_{2n}=\alpha_{3n}=0} - \chi_{b.f.}^2, \quad (64)$$

where $\chi^2|_{\alpha_{2n}=\alpha_{3n}=0}$ is the χ^2 value with the assumption of $\alpha_{2n} = \alpha_{3n} = 0$ ($n = 1, 2, 3$), and $\chi_{b.f.}^2$ is the χ^2 value for the best fit. The expression of χ^2 is used

$$\chi^2 = \min_{\Theta, \xi=\{\xi_s, \xi_b\}} \left[2 \sum_i \left(\eta_i(\Theta, \xi) - n_i + n_i \ln \frac{n_i}{\eta_i(\Theta, \xi)} \right) + p(\xi, \sigma) + P(\Theta_{\text{OSC}}) \right]. \quad (65)$$

The sum in this expression is over the i energy bins of the experimental configuration, with simulated true event rates of n_i and simulated event rates $\eta_i(\Theta, \xi)$ for the hypothesis parameters $\Theta \equiv \{\theta_{ij}, \Delta m_{ij}^2, \text{NSI parameters}\}$ and systematic error parameters ξ . Based on different conventions or assumptions, we may adopt the different parametrisation for NSI parameters; in this subsection, we use α_{mn} . The systematic errors of the experiments are treated using the method of pulls, parameterized as ξ_s for the signal error and ξ_b for the background error. These parameters are given Gaussian priors which form the term $p(\xi, \sigma) = \xi_s^2/\sigma_s^2 + \xi_b^2/\sigma_b^2$, where $\sigma = \{\sigma_s, \sigma_b\}$ are the sizes of the systematic errors given in Ref. [69]. $P(\Theta_{\text{OSC}})$ comprises a sum of Gaussian priors for oscillation parameters Θ_{OSC} , except for δ . The central values and widths are respectively used the best fit and 1σ width of NuFit results, and are given in Tab. 9. The value of $\chi_{b.f.}^2$ is always 0, as the best fit is exactly the true value. In the following results, we allow α_{12} and α_{13} to be free to vary. While varying the true value for one of $\{\alpha_{21}, \alpha_{22}, \alpha_{23}, \alpha_{31}, \alpha_{32}, \alpha_{33}\}$, we set true values of α_{12} and α_{13} to be 0.

We scan all possible true values for the targeted parameter to test the “ A_4 symmetry” hypothesis, i.e. $\alpha_{2n} = \alpha_{3n} = 0$ (for $n = 1, 2, 3$) in Figure 5. The solid curves and dashed curves correspond to

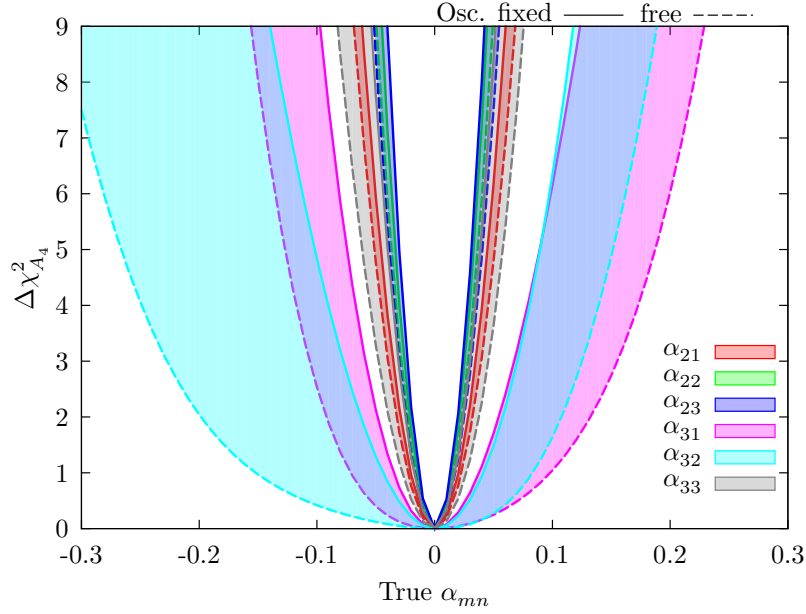


Figure 5: $\Delta\chi^2_{A_4}$ to exclude the “ A_4 symmetry” hypothesis ($\alpha_{2n} = \alpha_{3n} = 0$) over the true value from -0.3 to 0.3 . α_{2n} or α_{3n} are forbidden under the flavour symmetry A_4 . Normal mass ordering with $\delta = 270^\circ$ is assumed. For generality, the solid (dashed) curves are presented for fixed (free) all oscillation parameters, which can be seen as the case with minimum (maximum) correlations with oscillation parameters. More details of the setting can be seen in Table 10. The oscillation parameters are taken from the current global fit results [68] (shown in Table 9).

oscillation parameters fixed at their best-fit values and values varying in 1σ ranges as given in Appendix A. The solid (dashed) curve can be seen as the case with minimum (maximum) correlations with oscillation parameters. This is for considering all possible correlation between or among parameters. For any flavour model consistent with oscillation data, the $\Delta\chi^2_{A_4}$ value is located between these two curves. We summarise the above setting in Appendix A.1. The larger $\Delta\chi^2_{A_4}$ values are seen for α_{21} , α_{22} , α_{23} and α_{33} . For the other two parameters α_{31} and α_{32} , with a worse performance, a minor asymmetry feature is seen. $\alpha_{31} < 0$ has the slightly higher significance than $\alpha_{31} > 0$. At $\alpha_{31} = 0.1$, the exclusion level can reach $1 \leq \Delta\chi^2_{A_4} \leq 6$; however, at $\alpha_{31} = -0.1$, $\Delta\chi^2_{A_4}$ ranges from 2.5 to 9.5. The asymmetry is in the opposite way for α_{32} , as $1.6 \leq \Delta\chi^2_{A_4} \leq 6.3$ ($0.4 \leq \Delta\chi^2_{A_4} \leq 4.8$) at $\alpha_{32} = 0.1$ (-0.1).

Parameter d.o.f.	α_{21}	α_{22}	α_{23}
6	$4.8\sigma \sim 5.7\sigma$	$4.8\sigma \sim 5.5\sigma$	$7.8\sigma \sim 10.2\sigma$
12	$3.7\sigma \sim 4.6\sigma$	$3.7\sigma \sim 4.4\sigma$	$6.9\sigma \sim 9.4\sigma$

Table 6: The averaged statistics significance to exclude A_4 symmetry at the 1σ bounds in Table 5 for two possible degrees of freedom (d.o.f.), with adopting Wilks’ theorem. These two cases are considered the maximum and minimum of the possible degrees of freedom. The range is for all possible correlations. The maximum (minimum) number of d.o.f. corresponds to the case that 6 free oscillation parameters and 8 free NSI parameters compared to the A_4 symmetry preserved case with 0 (6) free oscillation parameters and 2 free NSI parameters; $|(6+8) - (0+2)| = 12$ for the maximum, while for the minimum $|(6+8) - (6+2)| = 6$.

To understand the statistics meaning of the result in Figure 5, we need to see Table 6. Giving a flavour model that predicts both oscillation and NSI parameters, we should adopt Wilks’ theorem. Considering the maximum and minimum of possible degrees of freedom for the χ^2 -distribution, in Table

6 we show the average statistical significance $N\sigma$ to exclude the A_4 symmetry by simply using Wilks' theorem in the case with the matter effect corresponding to the 1σ bounds in Table 5. The exclusion level for α_{23} is from 7σ to about 10σ , while that for α_{21} and α_{22} is ranged from $\sim 4\sigma$ to $\sim 6\sigma$.

We conclude this subsection that DUNE has a high potential to test textures predicted by the “ A_4 symmetry” hypothesis, which predicts only diagonal entries of ϵ .

5.3 Testing “ Z_2 symmetry” in DUNE

From the EFT point of view, combining dimension-8 operators with Z_2 -preserving flavon VEV can predict plenty of off-diagonal NSI textures. Therefore, testing the “ Z_2 symmetry” by using Z_2 -motivated NSI textures is more complicated than testing the “ A_4 symmetry”. Fortunately, some of them have stronger constraints than the others if UV completions of these operators are accounted, and only \mathbb{T}_1 , \mathbb{T}_2 , \mathbb{T}_3 and \mathbb{T}_4 may reach the percent level, as shown in Section 4.2. To simplify our discussion, we will only focus on these textures. We re-parametrise their linear combination as follows

$$\begin{pmatrix} -x & x+y-z-iw & x+y+z+iw \\ x-z+iw & z & y-iw \\ x+z-iw & y+iw & -z \end{pmatrix} \quad (66)$$

for the phenomenological benefit, where $x \equiv \alpha_2$, $y \equiv -\frac{\alpha_1}{3} + \frac{2\alpha_2}{3\sqrt{2}}$, $z \equiv \frac{\alpha_3}{\sqrt{3}}$ and $w \equiv \frac{\alpha_{31}}{\sqrt{6}}$. This parametrisation piles two strong constraints $\Delta\epsilon_{\mu\tau}$ and $\Delta\tilde{\epsilon}_{\tau\tau}$ to y and z respectively. As we will see later, this helps us to focus on a simple but not highly excluded structure for the NSI matrix.

Global Fit		Global Fit		DUNE sensitivity	
w^u	–	w^d	–	w	$[-0.013, 0.025]$
x^u	$[-0.034, 0.013]$	x^d	$[-0.035, 0.012]$	x	$[-0.1, 0.1]$
y^u	$[-0.004, 0.003]$	y^d	$[-0.004, 0.003]$	y	$[-0.01, 0.01]$
z^u	$[-0.002, 0.005]$	z^d	$[-0.002, 0.005]$	z	$[-0.007, 0.017]$

Table 7: The 1σ bounds for $x^{u,d}$, $y^{u,d}$, and $z^{u,d}$, by global fit [27] shown in Table 4, and expected 1σ bounds w , x , y , and z , for DUNE with fixed oscillation parameters, assuming true values $w = x = y = z = 0$. The upper-scripts u , d denote NSIs only with u and d quarks, respectively. For both fitting, we allow the other NSI parameters to vary, except for w in the fit using global fit results. To avoid conflicting to the “real $\epsilon_{\alpha\neq\beta}$ ” assumption of global fit, we set $w = 0$ in the second and fourth columns.

Table 7 shows the 1σ constraint on x , y , z , w in Eq. (66) translated from Table 4, and predicted sensitivity for DUNE with fixed oscillation parameters, assuming $w = x = y = z = 0$. For both cases, we test one parameter and allow the others to vary, except for w in the fitting with global fit results. Keeping in mind that a rough factor ‘3’ should be multiplied to $x^{u,d}$, $y^{u,d}$ and $z^{u,d}$ when comparing with x , y and z , we find the precision on x , y , and z for DUNE is competitive to current global fit results. Besides, DUNE is sensitive to the imaginary part w , which however is assumed at zero in the global fit.

We find the result in Table 7 imposes very restricting bounds for y and z around zeros through the elements $\tilde{\epsilon}_{\tau\tau}$ and $\epsilon_{\mu\tau}$, and the possibility of nonzero x . This result motivates us the structure

$$\epsilon = \begin{pmatrix} 0 & x & x \\ x & x & 0 \\ x & 0 & x \end{pmatrix}. \quad (67)$$

Two sum rules can be read out from Eq. (67),

$$\epsilon_{e\mu} = \epsilon_{e\tau} = -\tilde{\epsilon}_{ee}, \quad (68)$$

$$\epsilon_{\mu\tau} = \tilde{\epsilon}_{\tau\tau} = 0. \quad (69)$$

In the following, we study the exclusion level for DUNE to exclude the matter-effect NSIs in the form of Eq. (67). The statistics quantity that we study is

$$\Delta\chi_{Z_2}^2 \equiv \chi^2|_x - \chi_{b.f.}^2, \quad (70)$$

where $\chi^2|_x$ is the χ^2 value defined in Eq.(65), assuming ϵ satisfies the structure Eq. (67). Thus for $\chi^2|_x$ we use x for the NSI parameters, while for $\chi_{b.f.}^2$, the parametrisation $\epsilon_{\alpha\beta}$ is used.

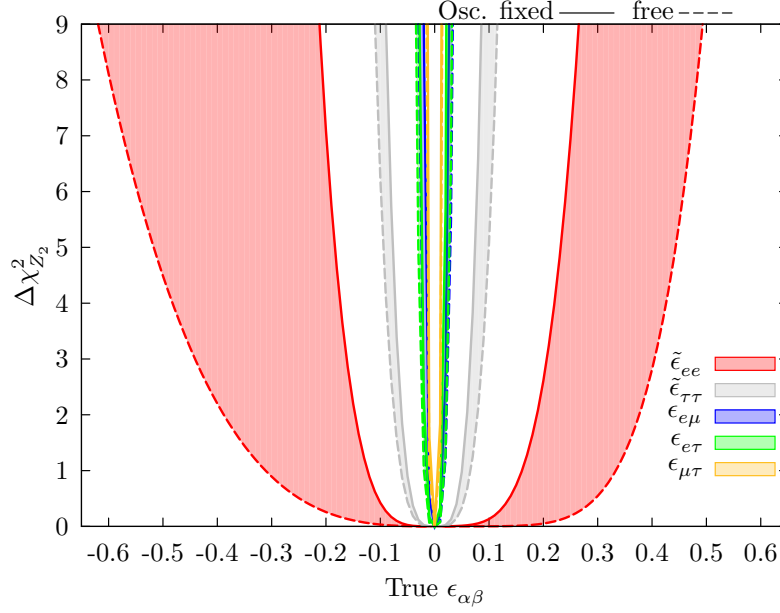


Figure 6: $\Delta\chi_{Z_2}^2$ value (defined in Eq. (70)) to exclude sum rules in Eqs. (68) and (69) over true value of $-0.65 < \epsilon_{\alpha\beta} < 0.65$, for normal mass ordering with $\delta = 270^\circ$. For generality, the solid (dashed) curves are presented for fixed (free) all oscillation parameters, which can be seen as the case with minimum (maximum) correlations with oscillation parameters. Also, we consider all possible numbers of degree of freedom; in the right panel we show how much the average statistics significance $N\sigma$ to exclude this model by simply using Wilks' approximation at the 1σ bounds in Table 4.

In Figure 6, we show $\Delta\chi_{Z_2}^2$ for all possible correlations from $\epsilon_{\alpha\beta}$ or $\epsilon_{\alpha\beta} = -0.65$ to 0.65 . We vary the true value of one certain $\epsilon_{\alpha\beta}$, but fix the others to be zero. We use the same experimental setting and the same oscillation parameters values as those in Section 5.2. For the first sum rule, in Eq. (68), within $[-0.05, +0.05]$, $\epsilon_{e\mu}$ and $\epsilon_{e\tau}$ can reach the significance $\Delta\chi_{Z_2}^2 > 10$. The performance for the ee component is the worst one. For the second sum rule, in Eq. (69), “ $\Delta\chi_{Z_2}^2 < 1$ ” significance covers roughly $-0.05 < \tilde{\epsilon}_{\tau\tau} < 0.05$ and $-0.03 < \epsilon_{\mu\tau} < 0.03$.

As discussed in Section 5.2, we show the statistics significance for every element of NSI matrix with two possible degrees of freedom, at the value of $\tilde{\epsilon}_{\alpha\alpha}$ and $\epsilon_{\alpha\beta}$ corresponding to 1σ bounds in Table 4. These two cases again are for the maximum and minimum of possible degrees of freedom. We find that for $\tau\tau$ and $\mu\tau$ elements, there is no chance to exclude this model. This is because of tight constraint for these two elements in global fit results. We see the high exclusion level for $\epsilon_{e\tau}$; it ranges from 4.7σ to 9.4σ . In the following for $\epsilon_{e\mu}$, the significance is expected from 2σ to 6.1σ . For the ee element, we also see a high significance from 1.1σ to 4.7σ .

d.o.f. \ Parameter	$\tilde{\epsilon}_{ee}$	$\tilde{\epsilon}_{\tau\tau}$	$\epsilon_{e\mu}$	$\epsilon_{e\tau}$	$\epsilon_{\mu\tau}$
7	$2.2\sigma \sim 4.7\sigma$	~ 0	$3.1\sigma \sim 6.1\sigma$	$5.7\sigma \sim 9.4\sigma$	~ 0
13	$1.1\sigma \sim 3.7\sigma$	~ 0	$2\sigma \sim 5.1\sigma$	$4.7\sigma \sim 8.6\sigma$	~ 0

Table 8: The averaged statistics significance to exclude the model Eq. (67) for the value of $\tilde{\epsilon}_{\alpha\alpha}$ or $\epsilon_{\alpha\beta}$ corresponding to 1σ bounds in Table 4 for two possible degrees of freedom, approximated by adopting Wilks' theorem. These two cases are considered the maximum and minimum of the possible degrees of freedom. The range is for all possible correlations. For the number of d.o.f., the maximum (minimum) is the case that 6 free oscillation parameters and 8 free NSI parameters compared to the hypothesis holding pattern Eq.(67) for NSIs with 0 (6) free oscillation parameters and 1 free NSI parameters; $|(6+8)-(0+1)|=13$ for the maximum, while for the minimum $|(6+8)-(6+1)|=7$.

6 Conclusion

Non-Abelian discrete flavour symmetries, as originally proposed to explain lepton flavour mixing, may contribute to other phenomenological signatures beyond the standard case of 3-generation neutrino oscillations. The test of flavour symmetries have been discussed for a while in the charged lepton sector, but has not been mentioned in the neutrino sector by far. In this paper, under the assumption of an A_4 flavour symmetry, we investigate the constraints on matter-effect non-standard interactions (NSIs) imposed by A_4 and, after its breaking, those imposed by the residual symmetry Z_2 . We establish connections between NSIs and flavour symmetries at two levels: the effective field theory level and the UV completion level.

At the effective field theory level, we impose A_4 symmetry to higher-dimensional operators ($d \leq 8$) which result in NSIs in neutrino oscillations. We only consider operators involving 4 SM fermions. We have carefully removed those operators introducing tree-level 4-charged-fermion interactions to avoid the strong constraints from the relevant flavour-violating processes. There are only one dimension-6 operator $\mathcal{O}^1 = \epsilon_{ac}\epsilon_{bd}(\overline{L_{a\alpha}}\gamma^\mu L_{b\beta})(\overline{L_{c\gamma}}\gamma^\mu L_{d\delta})$ and seven dimension-8 operators $\mathcal{O}^{2,3,4,5,6} = (\overline{\nu_{\alpha L}}\gamma^\mu \nu_{\beta L})(\overline{F_\gamma}\gamma_\mu F_\delta)$ (for $F = U_R, D_R, E_R, Q, L$), $\mathcal{O}^7 = (\overline{L_\alpha}\tilde{H}\gamma^\mu L_{b\beta})(\overline{Q_{b\gamma}}\gamma_\mu \tilde{H}^\dagger Q_\delta)$ and $\mathcal{O}^8 = \epsilon_{bc}(\overline{L_\alpha}\tilde{H}\gamma^\mu L_{b\beta})(\overline{Q_\gamma}H\gamma_\mu Q_{c\delta})$ contributing to matter-effect NSIs, shown in Table 1. Following the general approach used in flavour models, the three lepton doublets L_1, L_2 and L_3 are arranged as a triplet of A_4 . For any other SM fermions, we perform a scan of all possible representations in the flavour space. Including a flavon with a Z_2 -preserving VEV, A_4 is broken to Z_2 , and we can obtain Z_2 -motivated NSI textures. Both A_4 -motivated textures and Z_2 -motivated textures have been systematically searched in this work, with the main result listed in Table 2

Then, we consider how to realise these operators by introducing new particles in renormalisable models of A_4 . The dimension-6 operator is realised by introducing electroweak singly-charged scalars as mediators. However, this case is strongly suppressed since couplings for L_1, L_2 and L_3 in A_4 are correlated with each other, and thus strong constraints from CLFV measurements cannot be avoided. Dimension-8 operators are realised by including heavy sterile neutrinos and charged scalars. The operators $\mathcal{O}^{2,3,4,5}$ involve extra fermions $F = U_R, D_R, E_R, Q$. By arranging F as singlets of A_4 , couplings for different generation fermions, i.e., F_i and F_j (for $i \neq j$), are not correlated with each other, and the constraints from CLFV or quark flavour violating processes do not apply to NSIs. Imposing A_4 does not give interesting observable NSI textures. After A_4 is broken to Z_2 , four interesting textures $\mathbb{T}_1, \mathbb{T}_2, \mathbb{T}_3$ and \mathbb{T}_4 , are obtained, as shown in Eq. (50). We regard them as major textures. The main constraints to these textures are from the measurement of the non-unitary effect of the lepton mixing. Including

the experimental constraints, coefficients of these textures may maximally reach 10^{-2} or 10^{-3} level. Arranging F as triplets of A_4 gives additional NSI textures, all strongly constrained by experiments, and we refer them to minor textures.

To understand what we can do with NSI texture in the near future, we apply the A_4 - and Z_2 -motivated NSI textures to analyse how to test the flavour symmetry by measuring NSIs in DUNE. We consider all possible correlations and the maximum and minimum numbers of free parameters, which affect the corresponding statistics significance. Two applications are studied. One is testing “ A_4 symmetry”. The off-diagonal entries of the NSI matrix are forbidden by A_4 symmetry, i.e., $\alpha_{21} = \alpha_{22} = \alpha_{23} = \alpha_{31} = \alpha_{32} = \alpha_{33} = 0$. Excluding this hypothesis can be used to exclude the “ A_4 symmetry”. We foresee that DUNE has the outstanding performance on it. For the case with the maximum and minimum of all possible degree of freedom for the χ^2 -distribution, in Table 6 we show the average statistical significance $N\sigma$ to exclude the A_4 symmetry by simply using Wilks’ theorem in the case with the matter effect corresponding to the 1σ bounds in Table 5. The exclusion level for α_{23} is from 7σ to about 10σ , while that for α_{21} and α_{22} is ranged from $\sim 4\sigma$ to $\sim 6\sigma$. High exclusion levels for α_{3n} ($n = 1, 2, 3$) are also expected. DUNE can constrain NSI parameters competitively with current global data. In particular, it can measure the imaginary part, labelled as w , with the percentage precision. We also suggest to test two sum rules of NSI parameters as shown in Eqs. (68) and (69). We show the statistics significance for excluding the model Eq. (67) for every elements of NSI matrix at the value corresponding to 1σ bounds in Table 4, in the cases with the maximum and minimum of possible degrees of freedom. We find that though for $\tau\tau$ and $\mu\tau$ elements, there is no way to exclude this model, the high exclusion level for $\epsilon_{e\tau}$; it ranges from 4.7σ to 9.4σ . For $\epsilon_{e\mu}$ and $\tilde{\epsilon}_{ee}$, the significance is expected from 2σ to 6.1σ (1.1σ to 4.7σ). We now see a good performance on both applications for DUNE.

To summarise, NSIs in neutrino oscillations have been studied in the framework of non-Abelian discrete flavour symmetries for the first time. Textures of NSIs are predicted by flavour symmetries. Measuring these textures can in principle provide a new way to test flavour symmetries and residual symmetries. It is a complimentary to the studies of flavour symmetries in standard neutrino oscillation measurements and CLFV processes. Our simulation result shows that even though matter NSI effects are predicted to be small for DUNE in general, these could provide extra informations that might extend our understanding of the flavour symmetry. And, we show how useful they are. What we raise up in this article is not only the theoretical feature of a flavour symmetry, but also the idea that we cannot waste these small but useful effects. We especially point out that if A_4 is conserved at the NSI level, it could be hard to see matter-effect NSIs in DUNE. This is because DUNE is less sensitive to those flavour-conserving ones. Therefore, the null result of matter-effect NSIs in DUNE could mean that ‘ A_4 symmetry’ is conserved at the NSI level. And this could still extend our knowledge on the symmetry of flavour at the higher energy.

Acknowledgements

We thank S. Pascoli for very useful discussions and improvements on the manuscript. We are also grateful to A. Olivares-Del Campo for double checking the probability approximation, N. W. Prouse for sharing T2HK simulations and J. Zhang for useful discussions. This work has been supported by the European Research Council under ERC Grant NuMass (FP7-IDEAS-ERC ERC-CG 617143), H2020 funded ELUSIVES ITN (H2020-MSCA-ITN-2015, GA-2015-674896-ELUSIVES), InvisiblePlus (H2020-MSCA-RISE-2015, GA-2015-690575-InvisiblesPlus) and the Science and Technology Facilities Council

(STFC).

A Neutrino oscillation parameters

In the standard case, neutrino oscillations are described by mass-squared differences Δm_{21}^2 , Δm_{31}^2 and Δm_{32}^2 with $\Delta m_{ji}^2 = m_j^2 - m_i^2$ and the mixing matrix U which is parametrised by three mixing angles θ_{ij} and a CP-violating phase δ as

$$U \equiv \begin{pmatrix} 1 & 0 & 0 \\ 0 & c_{23} & s_{23} \\ 0 & -s_{23} & c_{23} \end{pmatrix} \begin{pmatrix} c_{13} & 0 & s_{13}e^{-i\delta} \\ 0 & 1 & 0 \\ -s_{13}e^{i\delta} & 0 & c_{13} \end{pmatrix} \begin{pmatrix} c_{12} & s_{13} & 0 \\ -s_{13} & c_{23} & 0 \\ 0 & 0 & 1 \end{pmatrix}, \quad (71)$$

where $s_{ij} = \sin\theta_{ij}$ and $c_{ij} = \cos\theta_{ij}$. Except for δ , we generally adopt the last global fit results in Table 9, taken from [68], for the true values and the priors. For the consistency, we should assume a flavour model for both oscillation and NSI parameters. However, we do not expect that it makes a large difference since the flavour model should be allowed by global fit results. Further, as the current global result is not changed significantly after including NO ν A data, of which results may have the impact of NSIs, our results do not lose predictability. Except for δ , we implement priors; we assume Gaussian distribution, centred at the true value with the width taken as the 1σ bound from the last global fit results, shown in Table 9. For δ , we do not implement a prior.

Parameter	Normal ordering	Inverted ordering
θ_{12} [°]	$33.56^{+0.77}_{-0.75}$	$33.56^{+0.77}_{-0.75}$
θ_{13} [°]	$8.46^{+0.15}_{-0.15}$	$8.49^{+0.15}_{-0.15}$
θ_{23} [°]	$41.6^{+1.5}_{-1.2}$	$50.0^{+1.1}_{-1.4}$
Δm_{21}^2 [$\times 10^{-5}$ eV ²]	$7.49^{+0.19}_{-0.17}$	$7.49^{+0.19}_{-0.17}$
Δm_{3l}^2 [$\times 10^{-3}$ eV ²]	$+2.524^{+0.039}_{-0.040}$	$-2.514^{+0.038}_{-0.041}$
δ [°]	270	270

Table 9: The true values used in this work, unless otherwise stated explicitly, with their uncertainties (the 1σ range of the priors we have used in our fit). These are based on NuFit 3.0 (2016) [68]. The definition of Δm_{3l}^2 are the same in NuFit 3.0, for normal ordering $\Delta m_{3l}^2 = \Delta m_{31}^2$, while for inverse one, $\Delta m_{3l}^2 = \Delta m_{32}^2$.

A.1 Parameter Setting for A_4 symmetry study

In Section 5.2, we study the potential to exclude the hypothesis preserving the A_4 symmetry for DUNE. The setting for oscillation and NSI parameters in the simulation is summarised in Table 10.

B Textures of NSIs at the source and detector predicted by A_4

In this appendix, we list the textures of NSIs at the source and detector in the framework of A_4 symmetry. These textures are directly dependent upon which representations the fermions are arranged in the flavour symmetry.

	Osc. Para.	α_{12}, α_{13}	α_{2n}, α_{3n}
true values	fix them at <i>b.f.</i>	fix them at 0	change one; fix the other at 0
tested values	all fixed or free	allow them varying	fix all at 0

Table 10: The summary of the setting for the true and tested values, used for studying $\Delta\chi_{A_4}^2$. The oscillation parameters (Osc. Para.) are fixed at the best fit (*b.f.*) of the global fit results in Tab. 9 for the true values. We study both scenarios with fixed and varying oscillation parameters with priors, for considering all possible correlations. The width of priors for oscillation parameters are used the size of 1σ uncertainty of global fit results in Tab. 9. The flavour symmetry A_4 only allows $\{\alpha_{12}, \alpha_{13}\}$, which are fixed at 0 for true values, but allowed to freely vary for tested values. The parameters $\{\alpha_{2n}, \alpha_{3n}\}$ are not allowed by A_4 . For their true values, we study each of them by changing its value from -0.3 to 0.3 , but fix the other at 0. For the tested values, we fix all of them at 0.

NSIs at the source and detector are expressed as 3×3 complex matrices ϵ^s and ϵ^d , respectively, contributing to superpositions of flavour states,

$$|\nu_\alpha^s\rangle = \frac{1}{n_\alpha^s} \left(|\nu_\alpha\rangle + \sum_\beta \epsilon_{\alpha\beta}^s |\nu_\beta\rangle \right), \quad \langle \nu_\beta^d| = \frac{1}{n_\beta^d} \left(\langle \nu_\beta| + \sum_\alpha \epsilon_{\alpha\beta}^d \langle \nu_\alpha| \right), \quad (72)$$

where $n_\alpha^s = \sqrt{\sum_\beta |\delta_{\alpha\beta} + \epsilon_{\alpha\beta}^s|^2}$, $n_\beta^d = \sqrt{\sum_\alpha |\delta_{\alpha\beta} + \epsilon_{\alpha\beta}^d|^2}$ (for $\alpha \neq \beta \neq \gamma \neq \alpha$) are normalisation factors. Replacing A with $-A$ and $\epsilon^{m,d,s}$ with $\epsilon^{m,d,s*}$, we obtain those for antineutrinos. The effective operators describing NSIs for neutrino production at the source and measured at the detector can be expressed as

$$\mathcal{L}_{\text{NSI}} = 2\sqrt{2}G_F \sum_{p=7}^{12} c_{\alpha\beta\gamma\delta}^p \mathcal{O}_{\alpha\beta\gamma\delta}^p + \text{h.c.} \quad (73)$$

Given the higher-dimensional operators in Eq. (19), the relation between the NSI parameters at the source and the detector $\epsilon_{\alpha\beta}^s, \epsilon_{\alpha\beta}^d$ and the higher-dimensional operators is given by

$$\epsilon_{\alpha\beta}^s = \sum_{p=7}^{12} n^{s,p} c_{\alpha\beta 11}^p, \quad \epsilon_{\alpha\beta}^d = \sum_{p=7}^{12} n^{d,p} c_{\alpha\beta 11}^p, \quad (74)$$

where $n^{s,p}$ and $n^{d,p}$ are order-one coefficients, related to the number densities of electron and neutron.

We only require the lepton doublets $L = (L_1, L_2, L_3)^T$ to be a triplet **3** of A_4 ($L\mathbf{3}$) for realise large mixing angles, but we do not specify representations of A_4 for the rest fermions. In other words, they could be any cases in the following:

- Three right-handed charged leptons E_{1R}, E_{2R}, E_{3R} are arranged as different singlets of A_4 or form a triplet **3**. The former case is helpful for realising hierarchical charged lepton masses. Without lose of generality, we consider two cases ($E_R\mathbf{1}$) and ($E_R\mathbf{3}$) for right-handed charged leptons:

$$\begin{aligned} (E_R\mathbf{1}) \quad & E_{1R} \sim \mathbf{1}, E_{2R} \sim \mathbf{1}', E_{3R} \sim \mathbf{1}'', \\ (E_R\mathbf{3}) \quad & E_R = (E_{1R}, E_{2R}, E_{3R}) \sim \mathbf{3}. \end{aligned} \quad (75)$$

- The left-handed quarks Q_1, Q_2, Q_3 may also be arranged as different singlets or form a triplet.

We consider four cases:

$$\begin{aligned}
(Q\mathbf{1}) \quad Q_1 &\sim \mathbf{1}, \\
(Q\mathbf{1}') \quad Q_1 &\sim \mathbf{1}', \\
(Q\mathbf{1}'') \quad Q_1 &\sim \mathbf{1}'', \\
(Q\mathbf{3}) \quad Q &= (Q_1, Q_2, Q_3)^T \sim \mathbf{3}.
\end{aligned} \tag{76}$$

Since Q_2 and Q_3 do not contribute to NSIs in neutrino oscillations, we do not care about their representations.

- Similarly, we will consider two cases for up-type and down-type right-handed quarks, respectively:

$$\begin{aligned}
(U_R\mathbf{1}) \quad U_{1R} &\sim \mathbf{1}, & (D_R\mathbf{1}) \quad D_{1R} &\sim \mathbf{1}, \\
(U_R\mathbf{1}') \quad U_{1R} &\sim \mathbf{1}', & (D_R\mathbf{1}') \quad D_{1R} &\sim \mathbf{1}', \\
(U_R\mathbf{1}'') \quad U_{1R} &\sim \mathbf{1}'', & (D_R\mathbf{1}'') \quad D_{1R} &\sim \mathbf{1}'', \\
(U_R\mathbf{3}) \quad U_R &= (U_{1R}, U_{2R}, U_{3R})^T \sim \mathbf{3}, & (D_R\mathbf{3}) \quad D_R &= (D_{1R}, D_{2R}, D_{3R})^T \sim \mathbf{3}.
\end{aligned} \tag{77}$$

All the above possibilities are considered in this appendix.

B.1 A_4 -invariant operators

We scan all A_4 -invariant operators $c_{\alpha\beta\gamma\delta}^{7-12} \mathcal{O}_{\alpha\beta\gamma\delta}^{7-12}$, which contribute to NSIs at the source and detector. Besides \mathbb{T}_{11} , \mathbb{T}_{12} , \mathbb{T}_{13} in Eq. (22), we have found six more NSI textures:

$$\begin{aligned}
\mathbb{T}'_{11} &= \begin{pmatrix} 0 & 1 & 0 \\ 0 & 0 & 1 \\ 1 & 0 & 0 \end{pmatrix}, & \mathbb{T}'_{12} &= \begin{pmatrix} 0 & -1 & 0 \\ 0 & 0 & 2 \\ -1 & 0 & 0 \end{pmatrix}, & \mathbb{T}'_{13} &= \begin{pmatrix} 0 & -1 & 0 \\ 0 & 0 & 0 \\ 1 & 0 & 0 \end{pmatrix}, \\
\mathbb{T}''_{11} &= \begin{pmatrix} 0 & 0 & 1 \\ 1 & 0 & 0 \\ 0 & 1 & 0 \end{pmatrix}, & \mathbb{T}''_{12} &= \begin{pmatrix} 0 & 0 & -1 \\ -1 & 0 & 0 \\ 0 & 2 & 0 \end{pmatrix}, & \mathbb{T}''_{13} &= \begin{pmatrix} 0 & 0 & 1 \\ -1 & 0 & 0 \\ 0 & 0 & 0 \end{pmatrix}.
\end{aligned} \tag{78}$$

The operators that may result in these correlations are listed in Table 11.

For $c_{\alpha\beta\gamma\delta}^{7-9} \mathcal{O}_{\alpha\beta\gamma\delta}^{7-9}$, the same discussions on $c_{\alpha\beta\gamma\delta}^2 \mathcal{O}_{\alpha\beta\gamma\delta}^2$ apply to these operators. $c_{\alpha\beta\gamma\delta}^{10-12} \mathcal{O}_{\alpha\beta\gamma\delta}^{10-12}$ provides more textures for NSIs at the source and detector. Here we take $\mathcal{O}_{\alpha\beta\gamma\delta}^{12}$ as an example to obtain these textures in details.

- If $L \sim E_R \sim Q \sim U_R \sim \mathbf{3}$, the A_4 -invariant combinations $(\bar{L}E_R)_{\mathbf{3}_S}(\bar{Q}U_R)_{\mathbf{3}_S}$ and $(\bar{L}E_R)_{\mathbf{3}_A}(\bar{Q}U_R)_{\mathbf{3}_S}$ result in \mathbb{T}_{12} and \mathbb{T}_{13} , respectively.
- If $L \sim E_R \sim Q \sim \mathbf{3}$ and $U_{1R} \sim \mathbf{1}'$, the A_4 -invariant combinations $(\bar{L}E_R)_{\mathbf{3}_S}(\bar{Q}U_R)_{\mathbf{3}}$ and $(\bar{L}E_R)_{\mathbf{3}_A}(\bar{Q}U_R)_{\mathbf{3}}$ result in \mathbb{T}'_{12} and \mathbb{T}'_{13} , respectively. Replacing $U_R \sim \mathbf{1}'$ by $U_R \sim \mathbf{1}''$ leads to another two textures \mathbb{T}''_{12} and \mathbb{T}''_{13} , respectively. These relations are also valid for $L \sim E_R \sim U_R \sim \mathbf{3}$, $Q \sim \mathbf{1}''$ and $\mathbf{1}'$, respectively.
- If $L \sim E_R \sim \mathbf{3}$ and $Q_1 \sim U_{1R} \sim \mathbf{1}, \mathbf{1}', \mathbf{1}''$, the A_4 -invariant combinations $(\bar{L}E_R)_{\mathbf{1}}(\bar{Q}U_R)_{\mathbf{1}}$ result in \mathbb{T}_{11} . If Q_1 and U_{1R} belong to different singlets of A_4 , we obtain \mathbb{T}'_{11} and \mathbb{T}''_{11} for $\bar{Q}_1 U_{1R} \sim \mathbf{1}'$ and $\mathbf{1}''$, respectively.

	Representations	A_4 -invariant operators	NSI textures
\mathcal{O}^{7-9}	$(L\mathbf{3})$	$(\bar{L}L)_1(\bar{F}F)_1$	\mathbb{T}_{11}
	$(L\mathbf{3}, F\mathbf{3})$	$(\bar{L}L)_{\mathbf{3}_S}(\bar{F}F)_{\mathbf{3}_S}$	\mathbb{T}_{12}
		$(\bar{L}L)_{\mathbf{3}_A}(\bar{F}F)_{\mathbf{3}_S}$	\mathbb{T}_{13}
$\mathcal{O}^{10,12}$	$(L\mathbf{3}, E_R\mathbf{3}, Q\mathbf{3}, U_R\mathbf{3})$	$(\bar{L}E_R)_1(\bar{Q}U_R)_1$	\mathbb{T}_{11}
		$(\bar{L}E_R)_{\mathbf{3}_S}(\bar{Q}U_R)_{\mathbf{3}_S}$	\mathbb{T}_{12}
		$(\bar{L}E_R)_{\mathbf{3}_A}(\bar{Q}U_R)_{\mathbf{3}_S}$	\mathbb{T}_{13}
	$(L\mathbf{3}, E_R\mathbf{3}, Q\mathbf{3}, U_R\mathbf{1}^{(\prime,\prime)})$ or $(L\mathbf{3}, E_R\mathbf{3}, Q\mathbf{1}^{(\prime,\prime)}, U_R\mathbf{3})$	$(\bar{L}E_R)_{\mathbf{3}_S}(\bar{Q}U_R)_{\mathbf{3}}$	$\mathbb{T}_{12}^{(\prime,\prime)}$
		$(\bar{L}E_R)_{\mathbf{3}_A}(\bar{Q}U_R)_{\mathbf{3}}$	$\mathbb{T}_{13}^{(\prime,\prime)}$
	$(L\mathbf{3}, E_R\mathbf{3}, Q\mathbf{1}, U_R\mathbf{1}^{(\prime,\prime)})$, $(L\mathbf{3}, E_R\mathbf{3}, Q\mathbf{1}', U_R\mathbf{1}'^{(\prime,0)})$ or $(L\mathbf{3}, E_R\mathbf{3}, Q\mathbf{1}'', U_R\mathbf{1}''^{(0,\prime)})$	$(\bar{L}E_R)_{\mathbf{1}^{(\prime,\prime)}}(\bar{Q}U_R)_{\mathbf{1}^{(\prime,\prime)}}$	$\mathbb{T}_{11}^{(\prime,\prime)}$
	$(L\mathbf{3}, E_R\mathbf{1}, Q\mathbf{3}, U_R\mathbf{3})$	$(\bar{L}E_R)_{\mathbf{3}}(\bar{Q}U_R)_{\mathbf{3}_S}$	$D_1\mathbb{T}_{11}$
	$(L\mathbf{3}, E_R\mathbf{1}, Q\mathbf{1}^{(\prime,\prime)}, U_R\mathbf{3})$ or $(L\mathbf{3}, E_R\mathbf{1}, Q\mathbf{3}, U_R\mathbf{1}^{(\prime,\prime)})$	$(\bar{L}E_R)_{\mathbf{3}}(\bar{Q}U_R)_{\mathbf{3}}$	$D_2\mathbb{T}_{11}^{(\prime,\prime)}$
\mathcal{O}^{11}	Results are obtained from those of $\mathcal{O}^{10,12}$ after the replacements $\bar{Q} \rightarrow \overline{D_R}$ and $U_R \rightarrow Q$.		

Table 11: Operators preserving A_4 symmetry and the predicted NSI textures at the neutrino source and detector, where F represents any fermion content in the SM and $\mathbf{1}^0 \equiv \mathbf{1}$, D_i are arbitrary diagonal matrices. The notations of the representations are understood as follows. For instance, $(L\mathbf{3}, E\mathbf{3}, Q\mathbf{1}^{(\prime,\prime)}, U\mathbf{3})$ means $L \sim \mathbf{3}, e \sim \mathbf{3}, Q \sim \mathbf{1}^{(\prime,\prime)}, u \sim \mathbf{3}$ and D_R can take arbitrary representations of A_4 . The textures $\mathbb{T}_{1n}^{(\prime,\prime)}$ are shown in Eq. (78).

- If $L \sim Q \sim U_R \sim \mathbf{3}$, $E_{1R} \sim \mathbf{1}, E_{2R} \sim \mathbf{1}', E_{3R} \sim \mathbf{1}''$, we obtain the A_4 -invariant combinations $\sum_i y_i (\bar{L}E_{iR})_{\mathbf{3}}(\bar{Q}U_R)_{\mathbf{3}}$ and $\sum_i y'_i (\bar{L}E_{iR})_{\mathbf{3}}(\bar{Q}U_R)_{\mathbf{3}_A}$, which we denote as $(\bar{L}E_R)_{\mathbf{3}}(\bar{Q}U_R)_{\mathbf{3}}$ and $(\bar{L}E_R)_{\mathbf{3}}(\bar{Q}U_R)_{\mathbf{3}_A}$, respectively. Here, y_i and y'_i are arbitrary parameters. We find for the first term

$$c_{\alpha\beta 11} = 0 \quad \text{for } \alpha \neq \beta. \quad (79)$$

Then the NSI matrix $\epsilon^{s,d}$ can be re-expressed as $D_1\mathbb{T}_{11}$, where D_1 is an arbitrary diagonal matrix. The second operator does not contribute to NSIs.

- If $L \sim U_R \sim \mathbf{3}$, $E_{1R} \sim \mathbf{1}, E_{2R} \sim \mathbf{1}', E_{3R} \sim \mathbf{1}''$ and $Q \sim \mathbf{1}$, the A_4 -invariant combinations $(\bar{L}E_R)_{\mathbf{3}}(\bar{Q}U_R)_{\mathbf{3}_S}$ only result in an arbitrary diagonal matrix, just like the former item, and we express the NSI matrix $\epsilon^{s,d}$ as $D_2\mathbb{T}_{11}$, where D_2 is an arbitrary matrix. Once we change the representation of Q to be $\mathbf{1}^{(\prime,\prime)}$, the order of the three components of the triplet $(\bar{Q}U_R)_{\mathbf{3}_S}$ will be changed, and we arrive at $D_2\mathbb{T}_{11}^{(\prime,\prime)}$.

Since $\mathcal{O}_{\alpha\beta\gamma\delta}^{10}$ is only different from $\mathcal{O}_{\alpha\beta\gamma\delta}^{12}$ by the Lorentz indices, it gives the same types of correlations as the latter. $\mathcal{O}_{\alpha\beta\gamma\delta}^{11}$ has a different particle arrangement from $\mathcal{O}_{\alpha\beta\gamma\delta}^{12}$. Performing the replacements $\bar{Q} \rightarrow \overline{D_R}$ and $Q \rightarrow U_R$, all the discussions on $\mathcal{O}_{\alpha\beta\gamma\delta}^{12}$ apply to $\mathcal{O}_{\alpha\beta\gamma\delta}^{11}$.

The textures in Eq. (78) only appear at the neutrino source and detector and the NSI matrices $\epsilon^{s,d}$ may be combinations of some of I_i , I'_i and I''_i , depending the choices of representations of A_4 to which E_R , Q , U_R and D_R belong. For instance, if $E_{1R} \sim \mathbf{1}$, $E_{2R} \sim \mathbf{1}'$, $E_{3R} \sim \mathbf{1}''$, $Q \sim \mathbf{3}$, $U_{1R} \sim \mathbf{1}$, $D_{1R} \sim \mathbf{1}$,

we get a combination of NSI textures at the source and the detector as that in matter,

$$\epsilon^{s,d} = \mathbb{T}_{11}\alpha_{11}^{s,d} + \mathbb{T}_{12}\alpha_{12}^{s,d} + \mathbb{T}_{13}\alpha_{13}^{s,d}. \quad (80)$$

where $\alpha_{1n}^{s,d}$ are complex parameters. Changing the representation of U_{1R} to $\mathbf{1}'$, we arrive at

$$\epsilon^{s,d} = \mathbb{T}_{11}\alpha_{11}^{s,d} + \mathbb{T}_{12}\alpha_{12}^{s,d} + \mathbb{T}_{13}\alpha_{13}^{s,d} + \mathbb{T}'_{11}\alpha_{11}'^{s,d} + \mathbb{T}_{12}\alpha_{12}'^{s,d} + \mathbb{T}_{13}\alpha_{13}'^{s,d}, \quad (81)$$

where $\alpha_{1n}^{(l)s,d}$ are complex parameters.

B.2 Z_2 -invariant operators

	Representations	Z_2 -invariant operators	NSI textures
$\chi\mathcal{O}^{7-9}$	$(L\mathbf{3})$	$\chi(\bar{L}L)_{\mathbf{3}_S}(\bar{F}F)_{\mathbf{1}}$	$\mathbb{T}_{12} + \mathbb{T}_{22}$
		$\chi(\bar{L}L)_{\mathbf{3}_A}(\bar{F}F)_{\mathbf{1}}$	$\mathbb{T}_{13} + \mathbb{T}_{23}$
	$(L\mathbf{3}, F\mathbf{3})$	$\chi((\bar{L}L)_{\mathbf{3}_S}(\bar{F}F)_{\mathbf{3}_S})_{\mathbf{3}_S}$	$2\mathbb{T}_{12} - \mathbb{T}_{22}$
		$\chi((\bar{L}L)_{\mathbf{3}_A}(\bar{F}F)_{\mathbf{3}_S})_{\mathbf{3}_S}$	$2\mathbb{T}_{13} - \mathbb{T}_{23}$
		$\chi((\bar{L}L)_{\mathbf{3}_S}(\bar{F}F)_{\mathbf{3}_S})_{\mathbf{3}_A}$	\mathbb{T}_{32}
		$\chi((\bar{L}L)_{\mathbf{3}_A}(\bar{F}F)_{\mathbf{3}_S})_{\mathbf{3}_A}$	\mathbb{T}_{33}
$\chi\mathcal{O}^{10,12}$	$(L\mathbf{3}, E_R\mathbf{3}, Q\mathbf{3}, U_R\mathbf{3})$	$\chi((\bar{L}E_R)_{\mathbf{3}_S}(\bar{Q}U_R)_{\mathbf{3}_S})_{\mathbf{3}_S}$	$2\mathbb{T}_{12} - \mathbb{T}_{22}$
		$\chi((\bar{L}E_R)_{\mathbf{3}_A}(\bar{Q}U_R)_{\mathbf{3}_S})_{\mathbf{3}_S}$	$2\mathbb{T}_{13} - \mathbb{T}_{23}$
		$\chi((\bar{L}E_R)_{\mathbf{3}_S}(\bar{Q}U_R)_{\mathbf{3}_S})_{\mathbf{3}_A}$	\mathbb{T}_{32}
		$\chi((\bar{L}E_R)_{\mathbf{3}_A}(\bar{Q}U_R)_{\mathbf{3}_S})_{\mathbf{3}_A}$	\mathbb{T}_{33}
	$(L\mathbf{3}, E_R\mathbf{3}, Q\mathbf{3}, U_R\mathbf{1}^{(l,\prime)})$ or $(L\mathbf{3}, E_R\mathbf{3}, Q\mathbf{1}^{(l,\prime)}, U_R\mathbf{3})$	$\chi((\bar{L}E_R)_{\mathbf{3}_S}(\bar{Q}U_R)_{\mathbf{3}})_{\mathbf{3}_S}$	$2\mathbb{T}_{12} - \mathbb{T}_{22}$
		$\chi((\bar{L}E_R)_{\mathbf{3}_A}(\bar{Q}U_R)_{\mathbf{3}})_{\mathbf{3}_S}$	$2\mathbb{T}_{13} - \mathbb{T}_{23}$
		$\chi((\bar{L}E_R)_{\mathbf{3}_S}(\bar{Q}U_R)_{\mathbf{3}})_{\mathbf{3}_A}$	\mathbb{T}_{32}
		$\chi((\bar{L}E_R)_{\mathbf{3}_A}(\bar{Q}U_R)_{\mathbf{3}})_{\mathbf{3}_A}$	\mathbb{T}_{33}
	$(L\mathbf{3}, E_R\mathbf{3}, Q\mathbf{1}, U_R\mathbf{1}^{(l,\prime)})$, $(L\mathbf{3}, E_R\mathbf{3}, Q\mathbf{1}', U_R\mathbf{1}^{(l,\prime,0)})$ or $(L\mathbf{3}, E_R\mathbf{3}, Q\mathbf{1}'', U_R\mathbf{1}^{(l,\prime,0)})$	$\chi((\bar{L}E_R)_{\mathbf{3}_S}(\bar{Q}U_R)_{\mathbf{1},\mathbf{1}',\mathbf{1}''})_{\mathbf{3}}$	$\mathbb{T}_{12} + \mathbb{T}_{22}$
		$\chi((\bar{L}E_R)_{\mathbf{3}_S}(\bar{Q}U_R)_{\mathbf{1},\mathbf{1}',\mathbf{1}''})_{\mathbf{3}}$	$\mathbb{T}_{13} + \mathbb{T}_{23}$
	$(L\mathbf{3}, E_R\mathbf{1}, Q\mathbf{3}, U_R\mathbf{3})$	$\chi(\bar{L}E_R)_{\mathbf{3}}(\bar{Q}U_R)_{\mathbf{1}}$	$D_3\mathbb{T}'_1\mathbb{T}_{11}$
		$\chi((\bar{L}E_R)_{\mathbf{3}}(\bar{Q}U_R)_{\mathbf{3}_S})_{\mathbf{3}_S}$	$D_4\mathbb{T}'_1\mathbb{T}_{12}$
		$\chi((\bar{L}E_R)_{\mathbf{3}}(\bar{Q}U_R)_{\mathbf{3}_S})_{\mathbf{3}_A}$	$D_5\mathbb{T}'_1\mathbb{T}_{13}$
	$(L\mathbf{3}, E_R\mathbf{1}, Q\mathbf{1}^{(l,\prime)}, U_R\mathbf{3})$ or $(L\mathbf{3}, E_R\mathbf{1}, Q\mathbf{3}, U_R\mathbf{1}^{(l,\prime)})$	$\chi((\bar{L}E_R)_{\mathbf{3}}(\bar{Q}U_R)_{\mathbf{3}})_{\mathbf{3}_S}$	$D_6\mathbb{T}'_1\mathbb{T}_{12}$
		$\chi((\bar{L}E_R)_{\mathbf{3}}(\bar{Q}U_R)_{\mathbf{3}})_{\mathbf{3}_A}$	$D_7\mathbb{T}'_1\mathbb{T}_{13}$
$\chi\mathcal{O}^{11}$	Results are obtained from those of $\chi\mathcal{O}^{10,12}$ after the replacements $\bar{Q} \rightarrow \bar{D}_R$ and $U_R \rightarrow Q$.		

Table 12: Operators preserving the residual symmetry Z_2 , $Z_2 \subset A_4$, and the resulted NSI textures at the neutrino source and detector, where F represents any fermion content in the SM. The NSI parameter correlations \mathbb{T}_{2n} and \mathbb{T}_{3n} are shown in Eq. (33). D_i are arbitrary diagonal matrices.

Once the operators \mathcal{O}^{7-12} couple to the flavon VEV, $\chi = (1, 1, 1)^T v_\chi$, new NSI textures at the source and detector are predicted, as summarized in Table 12. $\chi_{\alpha'}\mathcal{O}_{\alpha\beta\gamma\delta}^{7-9}$ give rise to the same textures as in

Eq. (33). For $\chi_{\alpha'} \mathcal{O}_{\alpha\beta\gamma\delta}^{10-12}$, we follow the same procedure as that in the last section, taking $\chi_{\alpha'} \mathcal{O}_{\alpha\beta\gamma\delta}^{12}$ as an example:

- If $L \sim E_R \sim Q \sim U_R \sim \mathbf{3}$, the Z_2 -invariant operators $\chi((\bar{L}E_R)_{\mathbf{3}_S}(\bar{Q}U_R)_{\mathbf{3}_S})_{\mathbf{3}_S}$, $\chi((\bar{L}E_R)_{\mathbf{3}_A}(\bar{Q}U_R)_{\mathbf{3}_S})_{\mathbf{3}_S}$, $\chi((\bar{L}E_R)_{\mathbf{3}_S}(\bar{Q}U_R)_{\mathbf{3}_A})_{\mathbf{3}_A}$ and $\chi((\bar{L}E_R)_{\mathbf{3}_A}(\bar{Q}U_R)_{\mathbf{3}_S})_{\mathbf{3}_A}$ result in the textures $3\mathbb{T}_{12} - \mathbb{T}_{22}$, $3\mathbb{T}_{13} + \mathbb{T}_{23}$, \mathbb{T}_{32} and \mathbb{T}_{33} , respectively. Changing the representations to $L \sim E_R \sim Q \sim \mathbf{3}$ and $U_{1R} \sim \mathbf{1}^{(\prime\prime)}$, or $L \sim E_R \sim U_R \sim \mathbf{3}$ and $Q_1 \sim \mathbf{1}^{(\prime\prime)}$, we arrive at the same textures.
- If $L \sim E_R \sim \mathbf{3}$ and $Q_1, U_{1R} \sim \mathbf{1}, \mathbf{1}', \mathbf{1}''$, the Z_2 -invariant combinations $\chi((\bar{L}E_R)_{\mathbf{3}_S}(\bar{Q}U_R)_{\mathbf{1}, \mathbf{1}', \mathbf{1}''})_{\mathbf{3}}$, $\chi((\bar{L}E_R)_{\mathbf{3}_A}(\bar{Q}U_R)_{\mathbf{1}, \mathbf{1}', \mathbf{1}''})_{\mathbf{3}}$ result in \mathbb{T}_{21} and \mathbb{T}_{22} , respectively.
- If $L \sim Q \sim U_R \sim \mathbf{3}$, $E_{1R} \sim \mathbf{1}$, $E_{2R} \sim \mathbf{1}'$, $E_{3R} \sim \mathbf{1}''$, the operator $\sum_i y_i'' \chi(\bar{L}E_{iR})_{\mathbf{3}}(\bar{Q}U_R)_{\mathbf{1}}$ requires

$$c_{ee11} = c_{e\mu11} = c_{e\tau11}, \quad c_{\mu e11} = c_{\mu\mu11} = c_{\mu\tau11}, \quad c_{\tau e11} = c_{\tau\mu11} = c_{\tau\tau11}, \quad (82)$$

where there is no correlation between $c_{\alpha\beta11}$ and $c_{\alpha'\beta'11}$ once $\alpha \neq \alpha'$. It gives rise to the NSI texture

$$\begin{pmatrix} y_1'' & y_1'' & y_1'' \\ y_2'' & y_2'' & y_2'' \\ y_3'' & y_3'' & y_3'' \end{pmatrix} = \begin{pmatrix} y_1'' & 0 & 0 \\ 0 & y_2'' & 0 \\ 0 & 0 & y_3'' \end{pmatrix} \mathbb{T}'_1 \mathbb{T}_{11}, \quad (83)$$

where

$$\mathbb{T}'_1 = \begin{pmatrix} 1 & 1 & 1 \\ 1 & 1 & 1 \\ 1 & 1 & 1 \end{pmatrix}. \quad (84)$$

$\chi((\bar{L}E_R)_{\mathbf{3}}(\bar{Q}U_R)_{\mathbf{3}_S})_{\mathbf{3}_S}$ and $\chi((\bar{L}E_R)_{\mathbf{3}}(\bar{Q}U_R)_{\mathbf{3}_S})_{\mathbf{3}_A}$ lead to

$$\begin{aligned} c_{ee11} &= -2c_{e\mu11} = -2c_{e\tau11}, \quad c_{\mu e11} = -2c_{\mu\mu11} = -2c_{\mu\tau11}, \quad c_{\tau e11} = -2c_{\tau\mu11} = -2c_{\tau\tau11}; \\ c_{e\mu11} &= -c_{e\tau11}, \quad c_{\mu\mu11} = -c_{\mu\tau11}, \quad c_{\tau\mu11} = -c_{\tau\tau11}, \end{aligned} \quad (85)$$

respectively, also no correlation between $c_{\alpha\beta11}$ and $c_{\alpha'\beta'11}$ for $\alpha \neq \alpha'$ in each case. From these two operators, we obtain the NSI textures

$$D_4 \mathbb{T}'_1 \mathbb{T}_{12}, \quad D_5 \mathbb{T}'_1 \mathbb{T}_{13}, \quad (86)$$

respectively, where D_i are independently arbitrary diagonal matrices. Replacing the representation of Q to be any singlet $\mathbf{1}$, $\mathbf{1}'$ or $\mathbf{1}''$, we obtain the Z_2 -invariant operators $\chi((\bar{L}E_R)_{\mathbf{3}}(\bar{Q}U_R)_{\mathbf{3}})_{\mathbf{3}_S}$ and $\chi((\bar{L}E_R)_{\mathbf{3}}(\bar{Q}U_R)_{\mathbf{3}})_{\mathbf{3}_A}$, which give the similar textures $D_6 \mathbb{T}'_1 \mathbb{T}_{12}$ and $D_7 \mathbb{T}'_1 \mathbb{T}_{13}$, respectively, with D_6 and D_7 being arbitrary diagonal matrices.

C Mathematical properties of \mathbb{T}_i

The textures \mathbb{T}_i satisfy the following interesting mathematical properties. They are helpful for our discussion in Section 4.

- \mathbb{T}_i (for $i = 1, 2, 3, 4$) form the following “closed” algebras,

$$\mathbb{T}_i^2 = \mathbb{T}_1, \quad \mathbb{T}_1 \mathbb{T}_i = \mathbb{T}_i, \quad \mathbb{T}_2 \mathbb{T}_3 = -i\mathbb{T}_4, \quad \mathbb{T}_2 \mathbb{T}_4 = i\mathbb{T}_3, \quad \mathbb{T}_3 \mathbb{T}_4 = -i\mathbb{T}_2. \quad (87)$$

- Given two 3×3 coupling matrices or mass matrices $M_1 = \alpha_0 \mathbb{1} + \sum_{i=1}^4 \alpha_i \mathbb{T}_i$ and $M_2 = \beta_0 \mathbb{1} + \sum_{i=1}^4 \beta_i \mathbb{T}_i$, their product $M_1 M_2$ is a linear combination of $\mathbb{1}$ and \mathbb{T}_i ,

$$\begin{aligned}
M_1 M_2 = & \alpha_0 \beta_0 \mathbb{1} + (\alpha_0 \beta_1 + \alpha_1 \beta_0 + \alpha_1 \beta_1 + \alpha_2 \beta_2 + \alpha_3 \beta_3 + \alpha_4 \beta_4) \mathbb{T}_1 \\
& + (\alpha_0 \beta_2 + \alpha_2 \beta_0 + \alpha_1 \beta_2 + \alpha_2 \beta_1 + i\alpha_4 \beta_3 - i\alpha_3 \beta_4) \mathbb{T}_2 \\
& + (\alpha_0 \beta_3 + \alpha_3 \beta_0 + \alpha_1 \beta_3 + \alpha_3 \beta_1 + i\alpha_2 \beta_4 - i\alpha_4 \beta_2) \mathbb{T}_3 \\
& + (\alpha_0 \beta_4 + \alpha_4 \beta_0 + \alpha_1 \beta_4 + \alpha_4 \beta_1 + i\alpha_3 \beta_2 - i\alpha_2 \beta_3) \mathbb{T}_4.
\end{aligned} \tag{88}$$

- If M_1 is reversible, the inverse matrix M_1^{-1}

$$M_1^{-1} = \frac{\alpha_0}{\det A} \left[\frac{\det A}{\alpha_0^2} \mathbb{1} + \left(\alpha_0 + \alpha_1 - \frac{\det A}{\alpha_0^2} \right) \mathbb{T}_1 - \alpha_2 \mathbb{T}_2 - \alpha_3 \mathbb{T}_3 - \alpha_4 \mathbb{T}_4 \right], \tag{89}$$

where $\det M_1 = \alpha_0(\alpha_0^2 + 2\alpha_0\alpha_1 + \alpha_1^2 - \alpha_2^2 - \alpha_3^2 - \alpha_4^2)$, is also a linear combination of $\mathbb{1}$ and \mathbb{T}_i .

By setting some of α_i or β_i to zero, the following corollaries are obtained:

- $\mathbb{1}$ and \mathbb{T}_1 form a closed algebra, if M_1, M_2 are linear combinations of $\mathbb{1}$ and \mathbb{T}_1 , their product and inverse matrices (if reversible) are also linear combinations of $\mathbb{1}$ and \mathbb{T}_1 .
- $\mathbb{1}, \mathbb{T}_1$ and \mathbb{T}_2 form a closed algebra, if M_1, M_2 are linear combinations of $\mathbb{1}, \mathbb{T}_1$ and \mathbb{T}_2 , their product and inverse matrices (if reversible) are also linear combinations of $\mathbb{1}, \mathbb{T}_1$ and \mathbb{T}_2 .
- $\mathbb{1}, \mathbb{T}_1$ and \mathbb{T}_3 form a closed algebra, if M_1, M_2 are linear combinations of $\mathbb{1}, \mathbb{T}_1$ and \mathbb{T}_2 , their product and inverse matrices (if reversible) are also linear combinations of $\mathbb{1}, \mathbb{T}_1$ and \mathbb{T}_3 .

D Oscillation probabilities with matter-effect NSIs

To understand the impact of α_{mn}^m (in the following, we simply use α_{mn}) on neutrino oscillation probabilities, we are based on the knowledge of the probabilities with non-zero $\epsilon_{\alpha\beta}^m$ (in the following, we simply use $\epsilon_{\alpha\beta}$). Therefore we firstly study the probability including the NSI matter effects in terms of $\epsilon_{\alpha\beta}$, and then by using the relations between two parameter sets Table 3, we can extend our understanding on how flavour symmetry model realises at oscillation probability through matter-effect NSI.

Assuming $\sqrt{\frac{\Delta m_{21}^2}{\Delta m_{31}^2}} \sim \sqrt{|\epsilon_{\alpha\beta}|} \sim s_{13}$ as the 1st order perturbation terms ξ , we expand the disappearance oscillation probability $P(\nu_\mu \rightarrow \nu_\mu)$ and appearance oscillation probability $P(\nu_\mu \rightarrow \nu_e)$. These equations are given with the leading-ordering coefficient for each $\epsilon_{\alpha\beta}$ to understand how each elements affect to the probability at the leading order^{vii},

$$\begin{aligned}
P(\nu_\mu \rightarrow \nu_\mu) = & P_0(\nu_\mu \rightarrow \nu_\mu) + \delta P_{\text{NSI}}(\nu_\mu \rightarrow \nu_\mu) \\
\approx & P_0(\nu_\mu \rightarrow \nu_\mu) \\
& - A\epsilon_{\mu\tau} \cos \phi_{\mu\tau} \left(\sin^3 2\theta_{23} \frac{L}{2E} \sin 2\Delta_{31} L + 4 \sin 2\theta_{23} \cos^2 2\theta_{23} \frac{1}{\Delta m_{31}^2} \sin^2 \Delta_{31} L \right) \\
& - A\tilde{\epsilon}_{\tau\tau} c_{23}^2 s_{23}^2 (c_{23}^2 - s_{23}^2) \left(\frac{L}{8E} \sin 2\Delta_{31} L - \frac{1}{\Delta m_{31}^2} \sin^2 \Delta_{31} L \right) \\
& + C_{\mu \rightarrow e; e\mu}^1 |\epsilon_{e\mu}| + C_{\mu \rightarrow e; e\tau}^1 |\epsilon_{e\tau}| + C_{\mu \rightarrow e; ee}^2 \tilde{\epsilon}_{ee},
\end{aligned} \tag{90}$$

^{vii}Our result is consistent with those in Ref. [70].

$$\begin{aligned}
P(\nu_\mu \rightarrow \nu_e) &= P_0(\nu_\mu \rightarrow \nu_e) + \delta P_{\text{NSI}}(\nu_\mu \rightarrow \nu_e) \\
&\approx P_0(\nu_\mu \rightarrow \nu_e) \\
&\quad + 8s_{13}|\epsilon_{e\mu}|s_{23}\frac{\Delta m_{31}^2}{\Delta m_{31}^2 - A}\sin\Delta_{31}^A L \\
&\quad \times \left(s_{23}^2\frac{A}{\Delta m_{31}^2 - A}\cos(\delta + \phi_{e\mu})\sin\Delta_{31}^A L + c_{23}^2\sin\frac{AL}{4E}\cos(\delta + \phi_{e\mu} - \Delta_{31}L) \right) \\
&\quad + 8s_{13}|\epsilon_{e\tau}|c_{23}s_{23}^2\frac{\Delta m_{31}^2}{\Delta m_{31}^2 - A}\sin\Delta_{31}^A L \\
&\quad \times \left(\frac{A}{\Delta m_{31}^2 - A}\cos(\delta + \phi_{e\tau})\sin\Delta_{31}^A L - \sin\frac{AL}{4E}\cos(\delta + \phi_{e\tau} - \Delta_{31}L) \right) \\
&\quad + \mathcal{C}_{\mu\rightarrow e;\mu\tau}^2|\epsilon_{\mu\tau}| + \mathcal{C}_{\mu\rightarrow e;ee}^2\tilde{\epsilon}_{ee} + \mathcal{C}_{\mu\rightarrow e;\tau\tau}^2\tilde{\epsilon}_{\tau\tau}, \tag{91}
\end{aligned}$$

where $P_0(\nu_\alpha \rightarrow \nu_\beta)$ is the transition probability for $\nu_\alpha \rightarrow \nu_\beta$ without NSI matter effects, $\Delta_{31} \equiv \frac{\Delta m_{31}^2}{4E}$, $\Delta_{31}^A \equiv \frac{\Delta m_{31}^2 - A}{4E}$. Here, for the coefficient $\mathcal{C}_{\text{channel}; \text{element}}^{\text{order}}$, the upper index gives the order of this coefficient, and the lower one gives the channel and the element.

channel	$\nu_\mu \rightarrow \nu_\mu$	$\nu_\mu \rightarrow \nu_e$
$\tilde{\epsilon}_{ee}$	$\mathcal{C}_{\mu\rightarrow\mu;ee}^2$	$\mathcal{C}_{\mu\rightarrow e;ee}^2$
$\tilde{\epsilon}_{\tau\tau}$	$\mathcal{C}_{\mu\rightarrow\mu;\tau\tau}^0$	$\mathcal{C}_{\mu\rightarrow e;\tau\tau}^2$
$\epsilon_{e\mu}$	$\mathcal{C}_{\mu\rightarrow\mu;e\mu}^1$	$\mathcal{C}_{\mu\rightarrow e;e\mu}^1$
$\epsilon_{e\tau}$	$\mathcal{C}_{\mu\rightarrow\mu;e\tau}^1$	$\mathcal{C}_{\mu\rightarrow e;e\tau}^1$
$\epsilon_{\mu\tau}$	$\mathcal{C}_{\mu\rightarrow\mu;\mu\tau}^0$	$\mathcal{C}_{\mu\rightarrow e;\mu\tau}^2$
α_{12}	$\mathcal{C}_{\mu\rightarrow\mu;ee}^2$	$\mathcal{C}_{\mu\rightarrow e;ee}^2$
α_{13}	$-\sqrt{2}\mathcal{C}_{\mu\rightarrow\mu;\tau\tau}^0$	$\frac{1}{2}\mathcal{C}_{\mu\rightarrow e;ee}^2 - \sqrt{2}\mathcal{C}_{\mu\rightarrow e;\tau\tau}^2$
α_{21}	$\frac{1}{\sqrt{6}}\mathcal{C}_{\mu\rightarrow\mu;\mu\tau}^0$	$\frac{1}{\sqrt{6}}\mathcal{RC}_{\mu\rightarrow e;e\mu}^1 + \frac{1}{\sqrt{6}}\mathcal{RC}_{\mu\rightarrow e;e\tau}^1$
α_{22}	$\frac{1}{\sqrt{3}}\mathcal{C}_{\mu\rightarrow\mu;\mu\tau}^0$	$\frac{1}{\sqrt{12}}\mathcal{RC}_{\mu\rightarrow e;e\mu}^1 + \frac{1}{\sqrt{12}}\mathcal{RC}_{\mu\rightarrow e;e\tau}^1$
α_{23}	$-\frac{1}{2}\mathcal{RC}_{\mu\rightarrow\mu;e\mu}^1 + \frac{1}{2}\mathcal{RC}_{\mu\rightarrow\mu;e\tau}^1$	$-\frac{1}{2}\mathcal{RC}_{\mu\rightarrow e;e\mu}^1 + \frac{1}{2}\mathcal{RC}_{\mu\rightarrow e;e\tau}^1$
α_{31}	$-\frac{1}{\sqrt{6}}\mathcal{IC}_{\mu\rightarrow\mu;e\mu}^1 + \frac{1}{\sqrt{6}}\mathcal{IC}_{\mu\rightarrow\mu;e\tau}^1$	$-\frac{1}{\sqrt{6}}\mathcal{IC}_{\mu\rightarrow e;e\mu}^1 + \frac{1}{\sqrt{6}}\mathcal{IC}_{\mu\rightarrow e;e\tau}^1$
α_{32}	$\frac{1}{\sqrt{12}}\mathcal{IC}_{\mu\rightarrow\mu;e\mu}^1 - \frac{1}{\sqrt{12}}\mathcal{IC}_{\mu\rightarrow\mu;e\tau}^1$	$\frac{1}{\sqrt{12}}\mathcal{IC}_{\mu\rightarrow e;e\mu}^1 - \frac{1}{\sqrt{12}}\mathcal{IC}_{\mu\rightarrow e;e\tau}^1$
α_{33}	$\frac{1}{2}\mathcal{IC}_{\mu\rightarrow\mu;e\mu}^1 + \frac{1}{2}\mathcal{IC}_{\mu\rightarrow\mu;e\tau}^1$	$\frac{1}{2}\mathcal{IC}_{\mu\rightarrow e;e\mu}^1 + \frac{1}{2}\mathcal{IC}_{\mu\rightarrow e;e\tau}^1$

Table 13: . The leading coefficient of each $\epsilon_{\alpha\beta}$ and α_{ij} , for $\nu_\mu \rightarrow \nu_\mu$ and $\nu_\mu \rightarrow \nu_e$. $\mathcal{RC}_{\alpha\rightarrow\beta;\gamma\delta}^x$ ($\mathcal{IC}_{\alpha\rightarrow\beta;\gamma\delta}^x$ is the coefficient for real (image) part of $\gamma\delta$ in $\alpha \rightarrow \beta$, which is of the order x).

In Eq. (90), coefficients of $\epsilon_{\mu\tau}$ and $\tilde{\epsilon}_{\tau\tau}$ appear at leading order, i.e., at the order $\mathcal{C}_{\mu\rightarrow\mu; \text{element}}^0$. However, the coefficient of $\tilde{\epsilon}_{\tau\tau}$ is proportional to the factor $(c_{23}^2 - s_{23}^2)$, which is suppressed since $\theta_{23} \sim 45^\circ$. Coefficients of $\tilde{\epsilon}_{ee}$, $\epsilon_{e\mu}$, $\epsilon_{e\tau}$, which are of the 2nd, 1st and 1st order, respectively, have less influence on $P(\nu_\mu \rightarrow \nu_\mu)$. Therefore, the impact of NSIs on the disappearance channel is dominated by $\epsilon_{\mu\tau}$. On the other hand, from Eq. (91), it is obvious that the largest contributions to the transition probability are from $\epsilon_{e\mu}$ and $\epsilon_{e\tau}$, with coefficients of the 1st order. In Table 13, we present coefficients for α_{mn} , based on Eqs. (90) and (91) and Table 3.

References

- [1] Y. Fukuda *et al.* [Super-Kamiokande Collaboration], Phys. Rev. Lett. **81** (1998) 1562 [hep-ex/9807003].
- [2] S. Fukuda *et al.* [Super-Kamiokande Collaboration], Phys. Rev. Lett. **86** (2001) 5651 [hep-ex/0103032]; Q. R. Ahmad *et al.* [SNO Collaboration], Phys. Rev. Lett. **87** (2001) 071301 [nucl-ex/0106015]; Q. R. Ahmad *et al.* [SNO Collaboration], Phys. Rev. Lett. **89** (2002) 011301 [nucl-ex/0204008].
- [3] M. H. Ahn *et al.* [K2K Collaboration], Phys. Rev. Lett. **90** (2003) 041801 [hep-ex/0212007]; K. Abe *et al.* [T2K Collaboration], Phys. Rev. Lett. **107** (2011) 041801 [arXiv:1106.2822 [hep-ex]].
- [4] K. Eguchi *et al.* [KamLAND Collaboration], Phys. Rev. Lett. **90** (2003) 021802 [hep-ex/0212021]; F. P. An *et al.* [Daya Bay Collaboration], Phys. Rev. Lett. **108** (2012) 171803 [arXiv:1203.1669 [hep-ex]]; J. K. Ahn *et al.* [RENO Collaboration], Phys. Rev. Lett. **108** (2012) 191802 [arXiv:1204.0626 [hep-ex]].
- [5] R. Acciarri *et al.* [DUNE Collaboration], arXiv:1512.06148 [physics.ins-det].
- [6] K. Abe *et al.* [Hyper-Kamiokande Collaboration], KEK-PREPRINT-2016-21, ICRR-REPORT-701-2016-1.
- [7] F. An *et al.* [JUNO Collaboration], J. Phys. G **43** (2016) 030401 [arXiv:1507.05613 [physics.ins-det]].
- [8] Z. Djurcic *et al.* [JUNO Collaboration], arXiv:1508.07166 [physics.ins-det].
- [9] M. Antonello *et al.* [MicroBooNE and LAr1-ND and ICARUS-WA104 Collaborations], arXiv:1503.01520 [physics.ins-det].
- [10] D. Adey *et al.* [nuSTORM Collaboration], arXiv:1308.6822 [physics.acc-ph].
- [11] J. Cao *et al.*, Phys. Rev. ST Accel. Beams **17** (2014) 090101 [arXiv:1401.8125 [physics.acc-ph]].
- [12] S. Choubey *et al.* [IDS-NF Collaboration], arXiv:1112.2853 [hep-ex].
- [13] H. Minakata and S. J. Parke, Phys. Rev. D **87** (2013) 113005 [arXiv:1303.6178 [hep-ph]]; S. Parke, Phys. Scripta T **158** (2013) 014013 [arXiv:1310.5992 [hep-ph]].
- [14] M. Blennow, P. Coloma, P. Huber and T. Schwetz, JHEP **1403** (2014) 028 [arXiv:1311.1822 [hep-ph]]; S. K. Agarwalla, Adv. High Energy Phys. **2014** (2014) 457803 [arXiv:1401.4705 [hep-ph]]; P. Coloma, H. Minakata and S. J. Parke, Phys. Rev. D **90** (2014) 093003 [arXiv:1406.2551 [hep-ph]]; M. Blennow, P. Coloma and E. Fernandez-Martinez, JHEP **1503** (2015) 005 [arXiv:1407.3274 [hep-ph]]; P. Ballett, S. F. King, S. Pascoli, N. W. Prouse and T. Wang, Phys. Rev. D **96** (2017) 033003 [arXiv:1612.07275 [hep-ph]].
- [15] T. Ohlsson, Rept. Prog. Phys. **76** (2013) 044201 [arXiv:1209.2710 [hep-ph]]; O. G. Miranda and H. Nunokawa, New J. Phys. **17** (2015) 095002 [arXiv:1505.06254 [hep-ph]].

- [16] S. Antusch, J. P. Baumann and E. Fernandez-Martinez, Nucl. Phys. B **810** (2009) 369 [arXiv:0807.1003 [hep-ph]].
- [17] M. B. Gavela, D. Hernandez, T. Ota and W. Winter, Phys. Rev. D **79** (2009) 013007 [arXiv:0809.3451 [hep-ph]].
- [18] M. B. Wise and Y. Zhang, Phys. Rev. D **90** (2014) 053005 [arXiv:1404.4663 [hep-ph]].
- [19] S. Antusch and O. Fischer, JHEP **1410** (2014) 094 doi:10.1007/JHEP10(2014)094 [arXiv:1407.6607 [hep-ph]].
- [20] D. V. Forero and W. C. Huang, JHEP **1703** (2017) 018 [arXiv:1608.04719 [hep-ph]].
- [21] J. Heeck and W. Rodejohann, Phys. Rev. D **84** (2011) 075007 [arXiv:1107.5238 [hep-ph]].
- [22] Y. Farzan, Phys. Lett. B **748** (2015) 311 doi:10.1016/j.physletb.2015.07.015 [arXiv:1505.06906 [hep-ph]].
- [23] Y. Farzan and I. M. Shoemaker, JHEP **1607**, 033 (2016) doi:10.1007/JHEP07(2016)033 [arXiv:1512.09147 [hep-ph]].
- [24] Y. Farzan and J. Heeck, Phys. Rev. D **94** (2016) no.5, 053010 doi:10.1103/PhysRevD.94.053010 [arXiv:1607.07616 [hep-ph]].
- [25] K. S. Babu, A. Friedland, P. A. N. Machado and I. Mocioiu, JHEP **1712** (2017) 096 doi:10.1007/JHEP12(2017)096 [arXiv:1705.01822 [hep-ph]].
- [26] D. Akimov *et al.* [COHERENT Collaboration], Science (2017) [arXiv:1708.01294 [nucl-ex]].
- [27] M. C. Gonzalez-Garcia and M. Maltoni, JHEP **1309** (2013) 152 [arXiv:1307.3092 [hep-ph]].
- [28] M. Masud, A. Chatterjee and P. Mehta, J. Phys. G **43** (2016) 095005 [arXiv:1510.08261 [hep-ph]]; A. de Gouvea and K. J. Kelly, Nucl. Phys. B **908** (2016) 318 [arXiv:1511.05562 [hep-ph]]; P. Coloma, JHEP **1603** (2016) 016 [arXiv:1511.06357 [hep-ph]].
- [29] J. Liao, D. Marfatia and K. Whisnant, Phys. Rev. D **93** (2016) 093016 [arXiv:1601.00927 [hep-ph]]; K. Huitu, T. J. Kärkkäinen, J. Maalampi and S. Vihonen, Phys. Rev. D **93** (2016) 053016 [arXiv:1601.07730 [hep-ph]]; P. Bakhti and Y. Farzan, JHEP **1607** (2016) 109 [arXiv:1602.07099 [hep-ph]]; M. Masud and P. Mehta, Phys. Rev. D **94** (2016) 013014 [arXiv:1603.01380 [hep-ph]]; P. Coloma and T. Schwetz, Phys. Rev. D **94** (2016) 055005 Erratum: [Phys. Rev. D **95** (2017) 079903] [arXiv:1604.05772 [hep-ph]]; M. Masud and P. Mehta, Phys. Rev. D **94** (2016) 053007 [arXiv:1606.05662 [hep-ph]]; M. Blennow, S. Choubey, T. Ohlsson, D. Pramanik and S. K. Raut, JHEP **1608** (2016) 090 [arXiv:1606.08851 [hep-ph]].
- [30] S. K. Agarwalla, S. S. Chatterjee and A. Palazzo, Phys. Lett. B **762** (2016) 64 [arXiv:1607.01745 [hep-ph]]; S. F. Ge and A. Y. Smirnov, JHEP **1610** (2016) 138 [arXiv:1607.08513 [hep-ph]]; S. Fukasawa, M. Ghosh and O. Yasuda, Phys. Rev. D **95** (2017) 055005 [arXiv:1611.06141 [hep-ph]]; K. N. Deepthi, S. Goswami and N. Nath, Phys. Rev. D **96** (2017) 075023 [arXiv:1612.00784 [hep-ph]]; J. Liao, D. Marfatia and K. Whisnant, JHEP **1701** (2017) 071 [arXiv:1612.01443 [hep-ph]].

- [31] P. Coloma, P. B. Denton, M. C. Gonzalez-Garcia, M. Maltoni and T. Schwetz, JHEP **1704** (2017) 116 [arXiv:1701.04828 [hep-ph]]; M. Masud, M. Bishai and P. Mehta, arXiv:1704.08650 [hep-ph]; K. N. Deepthi, S. Goswami and N. Nath, Nucl. Phys. B **936** (2018) 91 [arXiv:1711.04840 [hep-ph]].
- [32] M. Blennow, P. Coloma, E. Fernandez-Martinez, J. Hernandez-Garcia and J. Lopez-Pavon, JHEP **1704** (2017) 153 [arXiv:1609.08637 [hep-ph]].
- [33] N. C. Ribeiro, H. Minakata, H. Nunokawa, S. Uchinami and R. Zukanovich-Funchal, JHEP **0712** (2007) 002 [arXiv:0709.1980 [hep-ph]]; P. Coloma, A. Donini, J. Lopez-Pavon and H. Minakata, JHEP **1108** (2011) 036 [arXiv:1105.5936 [hep-ph]].
- [34] J. Tang and Y. Zhang, Phys. Rev. D **97** (2018) no.3, 035018 doi:10.1103/PhysRevD.97.035018 [arXiv:1705.09500 [hep-ph]].
- [35] Z. Rahman, A. Dasgupta and R. Adhikari, J. Phys. G **42**, 065001 (2015) doi:10.1088/0954-3899/42/6/065001 [arXiv:1503.03248 [hep-ph]].
- [36] A. Dasgupta, Z. Rahman and R. Adhikari, arXiv:1210.4801 [hep-ph].
- [37] P. Coloma, A. Donini, J. Lopez-Pavon and H. Minakata, JHEP **1108**, 036 (2011) doi:10.1007/JHEP08(2011)036 [arXiv:1105.5936 [hep-ph]].
- [38] E. Ma and G. Rajasekaran, Phys. Rev. D **64** (2001) 113012 [hep-ph/0106291].
- [39] G. Altarelli and F. Feruglio, Nucl. Phys. B **720** (2005) 64 [hep-ph/0504165].
- [40] G. Altarelli and F. Feruglio, Nucl. Phys. B **741** (2006) 215 [hep-ph/0512103].
- [41] C. S. Lam, Phys. Rev. D **78** (2008) 073015 [arXiv:0809.1185 [hep-ph]].
- [42] P. F. Harrison, D. H. Perkins and W. G. Scott, Phys. Lett. B **530** (2002) 167 [hep-ph/0202074]; Z. Z. Xing, Phys. Lett. B **533** (2002) 85 [hep-ph/0204049]; P. F. Harrison and W. G. Scott, Phys. Lett. B **535** (2002) 163 [hep-ph/0203209]; X. G. He and A. Zee, Phys. Lett. B **560** (2003) 87 [hep-ph/0301092].
- [43] For some reviews, see G. Altarelli and F. Feruglio, Rev. Mod. Phys. **82** (2010) 2701 [arXiv:1002.0211 [hep-ph]]; S. F. King and C. Luhn, Rept. Prog. Phys. **76** (2013) 056201 [arXiv:1301.1340 [hep-ph]]; S. F. King, A. Merle, S. Morisi, Y. Shimizu and M. Tanimoto, New J. Phys. **16** (2014) 045018 [arXiv:1402.4271 [hep-ph]].
- [44] E. Ma, Phys. Rev. D **82** (2010) 037301 [arXiv:1006.3524 [hep-ph]].
- [45] R. de Adelhart Toorop, F. Bazzocchi, L. Merlo and A. Paris, JHEP **1103** (2011) 035 [arXiv:1012.1791 [hep-ph]]; R. de Adelhart Toorop, F. Bazzocchi, L. Merlo and A. Paris, JHEP **1103** (2011) 040 [arXiv:1012.2091 [hep-ph]].
- [46] A. Degee, I. P. Ivanov and V. Keus, JHEP **1302** (2013) 125 [arXiv:1211.4989 [hep-ph]]; V. Keus, S. F. King and S. Moretti, JHEP **1401** (2014) 052 [arXiv:1310.8253 [hep-ph]].
- [47] J. Heeck, M. Holthausen, W. Rodejohann and Y. Shimizu, Nucl. Phys. B **896** (2015) 281 [arXiv:1412.3671 [hep-ph]]; I. de Medeiros Varzielas, O. Fischer and V. Maurer, JHEP **1508** (2015) 080 [arXiv:1504.03955 [hep-ph]].

- [48] T. Kobayashi, Y. Omura, F. Takayama and D. Yasuhara, JHEP **1510** (2015) 042 [arXiv:1505.07636 [hep-ph]].
- [49] S. Pascoli and Y. L. Zhou, JHEP **1610** (2016) 145 [arXiv:1607.05599 [hep-ph]].
- [50] Y. Muramatsu, T. Nomura, Y. Shimizu and H. Yokoya, Phys. Rev. D **97** (2018) 015003 [arXiv:1707.06542 [hep-ph]].
- [51] S. Pascoli and Y. L. Zhou, JHEP **1606** (2016) 073 [arXiv:1604.00925 [hep-ph]].
- [52] I. Girardi, S. T. Petcov, A. J. Stuart and A. V. Titov, Nucl. Phys. B **902** (2016) 1 [arXiv:1509.02502 [hep-ph]]; S. F. King, J. Phys. G **42**, 123001 (2015) [arXiv:1510.02091 [hep-ph]]; C. C. Li, J. N. Lu and G. J. Ding, Nucl. Phys. B **913** (2016) 110 [arXiv:1608.01860 [hep-ph]]; S. K. Kang, Y. Shimizu, K. Takagi, S. Takahashi and M. Tanimoto, arXiv:1804.10468 [hep-ph].
- [53] A. N. Khan, Phys. Rev. D **93** (2016) 093019 [arXiv:1605.09284 [hep-ph]].
- [54] B. Sevda, M. Deniz, S. Kerman, L. Singh, H. T. Wong and M. Zeyrek, Phys. Rev. D **95** (2017) 033008 [arXiv:1611.07259 [hep-ex]].
- [55] O. G. Miranda, M. A. Tortola and J. W. F. Valle, JHEP **0610** (2006) 008 [hep-ph/0406280]; F. J. Escrihuela, O. G. Miranda, M. A. Tortola and J. W. F. Valle, Phys. Rev. D **80** (2009) 105009 Erratum: [Phys. Rev. D **80** (2009) 129908] [arXiv:0907.2630 [hep-ph]].
- [56] E. Fernandez-Martinez, J. Hernandez-Garcia and J. Lopez-Pavon, JHEP **1608** (2016) 033 [arXiv:1605.08774 [hep-ph]].
- [57] D. Wyler and L. Wolfenstein, Nucl. Phys. B **218** (1983) 205; R. N. Mohapatra, Phys. Rev. Lett. **56** (1986) 561; R. N. Mohapatra and J. W. F. Valle, Phys. Rev. D **34** (1986) 1642.
- [58] K. Hayasaka *et al.*, Phys. Lett. B **687** (2010) 139 [arXiv:1001.3221 [hep-ex]].
- [59] B. Aubert *et al.* [BaBar Collaboration], Phys. Rev. Lett. **104** (2010) 021802 [arXiv:0908.2381 [hep-ex]].
- [60] A. M. Baldini *et al.* [MEG Collaboration], Eur. Phys. J. C **76** (2016) 434 [arXiv:1605.05081 [hep-ex]].
- [61] R. N. Mohapatra, M. K. Parida and G. Rajasekaran, Phys. Rev. D **69** (2004) 053007 [hep-ph/0301234].
- [62] C. Biggio, M. Blennow and E. Fernandez-Martinez, JHEP **0903** (2009) 139 [arXiv:0902.0607 [hep-ph]].
- [63] C. Biggio, M. Blennow and E. Fernandez-Martinez, JHEP **0908** (2009) 090 [arXiv:0907.0097 [hep-ph]].
- [64] Q. H. Cao, G. Li, K. P. Xie and J. Zhang, Phys. Rev. D **97** (2018) 115036 [arXiv:1711.02113 [hep-ph]].
- [65] S. S. Wilks, Annals Math. Statist. **9**, no. 1, 60 (1938).

- [66] P. Huber, M. Lindner and W. Winter, Comput. Phys. Commun. **167** (2005) 195 [hep-ph/0407333].
- [67] P. Huber, J. Kopp, M. Lindner, M. Rolinec and W. Winter, Comput. Phys. Commun. **177** (2007) 432 [hep-ph/0701187].
- [68] I. Esteban, M. C. Gonzalez-Garcia, M. Maltoni, I. Martinez-Soler and T. Schwetz, JHEP **1701** (2017) 087 [arXiv:1611.01514 [hep-ph]].
- [69] T. Alion *et al.* [DUNE Collaboration], arXiv:1606.09550 [physics.ins-det].
- [70] T. Kikuchi, H. Minakata and S. Uchinami, JHEP **0903** (2009) 114 [arXiv:0809.3312 [hep-ph]].